SAPIENZA UNIVERSITY OF ROME

Department of Physiology and Pharmacology
"V. Erspamer"

A Dissertation in Fulfillment of the Requirements for the
Degree of Doctor of Philosophy in Toxicology

Glia-neuron interplay in health and disease: pharmacological evidence for this required teamwork

Ph.D Thesis of:
Dr. Maria Rosanna Bronzuoli

SUPERVISOR:
Prof. Luca Steardo

CO-SUPERVISORS:
Prof. Maiken Nedergaard
Dr. Caterina Scuderi

Director of the Ph.D Program
Prof. Vincenzo Cuomo

INDEX

SUMMARY

During these three years, my PhD studies evaluated the role of the cross-talk between glia and neurons in physiological and/or pathological conditions, paying attention to neuroinflammatory processes in neuropsychiatric disorders, mainly in Alzheimer's disease (AD).

Glia is a cell population highly present in the central nervous system (CNS) with the purpose, among other functions, to support neurons. In fact, many of these cells are closely in contact with neurons, actively participating to homeostatic support and synaptic transmission. For instance, astrocytes are considered integral part of the tripartite synapse. By this way, recent discoveries made possible to change perspective regarding the neuro-centric view of chronic neurodegenerative disorders, expanding the horizon to new players involved in the physiological and/or pathologic processes that take place in CNS. Better understanding the contribution of non-neuronal cells to these processes will be crucial for the development of new therapeutic approaches to counteract neurodegeneration.

Moving from these assumptions, my studies focused on evaluating the role of glial cells in inducing and triggering the inflammatory processes during neurodegeneration and, in particular, on the events that lead these cells to an activated state named reactive gliosis. Moreover, the consequences caused by these processes on neuronal survival, and in a macroscopic manner, on learning and memory, were evaluated.

To achieve such goals, I worked with different preclinical models of AD, both *in vitro* and *in vivo*, attempting to recreate at best the pathological hallmarks of pathology. In addition, since the crucial role of glial cells in the maintenance of brain homeostasis and their close connection with neuronal functioning and survival, the action of different molecules on neuroinflammation, as well as on neuronal survival, were tested.

The first part of the PhD program focused on the role of SIRT1 and SIRT2 modulation in an *in vitro* model of beta amyloid (Aβ) toxicity. Sirtuins (SIRTs) are a family of NAD^+-dependent enzymes, involved in the control of a variety of biological processes that have the potential to modulate neurodegeneration. The possibility to activate SIRT1 or inhibit SIRT2 in order to prevent reactive gliosis induced by $A\beta_{(1-42)}$ was tested in primary rat astrocytes. Aβ-activated astrocytes were treated with either resveratrol (RSV), a SIRT1 activator, or AGK-2, a SIRT2-selective inhibitor. Results shown that RSV and AGK-2 controlled both astrocytes activation and inflammation (Section I).

During the same period, I was involved in a study aimed at investigating the anti-inflammatory and neuroprotective properties of palmitoylethanolamide (PEA) in an *in vivo* model of AD. To this purpose, adult rats were injected with $A\beta_{(1-42)}$ in hippocampus and, starting from the day of surgery, were intraperitoneally treated with PEA for 7 days. Moreover, to assess PEA molecular mechanism, a group of rats was i.p. treated with GW6471, a selective peroxisome proliferator-activated receptor-α (PPAR-α) antagonist.

Results from molecular biology and behavioural experiments confirmed that $A\beta_{(1-42)}$ infusion causes reactive gliosis, exacerbating amyloidogenesis, tau hyperphosphorylation, and cognitive deficit. PEA treatment had a great anti-inflammatory and neuroprotective action, restoring the behavioural outcomes by activating PPAR-α (Section II).

During the second part of my PhD, I further explored the pharmacological properties of PEA by using a triple transgenic mouse model of AD (3xTg-AD). These mice harbour three human transgenes strongly correlated with AD (APP_{swe}, $PS1_{M146V}$ and tau_{P301L}), and express both senile plaques (SPs) and neurofibrillary tangle (NFTs). 3xTg-AD and Non-Tg mice received vehicle or ultra-micronized PEA (um-PEA) for three months through a depot delivery system subcutaneously implanted. Hippocampal tissues from mice of two different ages, 6-month-old (corresponding to a pre-symptomatic stage) and 12-month-old (corresponding to full-blown disease) were tested.

Results shown that hippocampi of 3xTg-AD mice, especially those deriving from 6-month-old animals, presented a reactive astrocytic state, impairment of the Akt/GSκ-3β pathway involved in tau phosphorylation and neuronal survival, and amyloidogenic pathway exacerbation. um-PEA chronic treatment was able to restore the deregulated parameters in each pathway studied, at both ages. It is noteworthy that um-PEA had a positive effect even in ageing when we tasted it in 12-month-old Non-Tg mice.

From these data, we can conclude that um-PEA has a promising effect on neuroinflammation and neuronal survival in 3xTg-AD model, especially in precocious stages of the disease, as well as on the aging process (Section III).

Last part of the research activity has been performed in Copenhagen, Denmark, at the Center of Basic and Translational Neuroscience of University of Copenhagen (KU). The research activity was followed by Prof. Maiken Nedergaard from KU.

These studies focused on long term potentiation (LTP), widely considered one of the primary mechanisms underlying learning and memory, processes strongly impaired in AD.

In order to further study the cross-talk between glia and neurons and, in particular, the physiological mechanisms involved in tripartite synapses, a chemical protocol, design by KU lab, able to induce LTP was used.

LTP is a form of synaptic plasticity characterized by a persistent strengthening of synapses and associated increase in dendritic spines volume taking place after high frequency stimulations. Although K^+ level in the dendritic cleft has been suggested to be involved in the process of synaptic potentiation, the effect of physiological K^+ concentration on the macroscopic increase in volume of dendritic spines is still poorly investigated. At this early step of the study, we focused on neurons in order to expand the study to other players involved in the induction of LTP and K^+ regulation, astrocytes.

This preliminary data shown that the area of dendritic spines in the CA1 region of hippocampus is increased after LTP induced by briefly superfusing acute mouse brain slices to a higher concentration of K^+ (20 mM). Notably, K^+ concentration where the measured changes occur has been demonstrated to peak around 8 mM, suggesting that the phenomenon is physiologically relevant (Section IV).

The present dissertation collects most of the results obtained during my PhD.

SECTION I

Sirtuin modulators control reactive gliosis in an in vitro model of Alzheimer's disease

INTRODUCTION

Alzheimer's disease (AD) represents one of the major health concerns and it is a research priority since there is a pressing need to develop new agents to prevent or treat it. A part of the progressive deposition of beta amyloid peptide (Aβ) and accumulation of phosphorylated tau, several other alterations occur in AD brain, all bringing to neuronal loss. Among these, growing interest has been attracted by the role of inflammation in the onset and progression of this disorder. In fact, senile plaques and neurofibrillary tangles (which are considered the more characteristic hallmarks of AD) co-localize with activated astrocytes, suggesting for these cells a key role in the pathogenesis of AD (Meda *et al.*, 2001; Craft *et al.*, 2006). Along this line, in several experimental models it has been demonstrated that Aβ peptide fragments markedly alter astrocytes functions. This process is accompanied with a noticeable neuroinflammatory response, accounting for the synthesis of different cytokines and pro-inflammatory mediators which amplify neuropathological damage (Mrak and Griffin, 2001a; Caricasole *et al.*, 2003; Tuppo and Arias, 2005; Griffin, 2006; Scuderi *et al.*, 2011, 2012, 2013). It is established that neuroinflammation is directly linked to neural dysfunction and cell death, representing a primary cause of neurodegeneration (Block and Hong, 2005). In fact, over-release of pro-inflammatory cytokines by glia cells causes neuronal dysfunction and synaptic loss, which correlate with memory decline. These phenomena are believed to precede neuronal death. Thus, research focused on developing therapeutic strategies directed at controlling the prolonged and uncontrolled glia activation should be encouraged.

An uncommon opportunity to improve inflammation and neurodegeneration simultaneously is provided by compounds able to modulate histone acetylation/deacetylation, since they participate in brain immune control and neuroprotection, in addition to their well-known effects on the molecular mechanisms associated to senescence and metabolic syndromes. Mounting evidence indicates that sirtuins (SIRTs) exert neuroprotective effects in several models of neurodegeneration (Outeiro *et al.*, 2008; Tang and Chua, 2008; de Oliveira *et al.*, 2010). SIRTs, a family of NAD^+-dependent enzymes with seven isoforms identified (SIRT1-7), are implicated in the control of a variety of biological processes including transcriptional silencing, chromosomal stability, cell cycle progression, apoptosis, autophagy, metabolism, growth suppression, inflammation, and stress response (Gan and Mucke, 2008; Haigis and Sinclair, 2010).

Recent observations indicate that both SIRT1 and SIRT2 regulate neuronal survival, but with divergent functional outcomes. Indeed, activation of SIRT1 mainly exerts neuroprotective actions, while SIRT2 fosters neurodegeneration. The reason for such opposite effect may be due to their different sub-cellular localization, which gives SIRT1 and SIRT2 distinct molecular targets (Harting and Knöll, 2010). It has been demonstrated that the overexpression of SIRT1 prevents neuronal death in tissue culture models of AD, amyotrophic lateral sclerosis, and polyglutamine toxicity, and it reduces hippocampal degeneration in a mouse model of AD (Kim *et al.*, 2007; Li *et al.*, 2007b). Moreover, treatment with resveratrol (RSV), a polyphenolic compound acting as a pharmacological activator of SIRT1, is protective in several experimental neurodegeneration paradigms (Anekonda, 2006; Sun *et al.*, 2010). RSV, like other polyphenol compounds including curcumin, displays a plethora of actions, behaving as a potent antioxidant agent, increasing SUMOylation, and activating protein kinase C, all mechanisms able to counteract astrocyte reactivity and protect neurons (Jefremov *et al.*, 2007; Hoppe *et al.*, 2013; Menard *et al.*, 2013). Finally, it has been observed that both SIRT1 overexpression and RSV treatment are able to significantly decrease the Aβ-induced activation of NF-κB, thus operating a simultaneous control on both neurodegeneration and neuroinflammation processes (Chen *et al.*, 2005). Indeed, NF-κB is a transcription factor which controls the expression of gene products involved in key cellular signaling, including those associated to inflammatory and degenerative events. Post-mortem studies on cerebral cortices from AD patients have established a correlation between loss of SIRT1 and the accumulation of Aβ and hyperphosphorylated tau proteins (Julien *et al.*, 2009). Growing evidence indicates that also SIRT2 is involved in regulating several brain processes including oligodendrocyte mitosis and differentiation, cytoskeletal dynamics necessary for trafficking, neurite outgrowth and synaptic remodelling. Unlike SIRT1, SIRT2 appears to promote neuronal death. In fact, blocking SIRT2 counteracted alpha synuclein toxicity in Parkinson's disease models (Outeiro *et al.*, 2007). However, less is known about the role of SIRT2 in AD.

On the basis of these considerations, we explored the effects of modulators of SIRTs on astrocyte activation and the subsequent inflammatory process. In particular, our experiments focalized the ability of RSV, a SIRT1 activator, and AGK-2, a SIRT2-selective inhibitor, to control astrocyte activation and to suppress the production of pro-inflammatory mediators in primary rat astrocytes exposed to Aβ peptide. These findings suggest that either RSV or AGK-2 may be an effective agent for neurodegenerative diseases initiated or maintained by inflammatory processes.

MATERIALS AND METHODS

Cell cultures and treatments

Newborn Sprague-Dawley rats (1 or 2 days old) were used to obtain primary astroglial cultures (Vairano *et al.*, 2002; Scuderi *et al.*, 2011). Briefly, brain cortices were homogenized and processed to obtain single cells. Astrocytes were cultured at a density of 3 × 106 cells/75-cm^2 flask and incubated at 37°C in a humidified atmosphere containing 5% CO_2. The culture medium used was Dulbecco's modified eagle medium (DMEM) supplemented with 5% inactivated fetal bovine serum, 100 IU/ml penicillin and 100 μg/ml streptomycin (all from Sigma-Aldrich, Milan, Italy), replaced 24 h after isolation and again one a week until astrocytes were grown to form a monolayer. Approximately 14-15 days after dissection, astrocytes were mechanically separated from microglia and oligodendrocytes. Obtained astrocytes were seeded onto 10-cm-diameter Petri dishes (1 × 106 cells/dish) or onto 24 well plates (1 × 105 cells/well). The monoclonal anti-glial fibrillary acidic protein (GFAP) was used to verify cell culture purity. Only cultures with more than 95% GFAP-positive cells were utilized. The 5% of non-astrocyte cells were microglia and oligodendrocytes.

All experiments were performed in accordance with the Italian Ministry of Health (DL 116/92), the Declaration of Helsinki, and the Guide for the Care and Use of Mammals in Neuroscience and Behavioral Research, and they were approved by the Institutional Animal Care and Use Committee at our institution.

Mature astrocytes were challenged with 0.23 μM $A\beta_{(1-42)}$ (Tocris Bioscience, Bristol, UK) in the presence or absence of the following substances: RSV (2 - 10 - 50 μM), a well-known SIRT1 activator, or AGK-2 (0.35 - 3.5 - 35 μM), a potent SIRT2-selective inhibitor (both from Sigma-Aldrich). After 24 (for viability and protein expression analyses) or 72 h (for proliferation assay) of treatment, astrocytes were collected for experiments. The concentration of the substances was chosen according to literature (Howitz *et al.*, 2003; Outeiro *et al.*, 2007; Scuderi *et al.*, 2011, 2012).

Analysis of astrocyte viability by neutral red uptake assay

Astrocyte viability was evaluated 24 h after treatments by the neutral red uptake assay according to Repetto *et al.* (2008), with some modifications (Scuderi and Steardo, 2013). Cells were seeded in 24-well plates and treated as previously described. 24 h after treatments, the plates were incubated for 3 h at 37°C with a neutral red working solution (50 μg/ml in PBS without calcium and magnesium, Sigma-Aldrich). The cells were washed and the dye removed from each

well through a destain solution (ethanol : deionized water : glacial acetic acid, 50:49:1, v/v). The absorbance was read at 540 nm using a microplate spectrophotometer (Epoch, Bio Teck, Winooski, VT, USA). The values of treated cells were referred to control non-exposed cultures, and expressed as percentage variation.

Analysis of astrocyte proliferation by trypan blue assay

Trypan blue exclusion assay was performed to monitor astrocyte proliferation 72 h after treatments. This method is based on the principle that living cells do not take up the dye, whereas dead cells do. To determine the number of cells and their viability using trypan blue, 20 µl of trypsinized and re-suspended cells were mixed with 20 µl of 0.4% solution of trypan blue dye (Sigma-Aldrich) for 1 min. Cells were immediately counted using a Bürker chamber with a light microscope. All counts were done using four technical duplicates of each sample.

Analysis of protein expression by western blotting

Western blot analyzes were performed on extracts of cell cultures challenged as previously described. 24 h after treatment, cells were detached from Petri dishes and each pellet was suspended in ice-cold hypotonic lysis buffer containing NaCl 150 mM; tris/HCl pH 7.5 50 mM; triton X-100 1%; ethylenediaminetetraacetic acid (EDTA) 1 mM, supplemented with PMSF 1 mM, aprotinin 10 µg/ml, leupeptin 0.1 mM (Roche, Mannheim, Germany). After incubation for 40 min at +4°C, homogenates were centrifuged at 14000 rpm for 15 min and the supernatant removed and stored in aliquots at -80°C until use. Equivalent amounts (70 µg) of each sample calculated by Bradford assay were resolved on 12% acrylamide SDS-PAGE precast gels (Bio-Rad Laboratories). Proteins were transferred onto nitro-cellulose. Membranes were blocked with 5% wt/v no-fat dry milk powder in tris-buffered saline-tween 0.1% (TBS-T) for 1 h before overnight incubation at +4°C with one of the following primary antibodies: rabbit anti-GFAP (1:50000, Abcam plc, Cambridge, UK), rabbit anti-S100β (1:1000, Epitomics, Burlingame, CA, USA), rabbit anti-inducible nitric oxide synthase (iNOS; 1:9000, Sigma-Aldrich), rabbit anti-cyclooxygenase-2 (COX-2; 1:1000, Cell Signaling Technology, MA, USA), rabbit anti-β-actin (1:1500, Santa Cruz Biotechnology, Santa Cruz, CA, USA). After being extensively washed in TBS-T, membranes were incubated for 1 h at +25 °C with the secondary horseradish peroxidase-conjugated antibody (HRP conjugated goat anti-rabbit IgG, 1:30000, Jackson Immunoresearch Europe, Suffolk, UK). The immunocomplexes were visualized using an ECL kit (Amersham, Bucks, UK). Protein expression was quantified by densitometric scanning of the X-ray films with

a GS 700 Imaging Densitometer (Bio-Rad laboratories) and a computer program (ImageJ software v1.44p, NIH, USA).

Statistical analysis

Analysis was performed using GraphPad Prism (GraphPad Software, San Diego, CA, USA). Data were analyzed by one way analysis of variance (ANOVA) to determine statistical differences between experimental groups. Multiple comparisons were performed with Bonferroni's test for *post hoc* analyzes. Differences between mean values were considered statistically significant when $p < 0.05$.

RESULTS

Effect of RSV and AGK-2 on astrocyte viability and proliferation

First of all, we decided to perform experiments to assess the effect of the SIRTs modulators on astrocyte viability and proliferation after $A\beta_{(1-42)}$ challenge. In fact, it has been already demonstrated that Aβ peptides are able to affect cell viability and to induce astrocyte proliferation (Allaman *et al.*, 2010; Scuderi *et al.*, 2012). Our results highlighted a significant increase in cell viability after 24 h treatment with $A\beta_{(1-42)}$ ($p < 0.01$; Figure 1A, C). RSV and AGK-2 were able to reduce this effect at the two higher concentrations used (Figure 1A, C). In addition, we found a reduction in cell viability after treatment with AGK-2 at the concentration of 35 μM on unstimulated cells, indicating a cytotoxic effect (Figure 1C). Trypan blue experiments revealed a significant astrocyte proliferation after 72 h treatment with $A\beta_{(1-42)}$ ($p < 0.01$; Figure 1B, D). Once again, both RSV and AGK-2 significantly controlled such increase at the two higher concentrations used. Surprisingly, RSV 50 μM and AGK-2 35 μM caused a reduction in proliferation rate also in unchallenged astrocytes (Figure 1B, D).

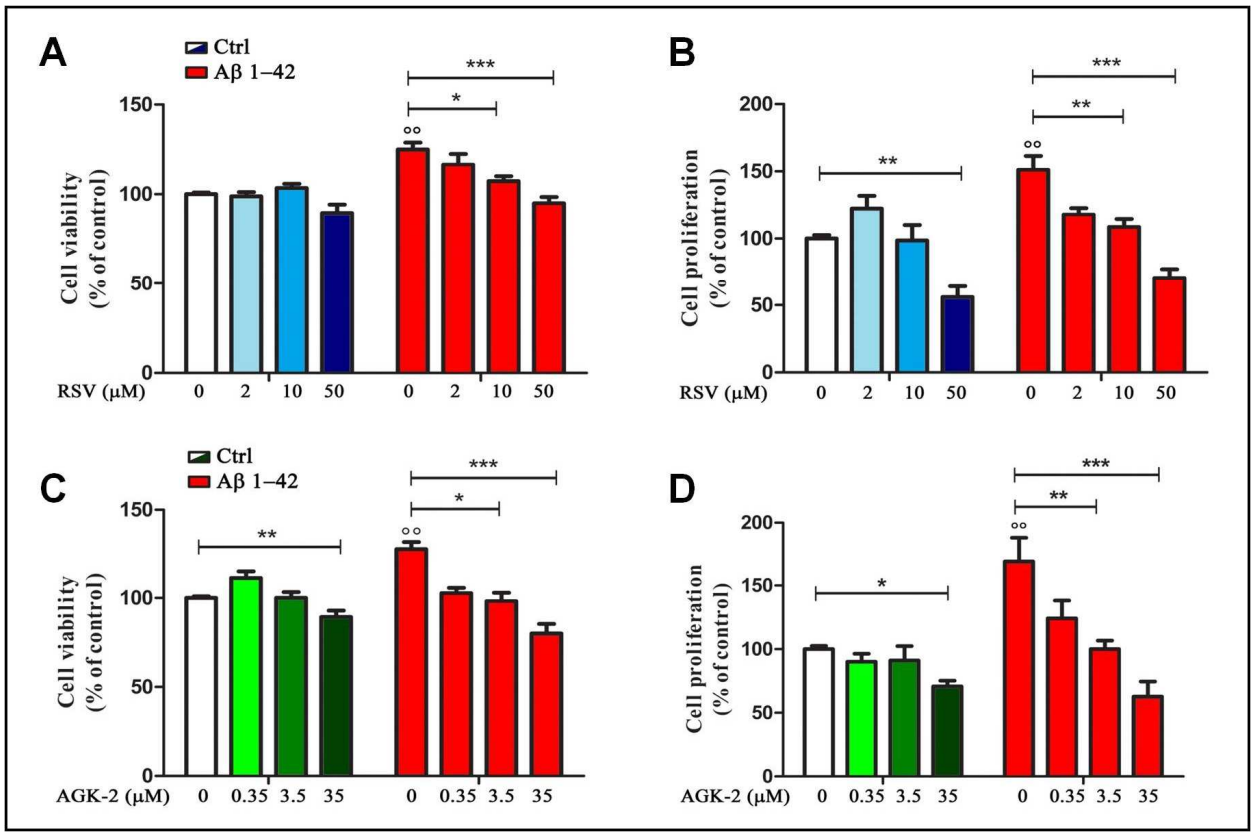

Figure 1 Resveratrol (RSV) and AGK-2 affect astrocyte viability and proliferation induced by Aβ$_{(1-42)}$ challenge

(A, C) Cells were challenged with 0.23 μM Aβ$_{(1-42)}$ in the presence or absence of one of the following substances: RSV (2 - 10 - 50 μM), a potent SIRT1 activator; AGK-2 (0.35 - 3.5 - 35 μM), a selective SIRT2 inhibitor. 24 h later cell viability was assessed by neutral red uptake assay. **(B, D)** 74 h after treatments cell proliferation was evaluated by trypan blue assay. Results are expressed as cell viability-fold increase versus unchallenged (open bars) or Aβ-challenged cells (black bars). Results are the mean ± SEM of four experiments in triplicate. Statistical analysis was performed by one-way ANOVA followed by Bonferroni multiple comparison test. °° $p < 0.01$ Aβ-challenged versus unchallenged cells; * $p < 0.05$; ** $p < 0.01$; *** $p < 0.001$ for multiple comparison among groups.

Effect of RSV and AGK.2 on astrocyte activation

In order to test the effect of RSV and AGK-2 on Aβ-induced astrogliosis, the expression of GFAP and S100β, specific markers of astrocyte activity, was explored. Reactive astrocytes display hypertrophied cell bodies and thickened processes exhibiting GFAP-immunoreactivity (O'Callaghan and Sriram, 2005; Olabarria *et al.*, 2010). Using western blot analysis, we observed a marked increase in the expression of GFAP after $A\beta_{(1-42)}$ challenge ($p < 0.01$; Figure 2). RSV was able to significantly attenuate such increase in a concentration-dependent manner (Figure 2A, B). Likewise, the Aβ-induced GFAP overexpression was counteracted by AGK-2 at the three concentrations used (Figure 2C, D).

Similarly, the expression of S100β was investigated by western blot. S100β is an astroglia-derived protein which acts as a neurotrophic factor and neuronal survival protein, even though the overproduction of S100β by activated astrocytes leads to further neurodegeneration. Elevated S100β levels are generally associated with a sustained reactive gliosis (Griffin, 2006; Donato and Heizmann, 2010). Results from cultured astrocytes showed a significant increase in S100β protein expression after $A\beta_{(1-42)}$ exposure ($p < 0.01$; Figure 2). Both RSV and AGK-2 controlled such an increase. Also in this case, RSV exerted its effect in a concentration-dependent manner (Figure 2A, B). Instead, all the AGK-2 concentrations completely abolished the Aβ-induced S100β increase (Figure 2C, D).

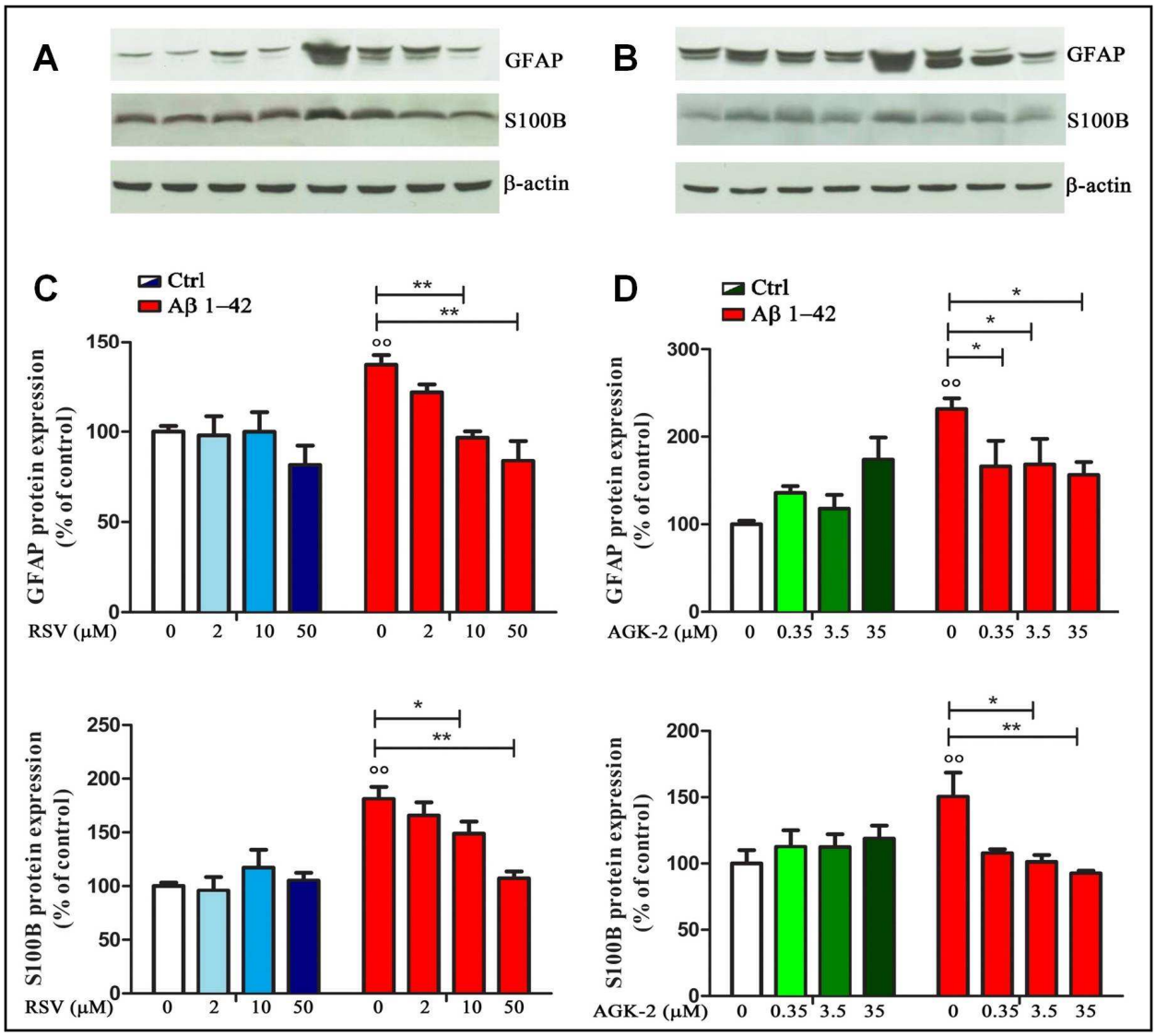

Figure 2 Effect of RSV and AGK-2 on GFAP and S100 β expression. 24 h after treatments, astrocytes were lysated and protein expression was evaluated

(A, B) Representative western blots for GFAP and S100β proteins in lysates from astrocytes challenged with $A\beta_{(1-42)}$ (0.23 μM) in the presence of **(C)** RSV (2 - 10 - 50 μM) or **(D)** AGK-2 (0.35 - 3.5 - 35 μM). Densitometric analyses normalized to β-actin loading controls. Results are the mean ± SEM of four experiments in triplicate. Statistical analysis was performed by one-way ANOVA followed by Bonferroni multiple comparison test. °° $p < 0.01$ Aβ-challenged versus unchallenged cells; * $p < 0.05$; ** $p < 0.01$; for multiple comparisons among groups.

Effect of RSV and AGK-2 on inflammation

Another set of experiments aimed at assessing the effect of RSV and AGK-2 on the production of inflammatory factors induced by $A\beta_{(1-42)}$ challenge. In fact, astrocyte activation is linked to the production of pro-inflammatory mediators which, in turn, stimulates gliosis and can kill neighbouring neurons (Mrak and Griffin, 2001a; Ferreira *et al.*, 2014). Treatment with $A\beta_{(1-42)}$ resulted in an increase in iNOS expression, as determined by western blot analysis ($p < 0.05$; Figure 3). Interestingly, this observed effect was reduced by both RSV and AGK-2 at the two higher concentrations used (Figure 3). Parallel results were obtained with immunoblot experiments aimed at studying COX-2 expression. In fact, $A\beta_{(1-42)}$ significantly increased COX-2 protein expression ($p < 0.05$; Figure 3). Also in this case, both RSV and AGK-2 significantly decreased such effect at the two higher concentrations used (Figure 3).

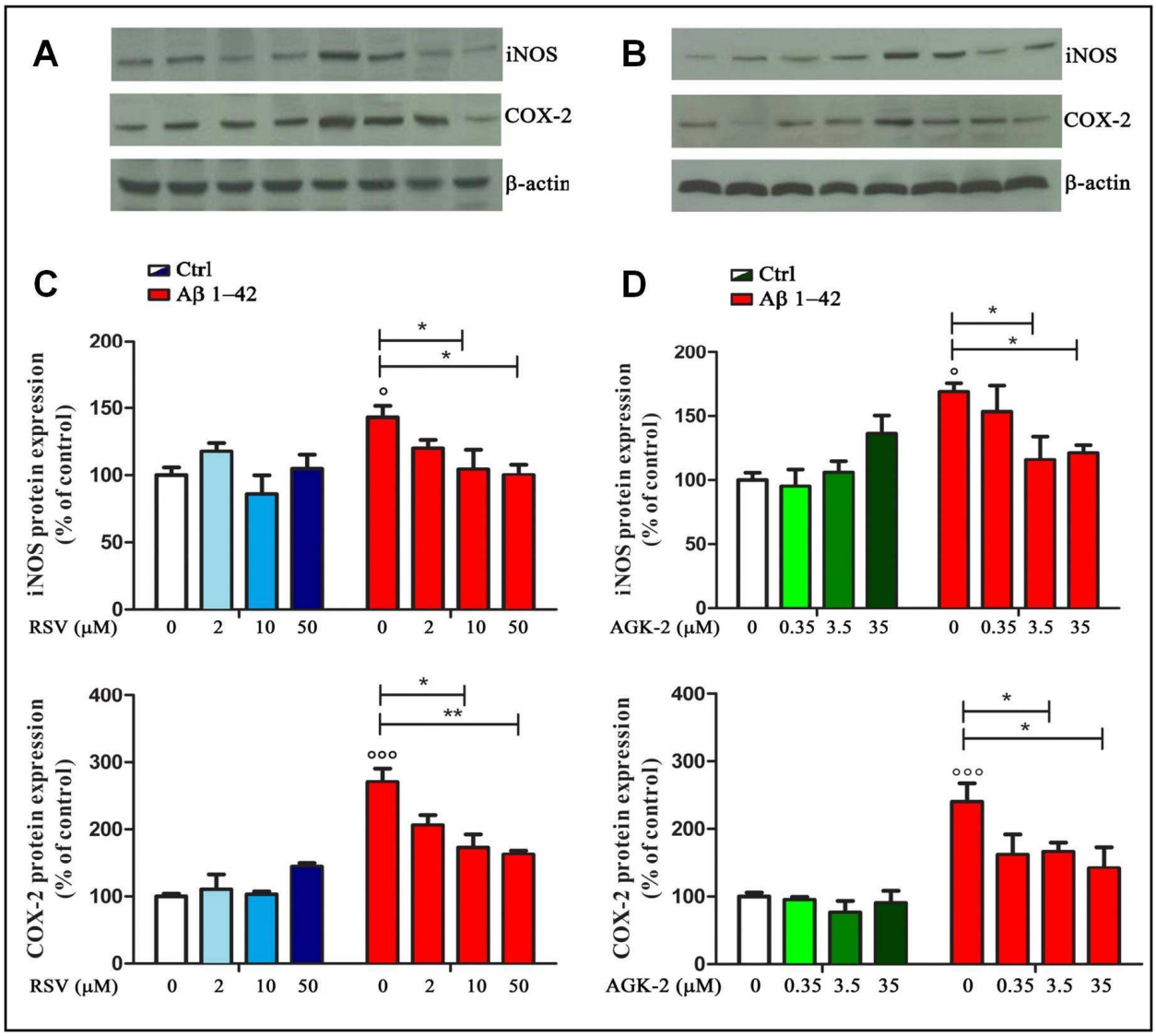

Figure 3 Effect of RSV and AGK-2 on iNOS and COX-2 expression
Astrocytes were treated with $A\beta_{(1-42)}$ (0.23 μM) in the presence of RSV (2 - 10 - 50 μM) or AGK-2 (0.35 - 3.5 - 35 μM). Western blot experiments were carried out 24 h after treatments. **(A, B)** Representative immunoblots for iNOS and COX-2 proteins. **(C**, **D)** Densitometric analyses normalized to β-actin loading controls. Results are the mean ± SEM of four experiments in triplicate. Statistical analysis was performed by one-way ANOVA followed by Bonferroni multiple comparison test. ° $p < 0.05$ and °°° $p < 0.001$ Aβ-challenged versus unchallenged cells; * $p < 0.05$; ** $p < 0.01$; for multiple comparison among groups.

DISCUSSION

The purpose of this study was to assess the efficacy of RSV, a well-known SIRT1 activator, and AGK-2, a potent SIRT2-selective inhibitor, in counteracting reactive gliosis, now considered one of the characteristic phenomena occurring in AD. AD leads to disability and death in a significant proportion of the world's aged population (Alzheimer's Association Report, 2013). However, the available treatments are limited and exert only symptomatic effects. Several promising drugs have recently failed to provide benefit, so there is an urgent need to develop new, and hopefully more efficacious drugs to affect AD course. To this attempt, in the last years researchers focused their attention on the role of reactive gliosis in the onset and progression of many neurodegenerative disorders, including AD. Produced results gave evidence that neuroinflammation and neurodegeneration mutually have a critical impact on AD course (Wyss-Coray and Rogers, 2012). For this reason, it is possible to assume that early combination of neuroprotective and anti-inflammatory treatments represents a particularly appropriate approach to AD (Di Filippo *et al.*, 2008). Although neurodegenerative disorders have distinct clinical manifestations, many of the underlying pathogenic processes are similar (intra- or extracellular accumulation of misfolded proteins, cytoskeletal abnormalities, disruption of calcium homeostasis, mitochondrial dysfunction, and inflammation), and most of them are strongly influenced by and increased during aging. In particular, in both early- and late-onset sporadic AD, aging represents a major contributing factor for the disease development and progression, although the precise role remains still unclear. Transcriptional profiling studies revealed that expression of genes that play central roles in synaptic plasticity, vesicular transport and mitochondria function is reduced, whereas expression of genes encoding for stress, inflammatory or immune factors is increased in aged human frontal cortex (Lu *et al.*, 2004). These findings implicate ongoing DNA damage, oxidative stress, and inflammation as contributors to the functional decline occurring in age-related neurodegenerative diseases, including AD.

In this context, the discovery of SIRTs, indicated as class III histone deacetylases (HDACs), offers a close relationship between aging, metabolism and neurodegeneration, thereby representing an innovative target to develop therapeutic strategies (Outeiro *et al.*, 2008). SIRTs play pleiotropic biological functions that range from repression of gene expression (through histone deacetylation) to regulation of cellular differentiation and/or apoptotic processes, from control of energetic cell metabolism to that of aging events. These enzymes have been extensively studied because of their involvement in mediating the effect of caloric restriction (CR) in fostering

longevity and healthy aging. In addition, many data indicate that SIRTs are potentially able to delay neurodegenerative diseases related to senescence, including AD. (Michan and Sinclair, 2007). It has been demonstrated that CR reduces the content of Aβ in the temporal cortex of squirrel monkeys, and such effect is inversely linked to SIRT1 expression in the same brain region (Qin *et al.*, 2006a). Moreover, in a transgenic mouse model of AD, the same authors previously demonstrated that CR antagonizes Aβ neuropathology by increasing the SIRT1 and NAD^+/nicotinamide ratio (Qin *et al.*, 2006b). Recently, SIRT2 inhibition has been proposed as a promising therapeutic strategy to achieve neuroprotection in *in vitro* and *in vivo* models of Parkinson's and Huntington's diseases (Outeiro *et al.*, 2007; Luthi-Carter *et al.*, 2010). Moreover, Spires-Jones *et al.* (2012) demonstrated that inhibition of SIRT2 is a safe and promising neuroprotective agent in both tau-associated frontotemporal dementia and AD.

It is recognized that Aβ affects cell viability and proliferation (Allaman *et al.*, 2010; Scuderi *et al.*, 2012). It is possible to speculate that these Aβ actions are due to its ability to enhance astrocyte metabolism turning on morpho-functional changes in such cells (Verkhratsky and Butt, 2007). Interestingly, our experiments highlighted alterations in astrocyte viability and proliferation after $A\beta_{(1-42)}$ challenge, and both RSV and AGK-2 markedly controlled these effects. SIRTs are considered as sensors of cell metabolic state because they finely modulate physiological processes. For this reason, it is important to establish the appropriate concentrations to avoid dangerous unwanted consequences. In fact, in our conditions, we found that the highest concentrations used of both RSV and AGK-2 caused cytotoxic effects.

As a consequence of exogenous insults, glial cells lost their physiological functions and acquire a reactive phenotype, characterized by profound morphological and functional alterations, such GFAP and S100β overexpression (O'Callaghan and Sriram, 2005; Donato *et al.*, 2013). In our model, we detected marked alteration of both these proteins. In fact, western blot analysis showed that astrocytes express higher GFAP and S100β protein levels after Aβ challenge. Interestingly, RSV and AGK-2 negatively modulated the expression of both GFAP and S100β.

As mentioned before, the direct correlation between the Aβ-induced toxicity and the production of pro-inflammatory mediators prompted us to investigate the expression of the two main inducible enzymes related to inflammation, iNOS and COX-2. In our experimental condition, we highlighted the existence of an inflammatory state induced by $A\beta_{(1-42)}$ treatment, as detected by the increased expression of both iNOS and COX-2. The alteration of these two proteins was significantly blunted by RSV and AGK-2, indicating a key role in regulating astrogliosis and important astrocyte changes, which contribute to disease progression. In the current study, it was observed that SIRT1 and SIRT2 can represent promising targets, whose manipulation could

prevent over-activation of neuroglia upon pro-inflammatory stimulation. These data suggest a SIRT-dependent mechanism to restrain detrimental effects of excessive astrocyte activation. Moreover, the findings bear major implications in the context of several inflammatory conditions of the CNS where astroglia is known to mediate deleterious consequences. In conclusion, the results of the present study provide evidence that SIRTs modulation can represent a strategy to counteract reactive gliosis, and suggest new avenues to walk for the discovery of novel and promising therapy for AD.

SECTION II

Palmitoylethanolamide controls reactive gliosis and exerts neuroprotective functions in a rat model of Alzheimer's disease

INTRODUCTION

Alzheimer's disease (AD) is the most common late-onset and progressive neurodegenerative disorder (Querfurth and LaFerla, 2010). It is characterized by progressive dementia including episodic memory impairments and involvement of other cognitive domains and skills (Dubois *et al.*, 2010). Although senile plaques (SPs) and neurofibrillary tangles (NFTs) are considered pathognomic (Blennow *et al.*, 2006), the concept that these are the only significant pathological changes occurring in AD brain is misleading. In fact, both *in vitro* and *in vivo* findings have demonstrated that beta amyloid (Aβ) fragments promote a marked neuroinflammatory response, accounting for the synthesis of different cytokines and pro-inflammatory mediators (Mrak and Griffin, 2001b). A chronic inflammation goes beyond physiological control and eventually detrimental effects override the beneficial effects. In fact, after their release, pro-inflammatory signaling molecules may act autocrinally to self-perpetuate reactive gliosis and paracrinally to kill neighbouring neurons, thus amplifying the neuropathological damage. Once started, the inappropriate and prolonged inflammatory process may contribute independently to neural dysfunction, cell death, and disease progression (Wyss-Coray, 2006; Block and Hong, 2005). Besides the sustained production of pathogenic substances, astrocytes fail to provide their neuro-supportive functions, making neurons more vulnerable to toxic molecules (Verkhratsky *et al.*, 2013). Therefore, targeting neuroinflammation might be an effective therapeutic strategy in AD (Fuller *et al.*, 2010; Esposito *et al.*, 2011; Cowley *et al.*, 2012; Medeiros and LaFerla, 2013).

At present, no therapies in clinical use are able to effectively impact the disease course. Therefore, new drugs able to simultaneously ameliorate the numerous pathogenic mechanism involved in AD are therapeutically promising.

Palmitoylethanolamide (PEA) has attracted much attention for its proven anti-inflammatory and neuroprotective properties reported in many neuropathological conditions other than AD. PEA, a naturally occurring amide of ethanolamine and palmitic acid, is a lipid messenger that mimics several endocannabinoid-driven actions, even though it does not bind cannabinoid receptors (Skaper *et al.*, 1996; Cadas *et al.*, 1997; Calignano *et al.*, 1998; Franklin *et al.*, 2003; Lo Verme *et al.*, 2005; Mackie and Stella, 2006; Murillo-Rodriguez *et al.*, 2006; Gatti *et al.*, 2012;

Keppel Hesselink *et al.*, 2013). PEA is abundant in the central nervous system (CNS) and it is conspicuously produced by glial cells (Cadas *et al*., 1997; Murillo-Rodriguez *et al.*, 2006). Many of its beneficial properties have been considered to be dependent on the activation of the peroxisome proliferator-activated receptor-α (PPAR-α) (Lo Verme *et al.*, 2005; Lo Verme *et al.*, 2006). Recent reports from our group showed the ability of PEA to attenuate *in vitro* the Aβ-induced upregulation of a wide range of inflammatory mediators by interacting at the PPAR-α nuclear site (Scuderi *et al.*, 2012; Scuderi and Steardo, 2013). Both PPAR-α and PEA are clearly detected in the CNS and their expression may largely change during pathological conditions (Petrosino *et al.*, 2010). It has been observed that Aβ significantly blunts PPAR-α in primary rat astrocytes, suggesting the possibility that the downregulation of this receptor may represent one of the molecular mechanisms by which Aβ induces astrocyte activation and possibly exerts toxicity. In addition, PEA is able to reverse the downregulation of PPAR-α induced by Aβ, thus mitigating the overexpression of pro-inflammatory molecules and signals (Scuderi *et al.*, 2011).

Therefore, we explored the anti-inflammatory and neuroprotective effects of PEA in an *in vivo* model of AD. The present study also incorporates pharmacological experiments to test the hypothesis that PPAR-α was involved in the effects induced by PEA administration. To this purpose, we co-administered PEA with the GW6471 (N-((2S)-2-(((1Z)-1-methyl-3-oxo-3-(4-(trifluoromethyl)phenyl)prop-1-enyl)amino)-3-(4-(2-(5-methyl-2-phenyl-1,3-oxazol-4-yl)ethoxy) phenyl)propyl)propanamide), a PPAR-α antagonist. These experiments are much needed because PEA is currently clinically used for a condition other than AD. Moreover, its safety and tolerability in humans further demonstrate the translational value of this work.

MATERIALS AND METHODS

Animals

Male adult Sprague-Dawley rats (250-275 g at the time of surgery; Charles River Laboratories, Calco, Italy) were individually housed in a temperature-controlled (20 ± 1 °C) vivarium and maintained under a 12 h light/dark cycle (07 : 00 AM lights on - 07 : 00 PM lights off). Food and water were available *ad libitum*. All experiments were carried out during the light phase. All procedures were approved by the Italian Ministry of Health (Rome, Italy) and performed in compliance with the guidelines of the European Communities Council (2010/63/UE).

Surgical procedures

Rats (n = 9-12 for each experimental group) were anesthetized intraperitoneally (i.p.) with sodium pentobarbital (50 mg/kg), placed in a stereotaxic frame and unilaterally inoculated with human $A\beta_{(1-42)}$ (Tocris Cookson, Bristol, UK) into the dorsal hippocampus (coordinates relative to the bregma: AP: -3 mm, ML: ±2.2 mm, and DV: -2.8 mm) (Paxinos *et al.*, 2007). The coordinates and dose of $A\beta_{(1-42)}$ were chosen according to literature and the results of a series of pilot experiments (Durán-González *et al.*, 2013). The peptide was dissolved in artificial cerebral-spinal liquid (aCSF) to the concentration of 2 μg/μl. Fibrillar amyloid was formed by incubation at least for 24 h at +37 °C (De Felice *et al.*, 2008). A volume of 2.5 μl was injected using a microdialysis pump, keeping the flow to the constant value of 0.5 μl/min. Injection needles were left in place for additional 60 s to facilitate the diffusion of solution. Control rats underwent the same procedure and were inoculated with an equivalent volume of aCSF.

Drug treatment

PEA and GW6471 were both from Tocris (Bristol, UK). PEA and GW6471 were dissolved in saline : PEG : Tween-80 in a 90 : 5 : 5 ratio (v/v) (Sigma-Aldrich, Milan, Italy). Control rats were i.p. given an equivalent volume of the proper vehicle. Vehicle, PEA (10 mg/kg), GW6471 (2 mg/kg), or both drugs were i.p. administered once a day for seven consecutive days, starting from the day of the surgery. The doses were chosen according to literature and the results of a series of pilot experiments (Sheerin *et al.*, 2004; Kapoor *et al.*, 2010) (data not shown).

Biochemical evaluations

Tissue collection Twenty-eight days after surgery, rats were killed by decapitation. For immunoblotting, ELISA, and RT-PCR experiments, hippocampi were isolated and frozen using 2-methylbutane. We focused on the hippocampus, which is one of the brain areas earliest and most severely affected by AD. For morphological analysis, whole brains were frozen in 2-methylbutane and stored at -80 °C.

Reverse transcriptase-polymerase chain reaction

Total RNA was extracted from homogenized hippocampi ipsilateral to the injection site using the lysis reagent provided in NZY total RNA isolation kit (NZYTech, Lda., Lisbon, Portugal) according to the manufacturer's protocol. The extracted RNA was subjected to DNase I (NZYTech, Lda) treatment at +25 °C for 15 min and eluted in 30 μl of RNase-free water. The total RNA concentration was determined by Nanodrop 1000 spectrophotometer (Thermo-scientific, Rockford, IL, USA) and purity of sample was determined according to the 260/280 nm ratio. One microgram of RNA was reversed transcribed into complementary DNA (cDNA) using oligo(dT) and random primers included in the first-strand cDNA synthesis kit (NZYTech, Lda.); then RNA/DNA hybrids were digested with RNaseH from *E. coli*, according to the manufacturer's specifications. All PCR experiments were performed using supreme NZYTaq DNA polymerase (NZYTech, Lda.) with specific primers for *rattus norvegicus* GFAP (forward primer 5′-TGG CCA CCA GTA ACA TGC AA-3′ reverse primer 5′-CTC GAT GTC CAG GGC TAG CT-3′), S100β (forward primer 5′-TCA GGG AGA GAG GGT GAC AA-3′ reverse primer 5′-ACA CTC CCC ATC CCC ATC TT-3′), and GAPDH (forward primer 5′-GCG AGA TCC CGC TAA CAT CAA ATG G-3′ reverse primer 5′-GCC ATC CAC AGT CTT CTG AGT GGC-3′) sequences, with the latter used as a housekeeping gene.

Each PCR was preceded by incubation for 5 min at +95 °C to activate Taq-polymerase enzyme and followed by 7 min at +72 °C to finish the extension of amplified sequences.

PCR amplification products were separated on 1.5% agarose gel (BioRad Laboratories, Milan, Italy) stained with GelRed (Biotium Inc., Hayward, CA, USA), visualized by ultraviolet light, acquired by Versadoc (BioRad Laboratories) and analyzed by a densitometry computer programme (ImageJ software v1.44p, NIH, Bethesda, MD, USA).

Western blot

Western blot analyses were performed on rat-isolated hippocampal region ipsilateral to the injection site. Each portion was suspended in ice-cold hypotonic lysis buffer (tris/HCl pH 7.5

50 mM, NaCl 150 mM, ethylenediaminetetraacetic acid (EDTA) 1 mM, 1% triton X-100) supplemented with the proper protease inhibitor cocktail (PMSF 1 mM, aprotinin 10 μg/ml, leupeptin 0.1 mM, all from Sigma-Aldrich). After incubation for 40 min at +4 °C, homogenates were centrifuged at 14000 rpm for 15 min and the supernatant removed and stored in aliquots at -80 °C until use.

Equivalent amounts (50 μg) of each sample calculated by Bradford assay were resolved on 12% acrylamide SDS-PAGE precast gels (BioRad Laboratories). Proteins were transferred onto nitrocellulose. Membranes were blocked with 5% w/v no-fat dry milk powder in tris-buffered saline-tween 0.1% (TBS-T) for 1 h before overnight incubation at +4 °C with one of the following primary antibodies: rabbit anti-GFAP (1 : 50000, Abcam plc, Cambridge, UK), rabbit anti-S100β (1 : 1000, Epitomics, Burlingame, CA, USA), rabbit anti-iNOS (1 : 9000, Sigma-Aldrich), rabbit anti-COX-2 (1 : 1000, Cell Signaling Technology, Inc, Danvers, MA, USA), rabbit anti-β-actin (1 : 1500, Santa Cruz Biotechnology, Santa Cruz, CA, USA), rabbit anti- β-catenin (1 : 1000, Cell Signaling Technology, Inc), rabbit anti-BACE1 (1 : 1000, Abcam plc), anti-APP (1 : 1000, Cell Signaling Technology, Inc), rabbit anti-Dkk-1 (1 : 1000, Santa Cruz Biotechnology), rabbit anti-phospho-Gsκ-3β (1 : 1000, Cell Signaling Technology, Inc), rabbit anti-phospho-tau (p[Ser396]tau, 1 : 500, Novus Biologicals, Littleton, CO, USA), goat anti-tau (1 : 500, Santa Cruz Biotechnology, CA, USA). After being extensively washed in TBS-T, membranes were incubated for 1 h at +25 °C in the proper secondary horseradish peroxidase-conjugated antibodies (HRP-conjugated goat anti-rabbit IgG, 1 : 30000, Jackson Immunoresearch Europe, Suffolk, UK; HRP-conjugated rabbit anti-goat, 1 : 5000, Abcam plc). The immunocomplexes were visualized using an ECL kit (Amersham, Bucks, UK). Protein expression was quantified by densitometric scanning of the X-ray films with a GS 700 Imaging Densitometer (Bio-Rad laboratories) and a computer programme (ImageJ software).

Enzyme-linked immunosorbent assay

Hippocampal regions ipsilateral to the injection site were homogenized in lysis buffer (tris-HCl pH 7.5 20 mM, NaCl 137 mM, NP40 1%, glycerol 10%, sodium orthovanadate 0.5 mM) containing a mix of protease inhibitors (PMSF 1 mM, aprotinin 10 μg/ml, leupeptin 1 μg/ml, all from Sigma-Aldrich), in a 5 : 1 ratio μl lysis buffer/mg tissue by a mechanical homogenization potter. The homogenates were centrifuged at 14000 rpm, at +4 °C for 30 min and the supernatant was immediately used for the assay. The concentrations of S100β, TNF-α, and IL-1β were measured with commercially available ELISA kit (Invitrogen, Milan, Italy) according to the procedures recommended by the manufacturer. The intensity of the colored product, recorded at

450 nm with an Epoch Microplate Spectrophotometer (BioTek Instruments, Inc., Winooski, VT, USA), was directly proportional to the concentration of cytokines in the sample.

Immunofluorescence

Extracted brains were transversely cut using a cryostat to obtain coronal sections containing the hippocampal region. Sections (10-μm thickness) were fixed for 4 min at room temperature with 4% paraformaldeyde (Merck, Darmstadt, Germany) in 0.12 M phosphate buffer, pH 7.4. After quenching auto-fluorescence with 0.05 M ammonium chloride, and saturation of non-specific sites with 3% normal donkey serum (BioCell Research Laboratories, Newport Beach, CA, USA), sections were incubated overnight at +4 °C with 0.5% albumin bovine serum/0.25% triton-TBS solution containing one of the following primary antibodies: rabbit anti-GFAP (1 : 500; Abcam plc), rabbit anti-S100β (1 : 1000, BD Transduction Laboratories, San Jose, CA, USA), mouse anti-MAP2 (1 : 250, Novus Biologicals). After washing, the sections were incubated with donkey Cy3-labeled anti-rabbit (or anti-mouse) IgG (1 : 400; Jackson ImmunoResearch Laboratories, West Grove, PA, USA). Negative controls were performed substituting specific Igs with an equivalent amount of non-specific Igs and omitting primary antibodies. After a final wash with PBS, slides were mounted with Vectashield mounting medium, containing DAPI for nuclear staining (Vector Laboratories, Burlingame, CA, USA). Pictures were taken using a fluorescence microscope (Eclipse E600; Nikon Instruments S.p.A., Firenze, Italy). Analysis of signal intensity was measured semi-quantitatively in each slice as optical density (OD) and considering the averaged OD of non-immunoreactive regions of the brain for background normalization using a specific computer program (ImageJ software). Since many variables affect the staining intensity of a tissue section, during the acquisition of images, we set the same values of gain and exposure for each channel.

Morris water maze test (MWM)

Task procedures Eighteen days after surgery, rats were handled 1 min per day for three consecutive days before training on the MWM task. The maze, located in a room containing several visual cues, was a circular tank (1.83 m in diameter and 0.58 m in height) filled with water (+23-24 °C) to a depth of 20 cm. During the spatial training and reversal learning, a hidden transparent Perspex platform (20-25 cm) was submerged 2.5 cm below the surface of the water in the northwest quadrant of the maze. The experiments were performed according to the procedure previously described (Koistinaho *et al.*, 2001; Campolongo *et al.*, 2013).

Spatial training (acquisition) Days 1-3. Rats were given a daily training session of four trials (60 s each one) for three consecutive days. On each trial, the animal was placed in the tank facing the wall at one of the four designated start positions and allowed to escape onto the hidden platform. If an animal failed to find the platform within 60 s during the first day of the training, it was manually guided to the platform. The rat was allowed to remain on the platform for 10 s and was then placed into a holding cage for 25 s until the start of the next trial. The time each animal spent to reach the platform was recorded as the escape latency.

Probe (memory retention) Day 4. The retention of the spatial training was assessed 24 h after the last training session. At the probe test, the platform was removed and rats were returned to the water maze for a 60 s trial. The parameter measured was the time spent by rats to reach the position where the platform was previously located (escape latency).

Reversal learning Day 5. Rats were given a single training session of five trials (60 s each one); the platform was placed into the quadrant on the opposite side where the platform was previously located. On each trial, the animal was placed in the tank facing the wall at one of the four designated start positions and allowed to escape onto the hidden platform. If an animal failed to find the platform within 60 s during the first trial, it was manually guided to the platform. The rat was allowed to remain on the platform for 10 s and was then placed into a holding cage for 15 s until the start of the next trial. The time each animal spent to reach the platform was recorded as the escape latency.

Behavioral data from the acquisition, probe, and reversal learning were acquired and analyzed using an automated video-tracking system (Smart, Panlab, Harvard Apparatus, Cornellà (Barcelona, Spain). The escape latency for the spatial training and reversal learning working memory, and the amount of time rats spent in the target zone in the probe test were analyzed.

Statistics

Analysis was performed using GraphPad Prism version 4.0 (GraphPad Software, San Diego, CA, USA). Data were analyzed by one or two-way analysis of variance and multiple comparisons were performed using the Bonferroni's *post hoc* test, when applicable. Data are shown as mean ± standard error of the mean (SEM) as specified in the figure legends. Differences between mean values were considered statistically significant when $p < 0.05$.

RESULTS

PEA counteracts Aβ-induced reactive gliosis

Gliosis is a common pathological process after brain injury and neurodegenerative disorders such as AD (Verkhratsky and Parpura, 2010; Verkhratsky *et al.*, 2012). On the basis of these evidences, we decided to investigate the possible modifications induced by the intrahippocampal inoculation of $A\beta_{(1-42)}$ and the potential beneficial effect of systemic administration of PEA. First, we studied the transcription and expression of the GFAP protein, which is considered one of the most important markers of astrocyte activation. Indeed, GFAP plays a role in mediating most of the signals involved in morphology and functional alterations observed during astrocyte activation (Verkhratsky and Butt, 2007). Immunofluorescence analysis of the hippocampal CA3 area ipsilateral to the injection site revealed that the levels of GFAP were significantly different between the vehicle-inoculated and Aβ-inoculated rats (Figure 1a, b). In fact, we observed an evident increase in the GFAP intensity, and astrocytes show stellate shape and multiple branched processes, which are typical of activated astrocytes (Figure 1b). Such effect was counteracted by systemic treatment with PEA. Indeed, GFAP immunopositivity was decreased in PEA-treated animals, and the shape of astrocytes resembles the one seen in control animals (Figure 1c). Further, the co-administration of PEA with GW6471, a selective PPAR-α antagonist, completely abolished PEA-induced effect (Figure 1d, f).

In line with this observation, results from RT-PCR and western blot experiments, performed in homogenates of hippocampi ipsilateral to the injection site, revealed that both transcription ($p < 0.05$) and expression ($p < 0.05$) of GFAP were significantly higher in Aβ-injected rats than in vehicle-injected rats (Figure 1g-j). Moreover, PEA significantly reduced the Aβ-induced GFAP induction in a PPAR-α-dependent manner (Figure 1g-j).

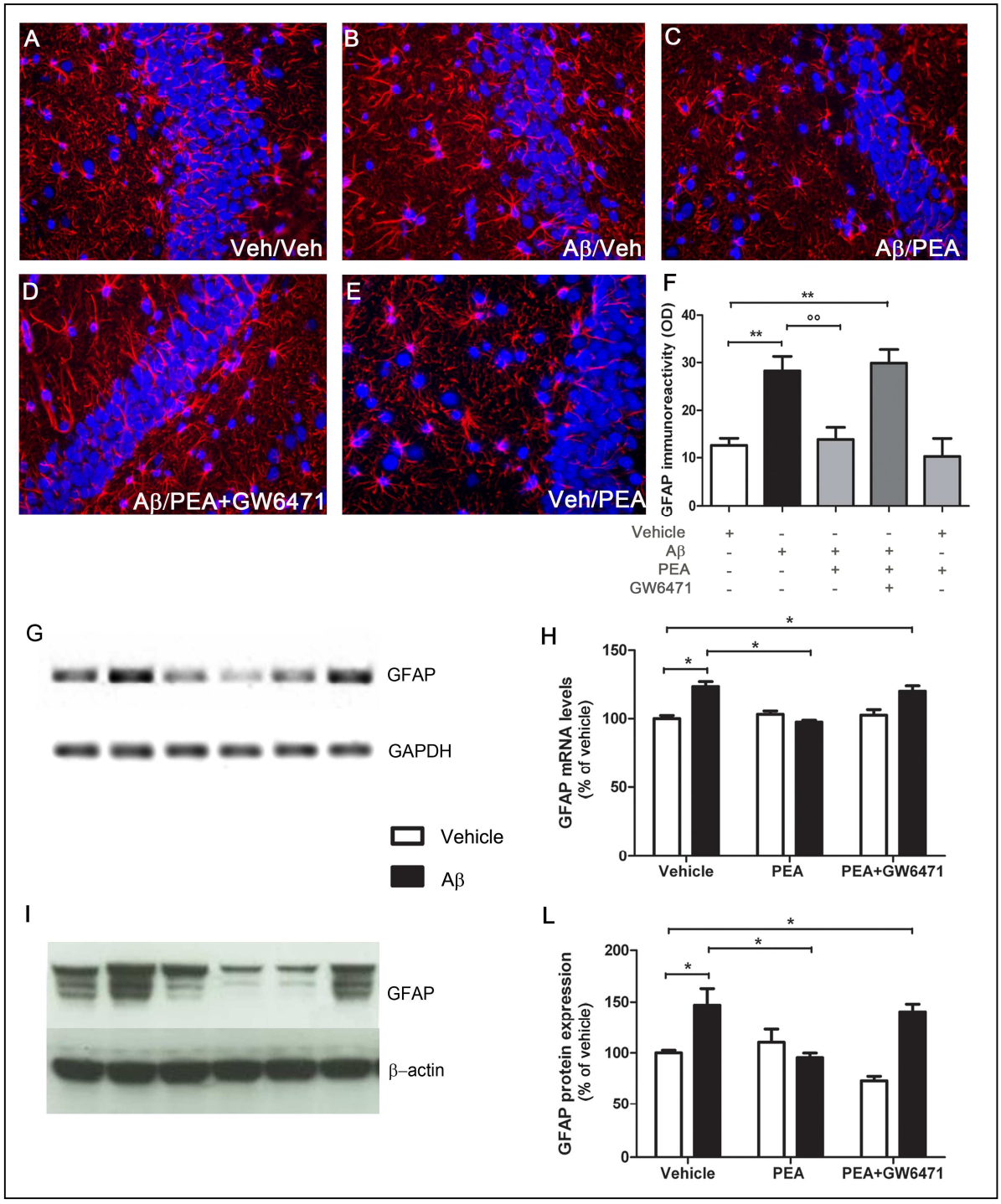

Figure 1 PEA effect on Aβ-induced GFAP protein transcription and expression
(a-e) Representative fluorescent photomicrographs (20X magnification) of GFAP immunostaining (red) in the CA3 region of hippocampi ipsilateral to vehicle or $A\beta_{(1-42)}$ injection obtained from rats i.p. treated with vehicle, PEA (10 mg/kg), GW6471 (2 mg/kg), or both drugs. Nuclei were stained with DAPI (blue). **(f)** Data obtained by the semiquantitative analysis of the OD of GFAP immunostaining. Data are expressed in arbitrary units as means ± SEM (** $p < 0.01$). **(g)** Results of GFAP RT-PCR amplification and **(h)** densitometric analysis of corresponding bands. Data were generated normalizing to GAPDH (* $p < 0.05$). **(i)** Representative western blots for GFAP protein from hippocampi ipsilateral to the injection site. **(j)** Densitometric analyses normalized to β-actin loading controls (* $p < 0.05$). Statistical analysis was performed by one-way **(f)** or two-way **(h, j)** ANOVA followed by Bonferroni multiple comparison test. Results presented as means ± SEM of five experiments.

Another mediator crucially involved in the reactive gliosis is the protein S100β. In physiological conditions, S100β behaves as a neurotrophin, promoting the growth of neuritis, stimulating astrocyte proliferation, and increasing free calcium concentrations in both neurons and astrocytes. On the contrary, in case of brain damage, large amounts of S100β are being passively released mainly from astrocytes to diffuse into CSF and blood brain, participating in the amplification of the inflammatory response by further activating microglia and astrocytes (Donato and Heizmann, 2010; Steiner *et al.*, 2011). Experiments revealed increased concentrations of S100β mRNA and protein, as well as increased densities of S100β-positive astrocytes, in Aβ-injected rats in comparison to the vehicle-injected rats (Figure 2). In particular, immunofluorescence analysis of the CA3 area of the hippocampi ipsilateral to the injection site revealed higher levels of S100β after $A\beta_{(1-42)}$ insult; PEA was able to prevent such increase through its interaction with PPAR-α (Figure 2a-f). RT-PCR, western blot, and ELISA experiments were performed to investigate S100β mRNA, protein expression, and release in hippocampal homogenates. Results indicated an upregulation of both transcription ($p < 0.01$) and expression ($p < 0.01$), as well as an increased release ($p < 0.01$) of S100β in Aβ-injected versus vehicle-injected rats. In these conditions, we observed that PEA controlled the Aβ-induced elevation of S100β content in a PPAR-α-dependent manner. In fact, GW6471, the selective antagonist for this receptor, completely abolished the effects of PEA (Figure 2g-k).

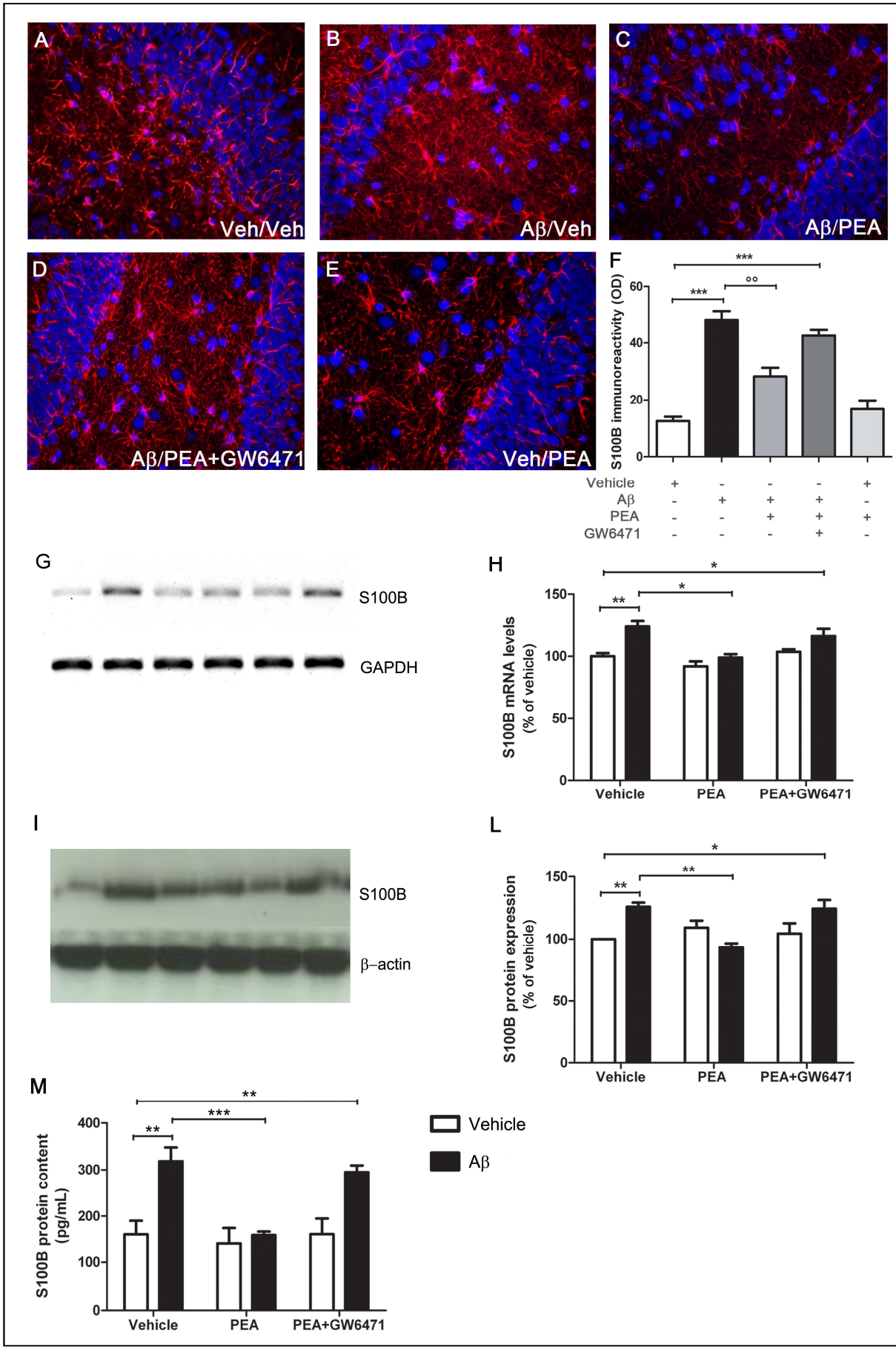
A
Veh/Veh
B
Aβ/Veh
C
Aβ/PEA
D
Aβ/PEA+GW6471
E
Veh/PEA
F
S100B immunoreactivity (OD)
***
°°
Vehicle
Aβ
PEA
GW6471
G
S100B
GAPDH
H
S100B mRNA levels (% of vehicle)
Vehicle
PEA
PEA+GW6471
I
S100B
β–actin
L
S100B protein expression (% of vehicle)
M
S100B protein content (pg/mL)
Vehicle
Aβ

Figure 2 Effect of PEA on Aβ-induced S100β protein transcription, expression, and release
(a-e) Representative fluorescent photomicrographs (20X magnification) of S100β immunostaining (red) in the CA3 region of hippocampi ipsilateral to vehicle- or $A\beta_{(1-42)}$ injection site obtained from rats i.p. treated with vehicle, PEA (10 mg/kg), GW6471 (2 mg/kg), or both drugs. Nuclei were stained with DAPI (blue). **(f)** Data obtained by the semiquantitative analysis of OD of S100β immunostaining. Data are expressed in arbitrary units as means ± SEM (*** $p < 0.001$; ** $p < 0.01$). **(g)** Results of S100β RT-PCR amplification and **(h)** densitometric analysis of corresponding bands. Data were generated normalizing to GAPDH (** $p < 0.01$; * $p < 0.05$). **(i)** Representative western blots for S100β protein from hippocampi ipsilateral to the injection site. **(j)** Densitometric analyses normalized to β-actin loading controls (** $p < 0.01$; * $p < 0.05$). **(k)** Measurement of S100β release by ELISA in homogenate hippocampi ipsilateral to the Aβ injection site (*** $p < 0.001$; ** $p < 0.01$). Statistical analysis was performed by one-way **(f)** or two-way **(h-k)** ANOVA followed by Bonferroni multiple comparison test. Results presented as means ± SEM of five experiments.

As mentioned before, a protracted glial activation is accompanied with the release of several pro-inflammatory mediators that can establish a self-sustaining detrimental cycle that leads to neuronal death, and thus to cognitive dysfunctions (Sastre *et al.*, 2006). Among these molecules, IL-1β has been particularly linked to the pathophysiology of AD, as IL-1β is involved in neurodegeneration (Griffin, 2011; Ben Menachem-Zidon *et al.*, 2014). Aβ stimulates IL-1β production which leads to a further increase in glial activation and still more expression of IL-1β. IL-1β is able to increase neuronal tau expression and tau hyperphosphorylation (Mrak, 2009), to upregulate the complex cdk5/p35, which plays a pivotal role in CNS development, and to induce inducible nitric oxide synthase (iNOS) with concomitant production of nitric oxide (NO) (Rojo *et al.*, 2008).

AD chronic neuroinflammation also shows the upregulation of TNF-α expression (Hallenbeck, 2010; Frankola *et al.*, 2011) mainly involved in the induction of inflammatory tissue damage and neuronal death (Rojo *et al.*, 2008). This neuroinflammatory stimulation is further characterized by activation of the complement cascade and induction of the prostanoid-generating enzyme cyclooxygenase-2 (COX-2) (Koistinaho *et al.*, 2011), elevated in many neuropathological conditions (Frank-Cannon *et al.*, 2009). This inducible enzyme causes neurodegeneration in several ways, including the generation of free radicals (Minghetti, 2004).

Our results demonstrated that $A\beta_{(1-42)}$ injection induced the upregulation of iNOS ($p < 0.01$) and COX-2 ($p < 0.01$) in comparison with vehicle-injected rats. PEA blunted $A\beta_{(1-42)}$ effect ($p < 0.01$) and the administration of GW6471 revealed that PPAR-α is partially involved in mediating PEA action ($p < 0.05$) (Figure 3a-c).

Similar findings were obtained when ELISA experiments were performed to quantify the release of IL-1β and TNF-α in homogenates of hippocampi ipsilateral to the injection site. We found a marked release of both these pro-inflammatory cytokines, and PEA, once again, was able to control their release. The administration of the selective PPAR-α antagonist, GW6471, completely abolished PEA effects, indicating the significant involvement of such a receptor (Figure 3d, e). These data clearly show that Aβ peptide causes a marked activation of glial cells, starting the so-called reactive gliosis process, which is efficaciously counteracted by PEA treatment. In addition, these data confirmed a clear involvement of PPAR-α receptor in mediating the effect of PEA.

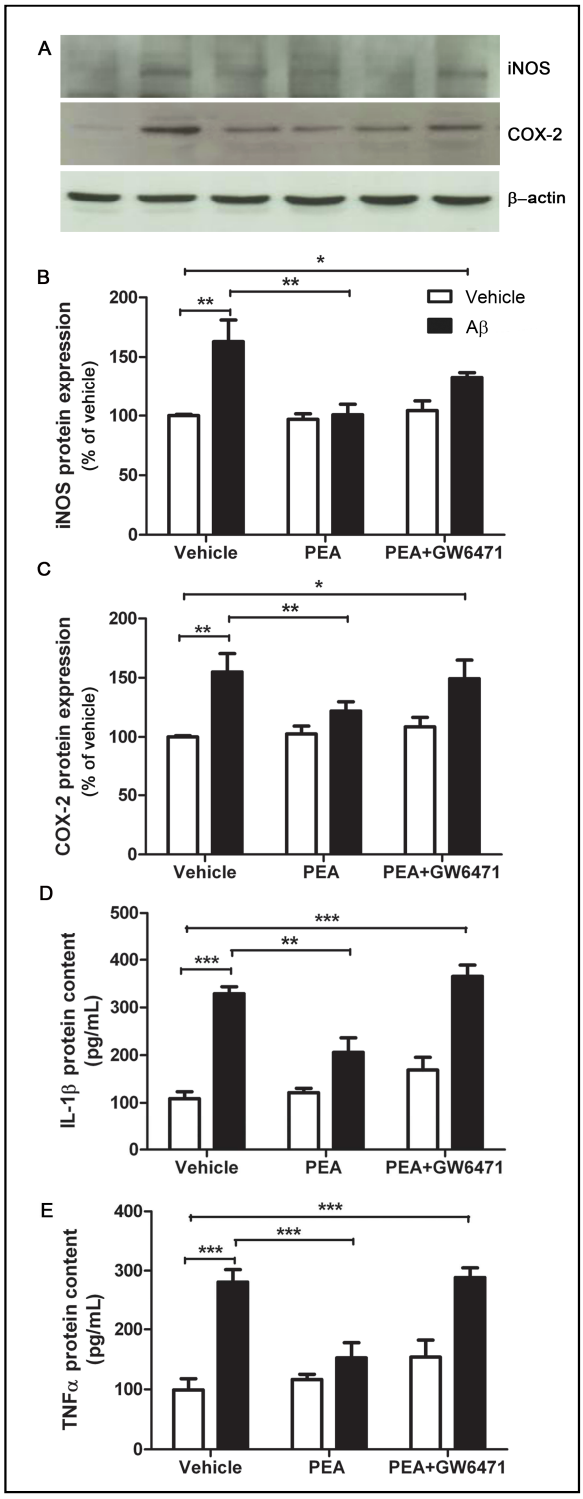

Figure 3 Effect of PEA on expression and release of inflammatory mediators induced by Aβ injection

(a) Representative western blots for iNOS and COX-2 proteins from hippocampi ipsilateral to the injection site and **(b, c)** relative densitometric analyses normalized to β-actin loading controls (** $p < 0.01$; * $p < 0.05$). Measurement of IL-1β **(d)** and TNF-α **(e)** release by ELISA in homogenate hippocampi ipsilateral to the Aβ injection site (*** $p < 0.001$; ** $p < 0.01$). Statistical analysis was performed by two-way ANOVA followed by Bonferroni multiple comparison test. Results presented as means ± SEM of five experiments.

PEA effects on amyloidogenic pathway

β-secretase (BACE1) is a type I transmembrane aspartyl protease. It is predominantly expressed in neuronal cells, and localizes to acidic compartments in the secretory pathway where the production of Aβ occurs. Indeed, Aβ generation is abolished in BACE1 knockout mice (Luo *et al.*, 2001), whereas Aβ formation is increased by the overexpression of BACE1 (Cole and Vassa, 2008). Cleavage of APP by BACE1 is the first step in a process essential for Aβ generation, and several studies demonstrated how BACE1 expression is able to control the dynamics of β-secretase activity in processing APP to generate Aβ (Li *et al*., 2006). Moreover, *in vitro* studies demonstrated that the AD-associated Swedish mutant APP is associated with increased BACE1 activity developing the phenotypes typical of axonal transport defects because of an enhanced cleavage of APP (Rodrigues *et al.*, 2012). Indeed, the regulation of APP transcription might play an important role in AD susceptibility. Several studies identified higher levels of APP mRNA in AD brains (Theuns and Van Broeckhoven, 2000), and highlighted that increased expression of APP correlates with Aβ deposition in brain with severe head injury (Gentleman *et al.*, 1993). Given the importance of these proteins in AD pathogenesis and progression, western blot analysis for BACE1 and APP was performed. Our results showed a significant BACE1 and APP protein expression increase ($p < 0.05$ and $p < 0.01$, respectively) in Aβ-injected rat compared with controls (Figure 4a), as confirmed by relative densitometric analysis (Figure 4b, c). This expression is statistically attenuated by PEA treatment ($p < 0.05$ and $p < 0.01$, respectively, for BACE1 and APP expression), when compared with the vehicle-treated group. The selective PPAR-α antagonist, GW6471, abolished PEA effects.

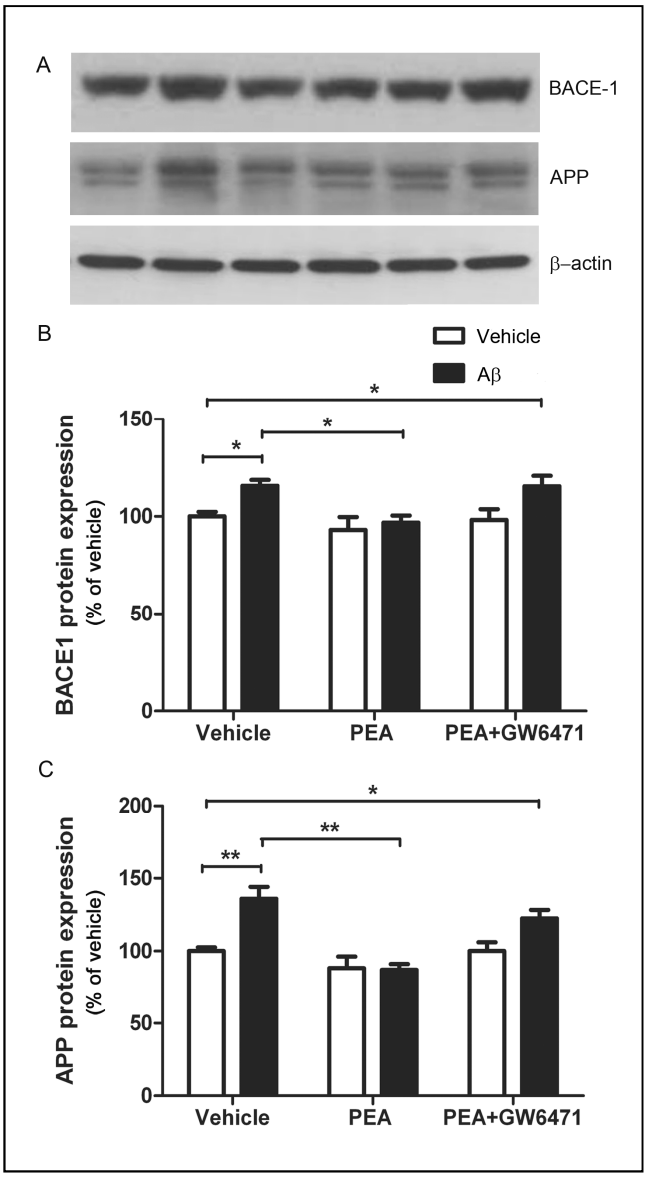

Figure 4 Effect of PEA on amyloidogenic pathway
(a) Representative western blots for BACE 1 and APP proteins from hippocampi ipsilateral to the injection site and **(b, c)** relative densitometric analyses normalized to β-actin loading controls (** $p < 0.01$; * $p < 0.05$). Statistical analysis was performed by two-way ANOVA followed by Bonferroni multiple comparison test. Results presented as means ± SEM of five experiments.

PEA rescues Wnt pathway thus modulating tau protein phosphorylation

The irregular phosphorylation of the microtubule-associated protein tau is a prominent aspect of AD. It is now established that glycogen synthase kinase 3β (Gsκ-3β) is involved in normal and pathological tau phosphorylation. Indeed, activation of the canonical Wnt pathway leads to two main molecular mechanisms represented by the inhibition of Gsκ-3β and the relative accumulation/degradation of β-catenin in the cytoplasm (Caricasole *et al.*, 2003). The latter signaling pathway has been found to be dysregulated in the AD brain (Inestrosa *et al.*, 2012). We have already demonstrated that S100β is able to induce the expression of Dickopff-1 (Dkk-1), causing tau protein hyperphosphorylation (Esposito *et al.*, 2008). In addition, recent data demonstrated the increased expression of Dkk-1 in brains of AD patients suggesting that dysfunction of the Wnt signaling could contribute to AD pathology (Zenzmaier *et al.*, 2009).

Utilizing western blot analysis, we evaluated the expression of the main proteins involved in the canonical Wnt pathway. Results of immunoblot experiments and their relative densitometric analysis are illustrated in Figure 5. Aβ-injected rats showed increased concentrations of Dkk-1 in comparison with vehicle-injected rats ($p < 0.05$). Under these conditions, PEA was able to control Dkk-1 expression in a PPAR-α-dependent manner (Figure 5b). This set of experiments also revealed a marked alteration in the levels of the Wnt pathway proteins. In fact, we found a significant increase in Gsκ-3β expression in Aβ-injected rats in comparison with vehicle-injected rats ($p < 0.001$). Such effect was totally abolished by the pharmacological treatment with PEA ($p < 0.001$) through a mechanism which partially involves PPAR-α (Figure 5c). In parallel, we observed a marked decrease of β-catenin protein in the hippocampus of Aβ-injected rats in comparison with vehicle-injected rats ($p < 0.01$). Physiological levels of β-catenin were founded in Aβ-injected rats systemically treated with PEA ($p < 0.05$) demonstrating, once again, the ability of this compound to counteract the damage induced by peptide inoculation. Co-administration of PEA with GW6471 attenuated such effect, demonstrating that PEA interacts with PPAR-α to achieve the observed effects (Figure 5d). Growing evidence indicates that disrupted Wnt signaling may be a direct link between Aβ toxicity and tau hyperphosphorylation, ultimately leading to neuronal degeneration. For this reason, we performed western blot experiments using a specific primary antibody able to bind tau protein on the phospho-Ser396, which is recognized to be the phosphorylation site mainly related to neurofibrillary pathology in AD brain (Cavallini *et al.*, 2013). The expression of phosphorylated tau (p-[Ser396]) was normalized for total tau content using a polyclonal primary antibody. Results highlighted a significant increase in the p-tau/tau ratio after $A\beta_{(1–42)}$ injection ($p < 0.01$), normalized by PEA ($p < 0.05$) in a manner partially dependent on its PPAR-α interaction (Figure 5e). Collectively, these data support a pivotal role of

PEA in modulating the Aβ-induced alterations in the Wnt pathway and normalizing the physiological level of phosphorylated tau protein.

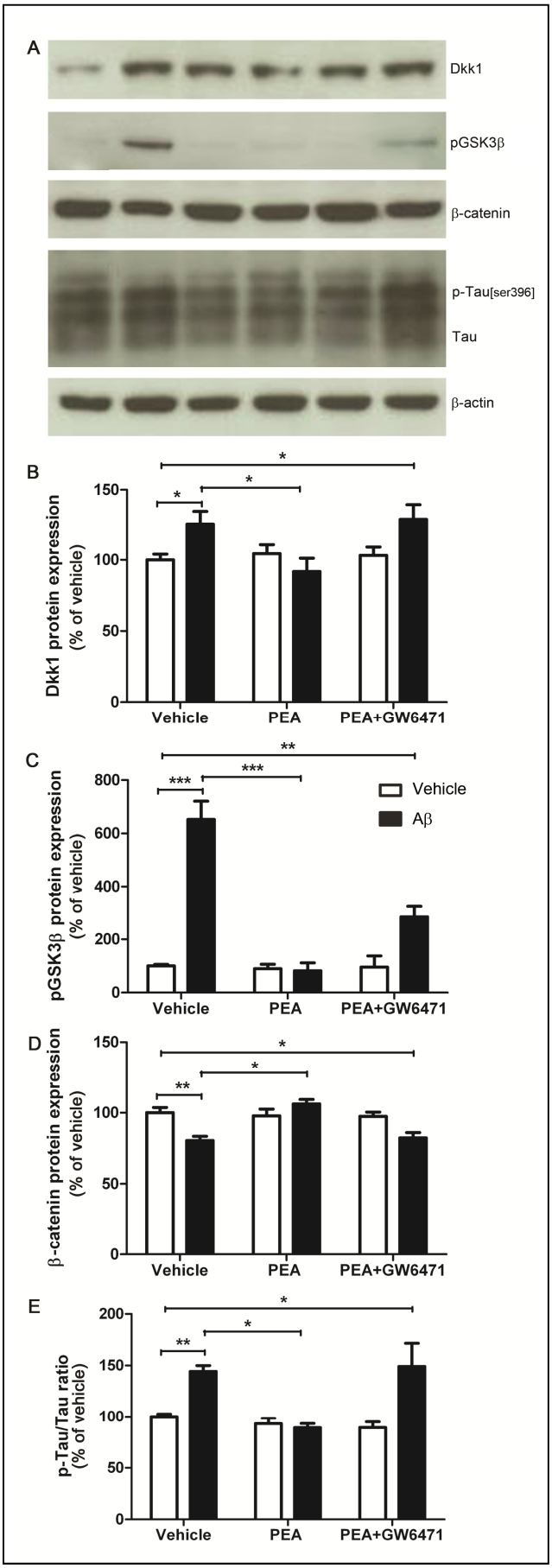
A
Dkk1
pGSK3β
β-catenin
p-Tau[ser396]
Tau
β-actin
B
Dkk1 protein expression (% of vehicle)
150
100
50
0
Vehicle
PEA
PEA+GW6471
C
pGSK3β protein expression (% of vehicle)
800
600
400
200
0
Vehicle
Aβ
D
β-catenin protein expression (% of vehicle)
E
p-Tau/Tau ratio (% of vehicle)
200

Figure 5 Effects of PEA on the Wnt pathway and tau protein phosphorylation
(a) Representative western blots from hippocampal proteins probed with the indicated antibodies. **(b-e)** Relative densitometric analyses. Data were generated normalizing proteins of interest to β-actin loading controls (*** $p < 0.001$; ** $p < 0.01$; * $p < 0.05$). Statistical analysis was performed by two-way ANOVA followed by Bonferroni multiple comparison test. Results presented as means ± SEM of five experiments.

PEA effects on neuronal integrity

To investigate the effects of $A\beta_{(1-42)}$ injection on neuronal survival, we measured the expression of the microtubule-associated protein 2 (MAP2) by immunofluorescence analysis. MAP2 is one of the main cytoskeletal proteins in neurons; in mammalian nervous system, MAP2 regulates microtubule dynamics, and it plays an important role in neurite outgrowth and dendrite development (Hirokawa, 1994). Morphologically, the reduction in neurite outgrowth is observed in neural cells from AD patients. Indeed, recent studies demonstrated that MAP2 expression pattern was significantly reduced compared with the control group, highlighting that mature neurons are significantly decreased in the patients' group (Dehghani *et al.*, 2013). In our study, results from MAP2-stained hippocampi indicated that $A\beta_{(1-42)}$ injection caused a severe depletion of neurons, especially in the dentate gyrus, compared with vehicle-injected rats ($p < 0.05$). By means of MAP2 staining and relative quantification of immunopositive cells, we observed that PEA treatment significantly reduced Aβ-provoked neuronal loss ($p < 0.05$) through its interaction with PPAR-α ($p < 0.05$) (Figure 6a-f). Moreover, our results indicate that PEA was able to exert an important neuroprotective effect through PPAR-α involvement.

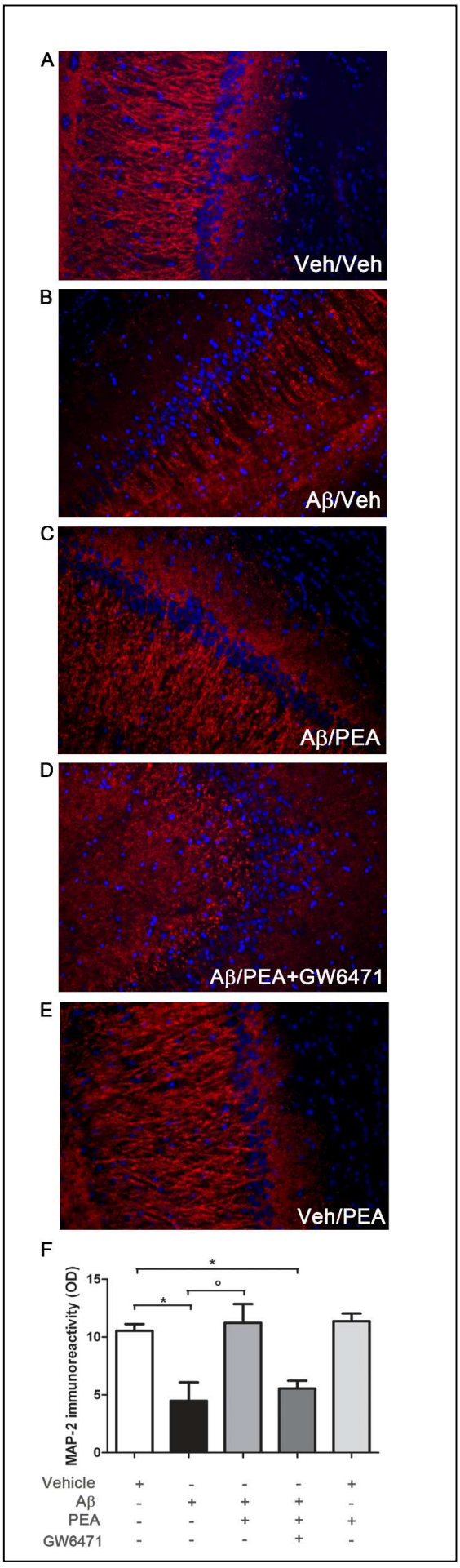
A
Veh/Veh
B
Aβ/Veh
C
Aβ/PEA
D
Aβ/PEA+GW6471
E
Veh/PEA
F
MAP-2 immunoreactivity (OD)
15
10
5
0
*
*
°
Vehicle + - - - +
Aβ - + + + -
PEA - - + + +
GW6471 - - - + -

Figure 6 PEA effect on neuronal integrity

(a-e) Representative fluorescent photomicrographs (20X magnification) of MAP2 immunostaining (red) in the CA3 region of hippocampi ipsilateral to vehicle or $A\beta_{(1-42)}$ injection site obtained from rats i.p. treated with vehicle, PEA (10 mg/kg), GW6471 (2 mg/kg), or both drugs. Nuclei were stained with DAPI (blue). **(f)** Data obtained by the semiquantitative analysis of the optical density (OD) of MAP2 immunostaining. Data are expressed in arbitrary units as means ± SEM of five experiments (* $p < 0.01$). Statistical analysis was performed by one-way ANOVA followed by Bonferroni multiple comparison test.

PEA rescues the Aβ-induced deficits in the reversal learning phase of the Morris water maze

To examine whether systemic treatment with PEA can result in recovery from memory deficit induced by hippocampal $A\beta_{(1-42)}$ infusion, the MWM task was carried out 3 weeks after surgery, as illustrated in the flow chart (Figure 7a). Rat weight was monitored every day until the beginning of behavioral tests. No alterations were observed (data not shown).

All groups were trained for three consecutive days on spatial training procedure of four trials session per day. During these sessions, rats had to learn to localize a hidden platform set always in a fixed place. All rats, regardless of any treatment, were equally able to acquire the cognitive task. Indeed, ANOVA for repeated measures (with trials as repeated measures) revealed a trial effect ($F_{(11,418)} = 35.031$; $p < 0.0001$) but did not reveal significant differences among groups in the acquisition performances ($F_{(11,418)} = 1.026$; $p = 0.422$) (Figure 7b).

The effect of $A\beta_{(1-42)}$ inoculation on long-term memory was analyzed 24 h after the last acquisition day on a single 60 s probe trial. During the probe test, the platform was removed from the water maze tank and the time spent in the target quadrant where the platform was previously located was measured as a parameter of long-term memory retention. ANOVA test revealed significant differences neither for the central treatment ($F_{(1,38)} = 0.506$; $p = 0.481$) nor for the peripheral treatment ($F_{(1,38)} = 0.464$; $p = 0.499$) nor for the interaction between central and peripheral treatments ($F_{(1,38)} = 0.623$; $p = 0.435$) showing that $A\beta_{(1-42)}$ did not alter long-term memory functions (Figure 7c).

On day 5, rats were tested for reversal learning capabilities during a unique session of five trials. The hidden platform was relocated into the quadrant on the opposite side where the platform was previously positioned, thus rats had to quickly understand the new experimental setting, and consequently to remodel their escape strategy. Figure 7d shows the effect of PEA administration on reversal learning performances during the first trial. ANOVA revealed a statistically significant interaction among treatments ($F_{(1,38)} = 10.278$; $p = 0.003$). *Post hoc* comparisons revealed a statistically significant difference between Aβ/vehicle (Veh) versus Veh/Veh, and Aβ/Veh versus Aβ/PEA animals ($p < 0.05$), thus showing that Aβ-injected rats were impaired in the fast adjustment to a change in the platform location compared with the vehicle-injected animals. Interestingly, we found that PEA administration statistically prevented the memory-impairing effect induced by Aβ ($p < 0.05$) (Figure 7d). No statistically significant differences were found among groups in the escape latency during trials 2-5 ($F_{(3,114)} = 1.36$; $p = 0.26$).

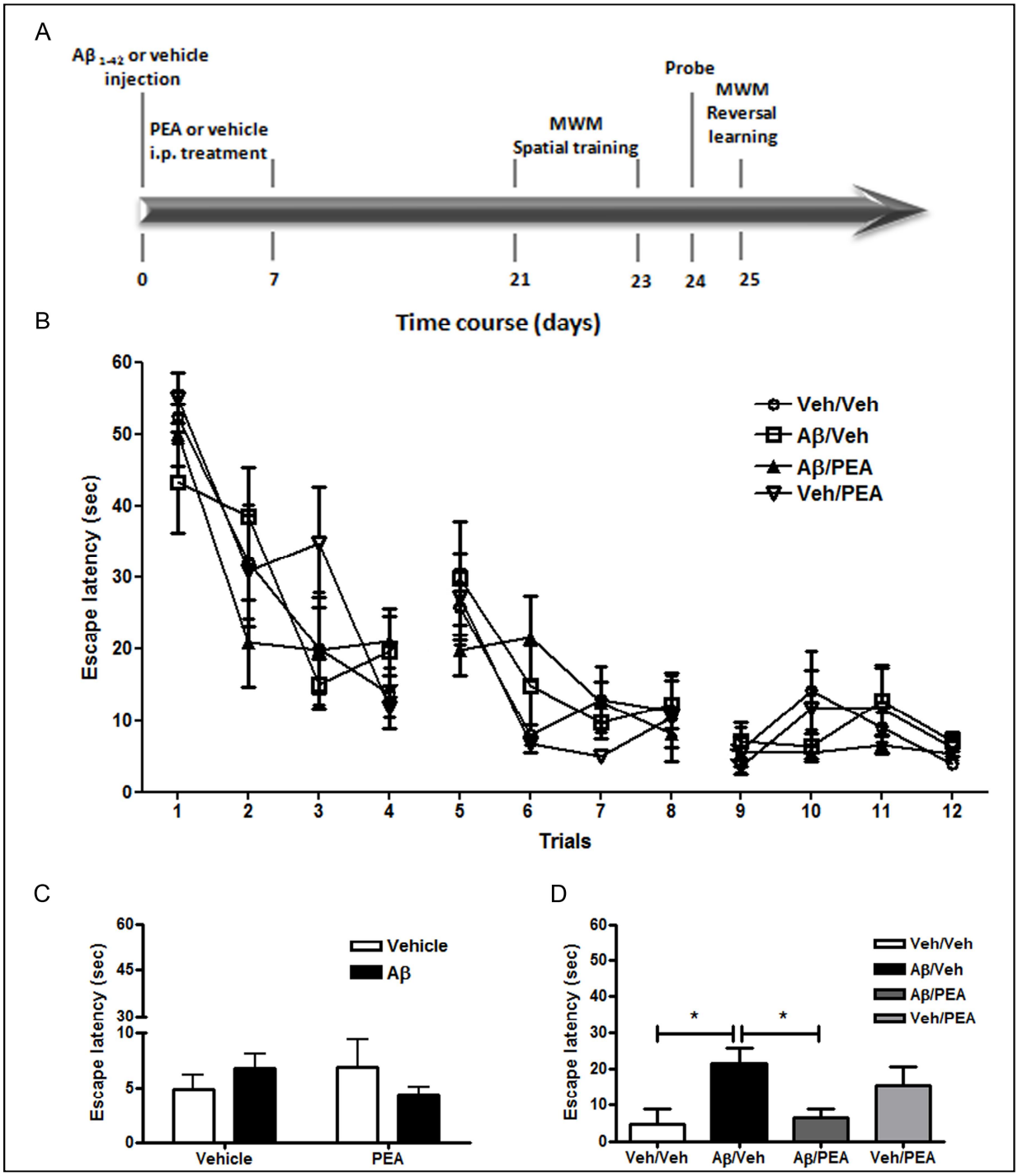

Figure 7 PEA rescues the Aβ-induced deficits in the reversal learning phase of the MWM
(a) Diagram of the experimental design. **(b)** Mean latency (seconds) for finding the escape platform during the spatial training. No significant differences were detected among all groups. **(c)** Mean latency (seconds) to reach the quadrant where the platform was located during the acquisition. No significant differences were detected among all groups. **(d)** Mean latency (seconds) for finding the escape platform during the reversal learning. Aβ/Veh rats showed longer escape latency versus Veh/Veh (* $p < 0.05$) and Aβ/PEA rats (* $p < 0.05$). Statistical analysis was performed by two-way ANOVA followed by Bonferroni multiple comparison test. Results are presented as means ± SEM.

DISCUSSION

The current results clearly demonstrate, for the first time in a rat model of AD, the ability of PEA to attenuate neuropathology by modulating neuroinflammation. This supports the view that astrocyte-unregulated activation can be considered an appropriate and promising therapeutic target for AD treatment. Furthermore, we demonstrated *in vivo* that PPAR-α is involved in mediating PEA beneficial effects. Such findings are new and of great interest because AD represents one of the major health concern, with a pressing need to develop new agents able to prevent or treat this disorder. Currently, an unresolved goal of preclinical investigation is to recognize tools capable to selectively regulate pro-inflammatory overactivation of neuroglia, restoring its physiological properties. The capacity of PEA to modulate the protective responses during inflammation suggests that endogenous PEA may be part of the complex homeostatic apparatus controlling the basal threshold of inflammatory processes. For this reason, we aimed to study the effects of PEA in a rat model of AD and here, we provide the first *in vivo* evidence that PEA exerts simultaneously anti-inflammatory and neuroprotective effects. It is commonly accepted that Aβ deposits can be associated with local cell loss, oxidative stress, and neuroglial activation. Glia possesses endogenous homeostatic mechanisms/molecules that can be seriously affected as a result of tissue damage. As a consequence, activated glial cells lose their physiological functions and acquire a reactive phenotype, characterized by profound morphological and functional alterations (Verkhratsky and Butt, 2007). Among these, GFAP and S100β overexpression is the best-known hallmark of activated astrocytes (O'Callaghan and Sriram, 2005; Donato *et al.*, 2013). In our model, we detected marked alteration of both these proteins. In fact, our results show that hippocampal astrocytes had significantly larger GFAP surface and express higher immunopositivity for S100β. Interestingly, PEA negatively modulated both GFAP and S100β transcription and expression, through its interaction with PPAR-α receptor.

In this study, we highlighted the existence of an inflammatory state induced by $A\beta_{(1-42)}$ infusion, as detected by the increased expression and release of the some key regulators of inflammatory process. Remarkably, PEA reduced iNOS and COX-2 overexpression and the enhanced release of IL-1β and TNF-α. Overall, these findings suggest that PEA exerts a key role in regulating astrogliosis and important functional changes, which contribute to disease progression.

Astrocytic cytokines may prompt the synthesis of acute-phase proteins such as APP (Blasko *et al.*, 2000) increasing the production of Aβ, regulating the cytokine cycle itself (Griffin,

2011), and inducing neuronal death (Mrak, 2009) responsible for the neurodegenerative consequences. Astrocytes could be induced by pro-inflammatory *stimuli* to promote the expression of BACE1, thus increasing the conversion of APP into the neurotoxic insoluble Aβ which could, in turn, induce astrocytes to produce more inflammation-like glial responses (Luterman *et al.*, 2000; Rojo *et al.*, 2008). Here, we demonstrate the ability of PEA to reduce the expression of BACE1 and APP, proteins directly involved in the amyloidogenic pathway. Collectively, these results identify PEA as a potential agent that is able to stop the detrimental cycle in which neuroinflammation and amyloidogenesis cooperate in sustaining the pathological state and the activation process of astrocytes.

Besides Aβ accumulation in SPs, the accumulation of hyperphosphorylated tau proteins that yield to NFTs formation is another hallmark characteristic in AD brain. Many data indicate that inhibition of the canonical Wnt pathway contributes to the pathophysiology of neurodegenerative disorders. Previous studies (Caricasole *et al.*, 2004) demonstrated the role for Dkk-1 in the mechanisms of Aβ toxicity. The ability of Aβ to induce the expression of Dkk-1 causes an increased activity of Gsκ-3β resulting in the hyperphosphorylation of tau protein. Here, we show, for the first time in an *in vivo* model, the ability of PEA to restore the alteration in the Wnt pathway caused by $A\beta_{(1-42)}$ hippocampal infusion, and to reduce phosphorylated tau protein overexpression. These findings indicate an important neuroprotective function for this endogenous compound and, once again, highlight an important involvement of PPAR-α. To deeply investigate the effect of PEA on neuronal circuitry, we decided to perform analysis on a neuronal marker, MAP2. Our findings showed an important role of PEA in restoring MAP2 expression that resulted reduced after Aβ injection, confirming its neuroprotective effect.

Finally, we decided to perform a MWM test to evaluate the effect of PEA on cognitive functioning. We found that $A\beta_{(1-42)}$-infused rats did not present deficits in the acquisition and in the long-term retention of the task. This is of translational value because clinical observations report that general and profound learning dysfunctions do not occur in the early course of AD. Importantly, we found that $A\beta_{(1-42)}$ infusion in the dorsal hippocampus results in reversal learning deficits, which could be partially compared to working-like memory in humans (Morris, 2001; Savonenko *et al.*, 2005). Impairment of working memory has been found to be a precocious marker for the future development of dementia (Sexton *et al.*, 2010; Espinosa *et al.*, 2013). Interestingly, PEA was able to restore the $A\beta_{(1-42)}$-induced deficits, suggesting its capability to improve reversal learning deficits.

The current investigation provides evidence that PEA, by activating PPAR-α, rescues altered molecular pathways as well as behavioral impairments that can mimic some early traits of

AD. Considering the extreme safety and tolerability of PEA in humans, our findings offer new opportunity in the already fruitless world of AD treatment.

SECTION III

Effects of ultra-micronized palmitoylethanolamide in a triple transgenic mice model of AD

INTRODUCTION

Alzheimer's disease (AD) is the most frequent cause of dementia in elderly that establishes a worldwide health problem. In the last year, around 47 million people worldwide were affected by dementia and, this number is expected to increase, plausibly reaching 131.5 million by 2050 (Prince *et al*., 2015). AD is a chronic condition first described by Alois Alzheimer in 1907, mainly characterized by a progressive cognitive impairment (Alzheimer, 1907). It is classically characterized by the presence of amyloid plaques (SPs), caused by aggregation of beta-amyloid (Aβ) deposits, and neurofibrillary tangles (NFTs) composed by hyperphosphorylated microtubule-binding protein tau (Selkoe, 2001). More recently, studies demonstrated that neuroinflammation is another key feature of the AD brains (McGeer and McGeer, 1999; Dandrea *et al*., 2001; Steardo Jr *et al.*, 2015). Altogether, these elements contribute to neuronal cell death and synaptic dysfunction, and, ultimately, to learning impairment and memory loss.

Neuroinflammation is guided by microglial cells, perivascular myeloid cells and reactive astrocytes surrounding SPs giving rise to the phenomenon of reactive gliosis (McGeer and McGeer, 2013; Osborn *et al*., 2016). This event has the initial aim of endogenous defence; however, the persistent activation establishes a self-fostering vicious cycle that contributes to AD progression (Steardo Jr *et al*., 2015). Reactive gliosis is characterized by the presence of reactive astrocytes that present an increase of glial fibrillary acid protein (GFAP) and hyperproduction of the neurotrophic factor S100β that, at higher non-physiological concentrations, becomes toxic. These activated cells become part of the inflammatory machinery, producing deleterious mediators like inducible nitric oxide synthase (iNOS), interleukin (IL)-1β and tumor necrosis factor (TNF)-α under control of the transcription factor NF-κB (Heneka *et al.*, 2010; Shih *et al.*, 2015). In turn, these factors trigger astrogliosis acting in an autocrine manner and, at the same time, are responsible for the death of neighbouring neurons thanks to the paracrine action (Burda and Sofroniew, 2014).

Tau protein is a microtubule-associated protein. In AD, it has been shown that tau is abnormally phosphorylated mainly by the glycogen synthase kinase-3β (Gsκ-3β), thus creating paired helical filaments (PHF-1) responsible for NFTs formation (Hanger *et al.*, 1992). Gsκ-3β enzymatic activity is regulated by its own phosphorylation. Indeed, Tyr216 phosphorylation

increases its activity. On the contrary, Ser9 phosphorylation operated by Akt-pathway inhibits its activity (Jope *et al.*, 2007). This pathway relates with neuronal survival, involving nuclear translocation of β-catenin by enhancing its transcriptional activity. Gsκ-3β inhibition, in addition to reducing tau phosphorylation, blocks β-catenin phosphorylation which can translocate into the nucleus and interact with DNA binding proteins inducing the transcription of pro-survival genes (Kim *et al*., 2013). By this manner, Akt/Gsκ-3β pathway promotes neuronal survival.

Reactive gliosis and tau iperphosphorylation are events closely related to the presence of Aβ accumulation. Indeed, Aβ increase, especially the more toxic $A\beta_{(1-42)}$ fragment, caused by an intense activity of the amyloidogenic pathway, plays a pivotal role in the progression of the disease (O'Brien and Wong, 2011).

At this point, we can affirm that each pathological event present in AD is somehow linked to all the others and, in order to better explore their relationship, the use of animal models is necessary. Among others, the triple transgenic model (3xTg-AD) of AD, harboring $PS1_{M146V}$, APP_{Swe}, and tau_{P301L} transgenes (Oddo *et al*., 2003b), helps researchers to address this issue.
These mice develop an age-dependent and progressive neuropathological phenotype that includes not only SPs and NFTs, with a penetrance of 100%, but even reactive gliosis in adulthood, detectable in the brain structures most impaired in AD, e.g. hippocampus, amygdala, and cerebral cortex (Oddo *et al*., 2003a; Griffith *et al.*, 2016). Nowadays, this model is one of the most used in pharmacological research (Romano *et al*., 2014; Kosaraju *et al*., 2016; Sawmiller *et al*., 2016).
With the aim of targeting neuroinflammation and neurodegeneration simultaneously, we decided to test the pharmacological effect of ultra-micronized palmitoylethanolamide (um-PEA) in 3xTg-AD mice. PEA is an endogenous lipidic mediator, compound produced from palmitic acid and ethanolamine reaction, largely present in the central nervous system (CNS) mainly due to astrocytic production (Cadas *et al*., 1997). It has been demonstrated that exogenous PEA crosses the BBB and reaches therapeutic concentrations in the brain (Artamonov *et al*., 1999), despite the presence of enzymes responsible for its hydrolysis, N-acylethanolamine acid amide hydrolase (NAAA) and fatty acid amide hydrolase (FAAH). Recently, um-PEA, a crystalline form on micrometric size of PEA was tested. In this form, the compound has smaller particle size, making it a useful alternative to improve its bioavailability (Petrosino *et al*., 2016). Several studies already shown neuroprotective, anti-neuroinflammatory, and analgesic properties of PEA (Petrosino and Di Marzo, 2016). In addition, recent studies performed by our group already shown the therapeutic efficacy obtained by PEA treatment in both *in vitro* and *in vivo* models of AD (Scuderi *et al*., 2011, 2012, 2014).

In this study, we wondered whether there are differences in efficacy of um-PEA treatment if administered before or after manifesting the pathological phenotype. For this reason, we started treatments at both 3 and 9 months of age.

Here, we decided to further explore pharmacological um-PEA properties in 3x-Tg-AD mice, investigating some of the main pathways involved in AD pathogenesis such as neuroinflammation, Akt/Gsκ-3β and amyloidogenic pathways. Moreover, we tested um-PEA treatment at 2 different months of ages, 6 and 12, with the aim to understand if there is any difference in compound efficacy whenever the administration is done in the pre-symptomatic or symptomatic stage.

MATERIALS AND METHODS

All procedures were conducted in conformity with the guidelines of the Italian Ministry of Health (D.L. 26/2014), and performed in compliance with the European Parliament directive 2010/63/EU.

Animals

A total of 48 male mice were tasted. Homozygous 6- and 12-month-old 3xTg-AD mice were compared to wild-type littermates (Non-Tg). The 3xTg-AD mice expressing APP_{swe}, $PS1_{M146V}$, and tau_{P301L} transgenes were genetically engineered by LaFerla and collaborators (Oddo, *et al.*, 2003a; 2003b). Polymerase chain reaction (PCR) after tail biopsies has been performed to confirm genotypes. All animals were maintained in controlled conditions (12-h light/12-h dark cycle, temperature +22°C, humidity 50% - 60%, fresh food and water *ad libitum*).

Chemicals

Um-PEA was kindly provided by Epitech group srl (Padua, Italy). Innovative Research of America (Sarasota, Florida) have made the depot delivery system containing um-PEA or the proper vehicle (Model NF-141). Once subcutaneously implanted, these pellets released a constant amount of drugs for 30 days. The implant was replaced two times in order to cover the 90 days treatment.

Study design

Pellets were implanted subcutaneously to 3- and 9-month-old 3xTg-AD and Non-Tg mice. By this system, mice received 10mg/kg/die of um-PEA or vehicle for 90 days (Figure 1). Dosage and administration route were chosen according to our previous data and available literature (Costa *et al*. 2002; Grillo *et al*., 2013).

Animals were first tested with behavioral studies, and subsequently sacrificed by decapitation to collect tissues. Hippocampi were isolated for western blotting and reverse transcriptase (RT)-PCR, and then stored at -80°C before analysis; whereas whole brains were frozen by 2-methylbutane and stored at -80°C before immunohistochemical analysis.

In figure 1 the experimental design is reported.

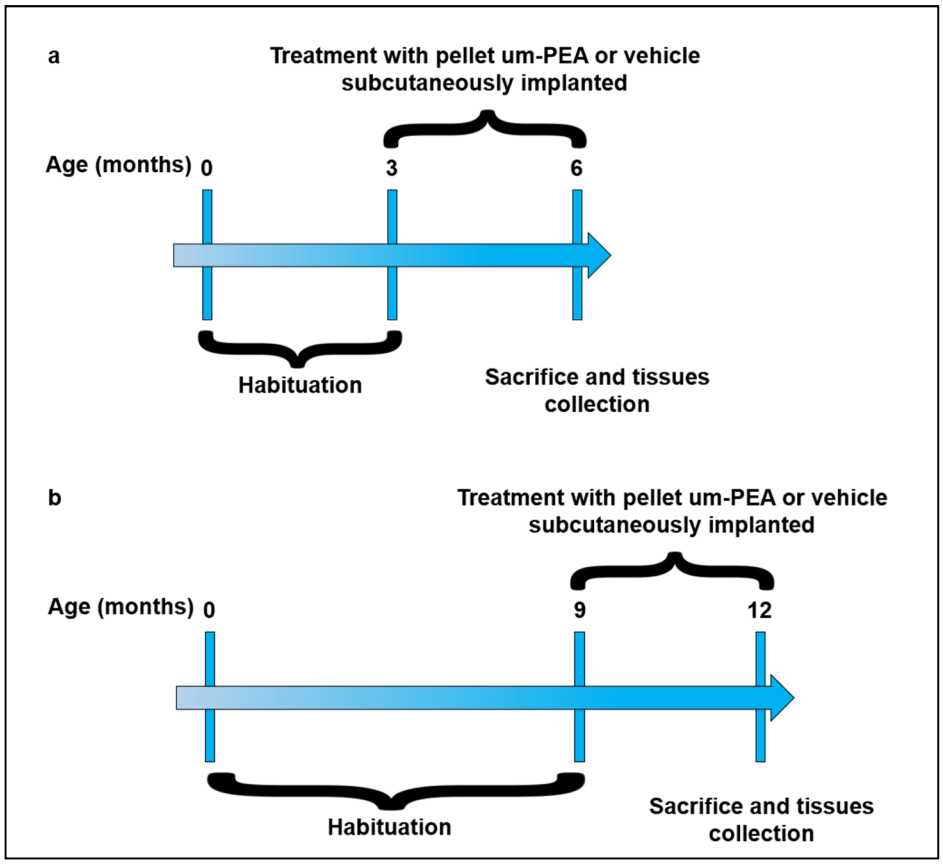

Figure 1 Study design
Schematic representation of the experimental design for both **(a)** 6-month-old and **(b)** 12-month-old Non-Tg and 3xTg-AD mice.

RNA isolation and RT-PCR

Total RNA was extracted from emi-hippocampal homogenates using the NZY total RNA isolation kit (NZYTech, Lisboa, Portugal) according to the company's datasheet. The total RNA concentration was measured by Nanodrop 1000 spectrophotometer (Thermo Fisher Scientific, MD, USA), so 1 μg of RNA was reversed transcribed to obtain cDNA by using oligo(dT) and random primers of the first-strand cDNA synthesis kit (NZYTech, Lisboa, Portugal). RNaseH from *E. coli* was used to digest RNA/DNA hybrids. All PCRs were performed using supreme NZYTaq DNA polymerase (NZYTech, Lisboa, Portugal) with specific primers (Sigma-Aldrich, Milan, Italy) for S100β (forward primer 5'-TAATGTGAGTGGCTGCGGAA-3' and reverse primer 5'-CCTCACCAAGGGCTAAGCAG-3'), GFAP (forward primer 5'-GGAGAGGGACAACTTTGCAC-3' and reverse primer 5'-GCTCTAGGGACTCGTTCGTG-3'), TNF-α (forward primer 5'-CAGCCGATGGGTTGTACCTT-3' and reverse primer 5'-CCGGACTCCGCAAAGTCTAA-3'), IL-1β (forward primer 5'-GGACCCCAAAAGATGAAGGGC-3' and reverse primer 5'-GGAAAAGAAGGTGCTCATGTCC-3'), IL-10 (forward primer 5'-GCCCTTTGCTATGGTGTCCT-3' and reverse primer 5'-CTCTGAGCTGCTGCAGGAAT-3'), iNOS (forward primer 5'-CAAGCTGATGGTCAAGATCCAGAG-3' and reverse primer 5'-GTGCCCATGTACCAACCATTGAAG-3'). GAPDH (forward primer 5'-GCTACACTGAGGACCAGGTTGTC-3' reverse primer 5'-CCATGTAGGCCATGAGGTCCAC-3') was used as gene reference.

Protein extraction and western blot analysis

Emi-hippocampi were homogenized in ice-cold hypotonic lysis buffer (Tris/HCl pH 7.5 50 mM, NaCl 150 mM, ethylenediaminetetraacetic acid (EDTA) 1 mM, 1% triton X-100, PMSF 1 mM, aprotinin 10μg/ml, leupeptin 0.1mM (all from Sigma-Aldrich Milan, Italy) and incubated for 40 min at +4 °C. Proteins dephosphorylation has been avoided by adding 0.3 mg of phosphatise inhibitor cocktail per ml of lysis buffer. The homogenates were then centrifuged at 14000 rpm for 30 minutes to discard membranes and keep aliquoted supernatant then stored at -80 °C waiting for the molecular processing. Bradford assay has been performed to calculate protein concentration in each sample in order to resolve an equal amount of proteins (50 μg) on 12% acrylamide SDS-PAGE precast gels (Bio Rad Laboratories, Milan, Italy). Afterwards, proteins were transferred onto nitrocellulose membranes through a semidry system (Bio Rad Laboratories, Milan, Italy). Membranes were blocked for 1 h with either 5% w/v no-fat dry milk or bovine serum albumin (BSA) powders in tris-buffered saline-tween (TBS-T) 0.1% (Tecnochimica, Rome, Italy).

Overnight incubation at +4 °C on a shaker was performed with one of the following primary antibodies: rabbit anti-S100β (1:1000, Epitomics, Burlingame, CA, USA), rabbit anti-GFAP (1:25000, Abcam, Cambridge, UK), rabbit anti-p[Ser536]-NF-κB p65 (1:2000, Cell Signaling, Danvers, MA, USA), rabbit anti-iNOS (1:8000, Sigma-Aldrich, Milan, Italy), rabbit anti-Gsκ-3β (1:1000, Cell Signaling, Danvers, MA, USA), rabbit anti-p[Ser9]-GSκ-3β (1:1000, Cell Signaling, Danvers, MA, USA), rabbit anti- p[Ser396]tau (1:1000, Thermo Fisher Scientific, Waltham, MA, USA), rabbit anti-Akt (1:500, Cell Signaling, Danvers, MA, USA), rabbit anti-p[Thr308]-Akt (1:5000, Cell Signaling, Danvers, MA, USA), rabbit anti-β-catenin (1:200, Cell Signaling, Danvers, MA, USA), mouse anti-MAP2 (1:250, Novus Biologicals, Littleton, CO, USA), rabbit anti-APP (1:1000, Cell Signaling, Danvers, MA, USA), rabbit anti-BACE1 (1:1000, Cell Signaling, Danvers, MA, USA), mouse anti-β-amyloid (1:200, Santa Cruz, Dallas, TX, USA), rabbit anti-β-actin (1:1500, Santa Cruz, Dallas, TX, USA).

After appropriate rinses in TBS-T 0.05%, membranes were incubated for 1h at room temperature with a specific secondary horseradish peroxidase (HRP)-conjugated antibody (HRP-conjugated goat anti-rabbit IgG, 1:10000 - 1:30000; HRP-conjugated goat anti-mouse, 1:10000; all from Jackson ImmunoResearch, Suffolk, UK) either in 5% w/v no-fat dry milk or BSA in TBS-T 0.1%. Immunocomplexes were detected by an ECL kit (GE Healthcare Life Sciences, Milan, Italy) and the signal obtained was quantified by ImageJ software after densitometric scanning of the X-ray films (GE Healthcare Life Sciences, Milan, Italy).

Immunohistochemistry

To evaluate GFAP and MAP2 levels and distribution, coronal slices (12 µm thickness) containing the hippocampal regions were collected by using a cryostat (Thermo Fisher Scientific, Waltham, MA, USA) and post-fixed with 4% paraformaldehyde in 0.1M phosphate buffer solution (PBS) (Tecnochimica, Rome, Italy) pH 7.4 for 7 minutes at +4C°. The slices were incubated with blocking solution (1% BSA, 0.25% triton X-100 in PBS 0.1M) for 2 h at room temperature and then incubated over night at +4 C° in 0.5% BSA, 0.25% triton X-100 TBS solution containing either rabbit anti-GFAP (1:1000, Abcam, Cambridge, UK) or mouse anti-MAP2 (1:250, Novus Biologicals, Littleton, CO, USA). The day after, sections were rinsed in PBS and then incubated with the proper secondary antibody (fluorescine-affinipure goat anti-rabbit IgG (H+L), 1:200; rhodamine-affinipure goat anti-mouse IgG (H+L), 1:300 - 1:400, Jackson ImmunoResearch, Suffolk, UK) and Hoecsth (1:75000, Sigma-Aldrich, Milan, Italy) in BSA 0.5%, triton X-100 0.25% TBS, for 2 hours at room temperature. Slices were washed and coverslipped using

Fluoromount acqueous mounting medium (Sigma-Aldrich, Milan, Italy). Pictures were captured with a wide-field microscope (Eclipse E600; Nikon Instruments, Rome, Italy).

Analysis were performed by ImageJ software and data expressed as a ratio of the difference between the mean of fluorescence signal and the background (ΔF), and the non-immunoreactive regions (F_0). To prevent that any change in the fluorescent signal could be due to artifacts, the exposure gain and time were kept constant during all image acquisitions.

Statistical Analysis

Data were analyzed by two way-ANOVA followed by Bonferroni's *post-hoc* multiple comparison test. Data are expressed as mean ± standard error of the mean (SEM). The level of statistical significance was $p < 0.05$. Statistical analysis was performed using GraphPad Prism 7 software.

RESULTS

um-PEA effect on reactive gliosis

Reactive gliosis is one of the main pathological hallmarks of AD (Verkhratsky *et al.*, 2010, 2012), and is characterized by glial activation, commonly detected by S100β and GFAP overexpression, and neuroinflammation. Here, we tested the effect of chronic um-PEA treatment on reactive gliosis in the hippocampi of 6- and 12-month-old 3xTg-AD mice, by considering both astrocytic and inflammatory markers (Figure 2).

We found that astrocytes from 6-month-old 3xTg-AD mice tended to be in an activated state as shown by a significant increase of S100β and GFAP transcripts (Figure 2a, b, c). This trend was not observed in the effective production of these proteins when tested by both western blot and immunofluorescence techniques (Figure 2h, i, l, o, q). um-PEA treatment was able to counteract GFAP, but not S100β, transcriptional increase (Figure 2a, b, c), without affecting their protein expression (Figure 2h, i, l, o, q).

In 12-month-old mice, a strong decrease of S100β mRNA was observed in 3xTg-AD mice when compared with age-matched Non-Tg (Figure 2a, b). Despite this reduction, the total amount of the relative protein resulted unaffected (Figure 2h, i). Furthermore, in transgenic mice a significant decrease of both transcription and expression of GFAP was found (Figure 2a, c, h, l, p, q). At this age, um-PEA treatment significantly increased S100β mRNA, without affecting its protein expression (Figure 2a, b, h, i). In the same experimental conditions, um-PEA increased both transcription and translation of GFAP (Figure 2a, c, p, q).

Interestingly, we recorded um-PEA action even in Non-Tg mice. We observed a reduced transcription of both astrocytic markers due to pharmacological treatment (Figure 2a, b, c).

Inflammation is the other main feature of reactive gliosis, involving the activation of different sets of genes, most of them guided by NF-κB transcription factor (Zamanian *et al*, 2012). NF-κB is upstream for the transcription of several pro- and anti-inflammatory mediators, like iNOS enzyme, IL-1β, TNF-α, and IL-10 (Lawrence, 2009; Shih *et al.*, 2015). In order to investigate um-PEA efficacy on inflammation, we studied NF-κB transactivation, occurring whenever its subunit p65 is phosphorylated in Ser536 (Jiang *et al.*, 2003).

We found that 6-month-old 3xTg-AD animals present an inflammatory state, proved by a statistically significant increase of p[Ser536]p65, when compared with Non-Tg littermates (Figure 2h, m). It is reasonable that this is the cause of the significant increase of pro-inflammatory TNF-α (Figure 2a, d) and IL-1β (Figure 2a, e) transcripts, and the significant decrease of IL-10 mRNA

(Figure 2a, f). In the transgenic model, at 6 months of age, the inflammatory state was confirmed by the significant increase of iNOS transcription and protein expression (Figure 2a, g, h, n). Chronic um-PEA treatment caused a marked decrease of p[Ser536]p65 subunit (Figure 2h, m), IL-1β (Figure 2a, e), and iNOS mRNAs (Figure 2a, g) but did not affect TNF-α transcription (Figure 2a, d). Moreover, um-PEA induced a significant transcriptional increase of the anti-inflammatory cytokine IL-10 (Figure 2a, f).

Different results were obtained in aged mice. Indeed, by comparing 3xTg-AD and Non-Tg mice, in the former we observed significant differences only for IL-10 and iNOS mRNAs, which resulted increased and decreased, respectively (Figure 2a, f, g). Despite um-PEA up-regulated iNOS mRNA, treatment resulted in a significant reduction of the corresponding protein amount (Figure 2a, g, h, n).

Notably, um-PEA treatment had a positive effect even in aged Non-Tg mice. We found that um-PEA was able to significantly reduce p[Ser536]p65 expression (Figure 2h, m), and strongly induce IL-10 transcription (Figure 2a, f). These data agree with the notion that neuroinflammation occurs also in physiological aging (Gabuzda and Yankner, 2013), confirming PEA anti-inflammatory properties.

Collectively, these results shown that 6-month-old 3xTg-AD mice present a mild astrocyte activation and an intense inflammatory status. By contrast, 12-month-old 3xTg-AD animals did not present reactive state neither neuroinflammation. The overall effect of um-PEA treatment was to stabilize the altered parameters related to reactive gliosis, bringing them to more physiological levels.

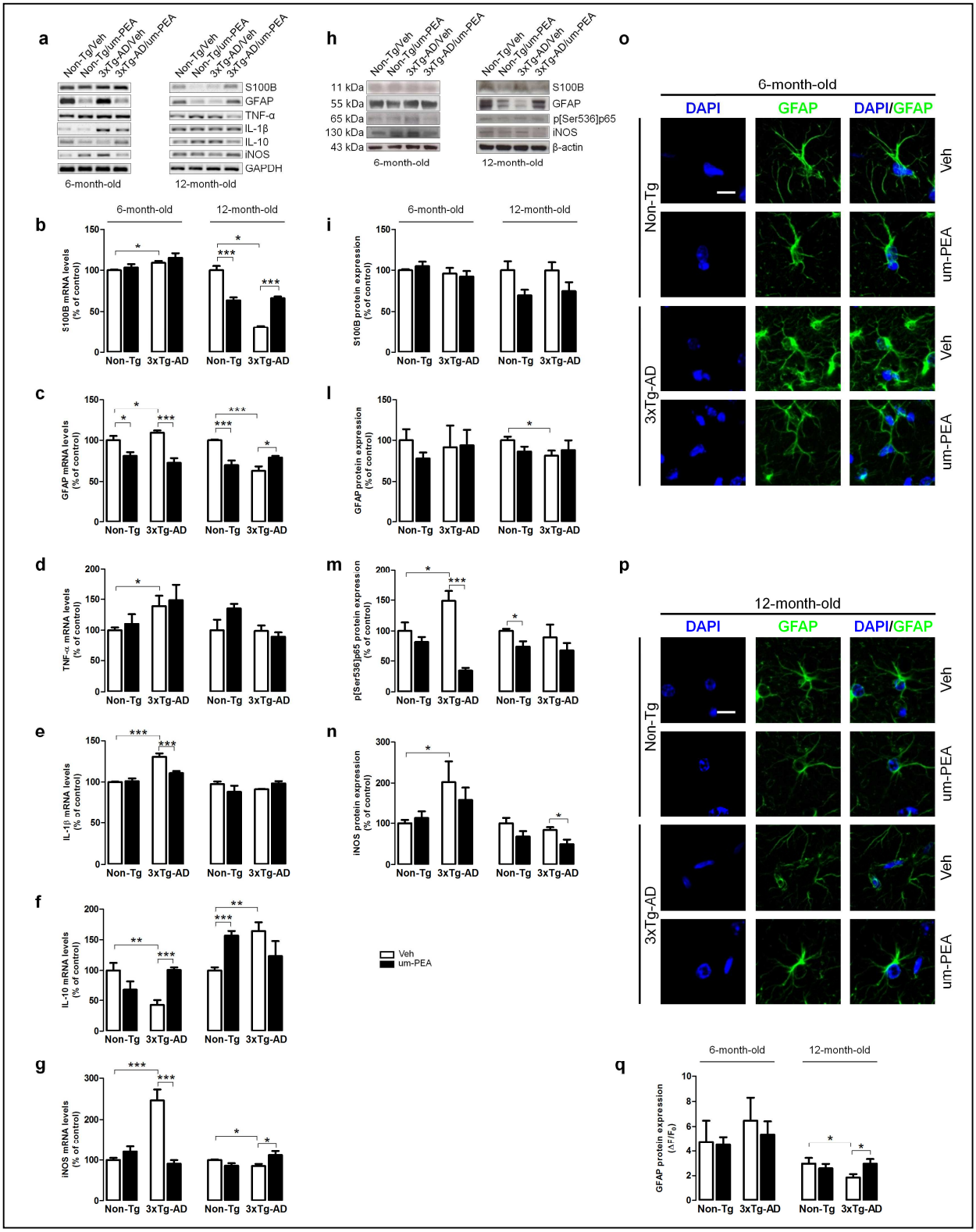
a
Non-Tg/Veh
Non-Tg/um-PEA
3xTg-AD/Veh
3xTg-AD/um-PEA
S100B
GFAP
TNF-α
IL-1β
IL-10
iNOS
GAPDH
6-month-old
12-month-old
h
11 kDa
55 kDa
65 kDa
130 kDa
43 kDa
S100B
GFAP
p[Ser536]p65
iNOS
β-actin
6-month-old
12-month-old
o
6-month-old
DAPI
GFAP
DAPI/GFAP
Non-Tg
3xTg-AD
Veh
um-PEA
p
12-month-old
b
S100B mRNA levels (% of control)
c
GFAP mRNA levels (% of control)
d
TNF-α mRNA levels (% of control)
e
IL-1β mRNA levels (% of control)
f
IL-10 mRNA levels (% of control)
g
iNOS mRNA levels (% of control)
i
S100B protein expression (% of control)
l
GFAP protein expression (% of control)
m
p[Ser536]p65 protein expression (% of control)
n
iNOS protein expression (% of control)
Non-Tg
3xTg-AD
Veh
um-PEA
q
GFAP protein expression (ΔF/F0)

Figure 2 PEA effect on reactive gliosis in hippocampus of 3xTg-AD mice, both 6- and 12-month-old

(a) Rapresentative results obtained from RT-PCR for S100β, GFAP, TNF-α, IL-1β, IL-10, iNOS mRNAs, and **(b-g)** densitometric analysis of corresponding bands normalized with GAPDH. Results are express as percentage of control (Non-Tg/Veh groups). **(h)** Representative western blots for S100β, GFAP, p[Ser536]p65, iNOS proteins and **(i-n)** densitometric analyses normalized with β-actin used as loading control. Results are express as percentage of control (NonTg/Veh groups). **(o-p)** Rappresentative fluorescent photomicrographs of GFAP (green) staining in the CA1 region of hippocampi at both 6 **(o)** and **(p)** 12 months of age, and **(q)** fluorescence analysis expressed as $\Delta F/F_0$. Nuclei were stained with DAPI (blue). Data are presented as means ± SEM and statistical analysis was performed by two-way ANOVA followed by Bonferroni multiple comparison test (* $p < 0.05$; ** $p < 0.01$; *** $p < 0.001$). Scale bar 10 um.

um-PEA role in tau phosphorylation and neuronal survival

Tau protein is a microtubule-associated protein that allows microtubules assembly and stabilization according to its phosphorylation (Cleveland *et al*., 1997). Tau protein hyperphosphorylation results in the production of PHFs which, in turn, are responsible for NFTs creation. These structural modifications lead to neuronal dysfunction and cognitive impairments (Zhu *et al*., 2007). Several kinases add phosphate groups on tau specific amino acids. Among these, Gsκ-3β is one of the kinases mainly involved in the creation of NFTs (Engel *et al*., 2006). Its activity is regulated by a serine/threonine-specific protein kinase, known as Akt (Grimes and Jope, 2001). Akt/Gsκ-3β pathway is involved in the neuronal survival regulation by controlling the expression of β-catenin, that mediates pro-survival signals (Yuan *et al.*, 2005). Activated Gsκ-3β causes β-catenin ubiquitination and degradation (Aberle *et al.*, 1997), resulting in neuronal death. This is patent in several neurological conditions, such as in AD (Zhang *et al.*, 1998; De Ferrari and Inestrosa, 2000; Li *et al.*, 2007a).

Here, we tested um-PEA effectiveness on tau phosphorylation via Akt/Gsκ-3β pathway (Figure 3), and the subsequent effect on neuronal survival (Figure 4).

We evaluated the expression of p[Thr308]Akt, the active form of this enzyme responsible of Gsκ-3β inactivation through Ser9 phosphorylation (Jope *et al.*, 2007), as well as tau protein damage through the amount of p[Ser396]tau.

Despite no changes in the total Akt quantity (Figure 3a, b), we found a significant decrease of p[Thr308]Akt in 6-month-old 3xTg-AD mice in comparison with Non-Tg littermates (Figure 3a, c). Accordingly, although no difference in the total amount of Gsκ-3β kinases was detected (Figure 3a, d), transgenic animals shown p[Ser9]Gsκ-3β reduction (Figure 3a, e). Lastly, we observed a significant p[Ser396]tau increase and a marked decrease in β-catenin expression in 3xTg-AD mice in comparison with age-matched Non-Tg (Figure 3a, f, g).

um-PEA treatment was able to induce a global regulation of the Akt/Gsκ-3β pathway in 6-month-old 3xTg-AD mice in comparison with Non-Tg. Indeed, we observed a significant increase of p[Thr308]Akt and p[Ser9]Gsκ-3β, resulting in a marked increase of β-catenin levels (Figure 3a, c, e, g), and decrease of p[Ser396]tau (Figure 3a, f).

At 12 months of age, we observed a significant reduction of the inactive form of Gsκ-3β with the subsequent increase of p[Ser396]tau in 3xTg-AD mice when compared with Non-Tg littermates (Figure 3a, e, f). Interestingly, um-PEA chronic treatment strongly counteracted p[Ser396]tau development (Figure 3a, f). At this age, all other parameters were not affected by either genotype or treatment.

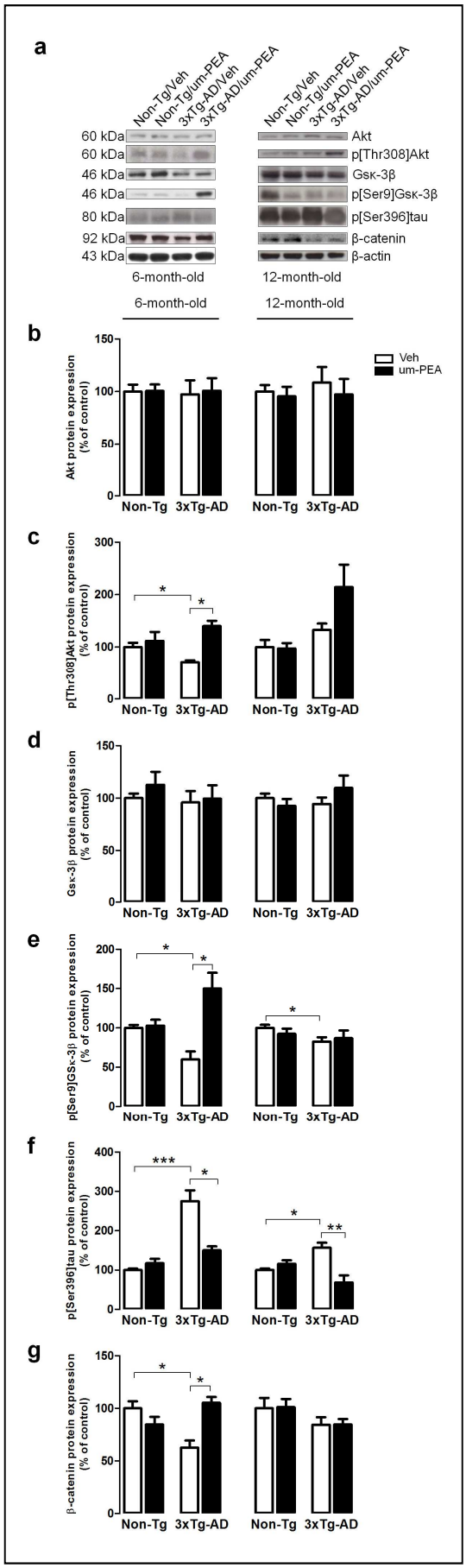
a
Non-Tg/Veh
Non-Tg/um-PEA
3xTg-AD/Veh
3xTg-AD/um-PEA
60 kDa
60 kDa
46 kDa
46 kDa
80 kDa
92 kDa
43 kDa
Akt
p[Thr308]Akt
Gsκ-3β
p[Ser9]Gsκ-3β
p[Ser396]tau
β-catenin
β-actin
6-month-old
12-month-old
b
Veh
um-PEA
Akt protein expression (% of control)
c
p[Thr308]Akt protein expression (% of control)
d
Gsκ-3β protein expression (% of control)
e
p[Ser9]GSκ-3β protein expression (% of control)
f
p[Ser396]tau protein expression (% of control)
g
β-catenin protein expression (% of control)
Non-Tg
3xTg-AD

Figure 3 PEA effect on tau phosphorylation in hippocampus of 3xTg-AD mice both 6- and 12-month-old

(a) Representative western blots for Akt, p[Thr308]Akt, GSκ-3β, p[Ser9]GSκ-3β, p[Ser396]tau, β-catenin and **(b-h)** densitometric analysis normalized to β-actin used as loading control. Results are express as percentage of control (Non-Tg/Veh groups). Data are presented as means ± SEM and statistical analysis was performed by two-way ANOVA followed by Bonferroni multiple comparison test (* $p < 0.05$; *** $p < 0.001$).

Since we detected marked alterations of Akt/Gsκ-3β pathway, we decided to investigate neuronal survival testing MAP2 expression (Figure 4). Results from western blot analyses did not show any difference among groups at both ages (Figure 4d, e). To deeper explore the different hippocampal areas, we performed additional immunofluorescence experiments. Obtained data revealed statistically significant differences only in the CA1 region. We found increased MAP2 immunopositivity in 6- (but not in 12-) month-old 3xTg-AD mice in comparison with Non-Tg animals (Figure 4 a, b, c). The same set of experiments revealed that um-PEA administration promoted neuronal survival. Indeed, we detected increased MAP2 signal in 3xTg-AD mice at both ages, but only at 6 months of age in Non-Tg ones (Figure 4 a, b, c).

In their entirety, these results indicate that transgenic mice show marked alterations in the Akt/Gsκ-3β pathway, especially at 6 months of age. However, these modifications seem to not be enough to cause neuronal death. The overall effect of um-PEA treatment was to stabilize the altered parameter related to Akt/Gsκ-3β pathway, and to promote neuronal survival in both genotypes.

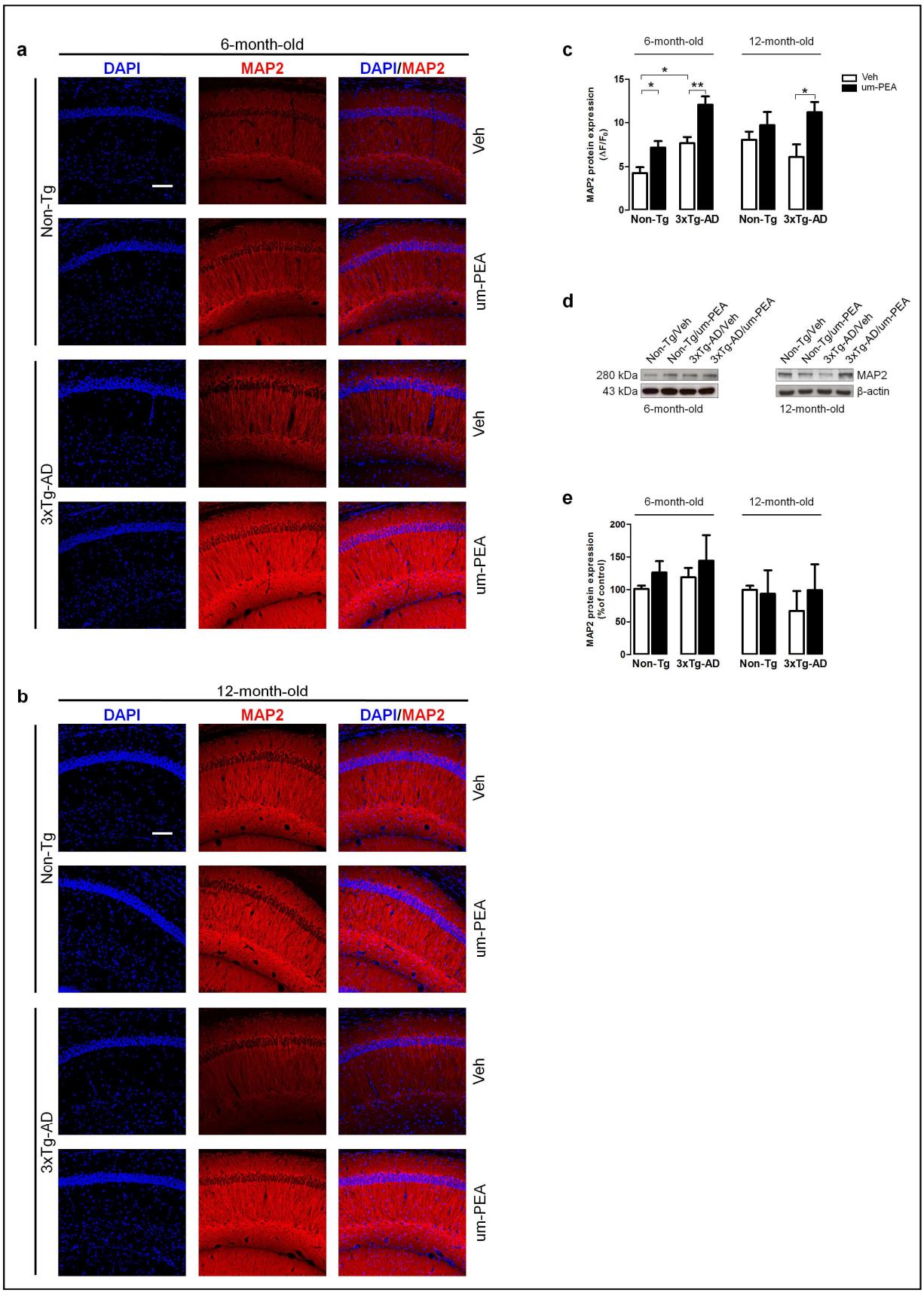
a
6-month-old
DAPI
MAP2
DAPI/MAP2
Non-Tg
3xTg-AD
Veh
um-PEA
b
12-month-old
c
6-month-old
12-month-old
Veh
um-PEA
MAP2 protein expression (ΔF/F0)
Non-Tg
3xTg-AD
d
Non-Tg/Veh
Non-Tg/um-PEA
3xTg-AD/Veh
3xTg-AD/um-PEA
280 kDa
43 kDa
MAP2
β-actin
e
MAP2 protein expression (%of control)

Figure 4 PEA effect on neuronal survival in hippocampus of 3xTg-AD mice, both 6- and 12-month-old

Rappresentative fluorescent photomicrographs of MAP2 (red) staining in the CA1 region of hippocampi at both 6 **(a)** and **(b)** 12 months of age, and **(c)** fluorescence analysis expressed as $\Delta F/F_0$. Nuclei were stained with DAPI (blue). **(d)** Representative western blots for MAP2 and **(e)** densitometric analyses normalized with β-actin used as loading controls. Results are express as percentage of control (Non-Tg/Veh groups). Data are presented as means ± SEM and statistical analysis was performed by two-way ANOVA followed by Bonferroni multiple comparison test (* $p < 0.05$; ** $p < 0.01$). Scale bar 100 um.

um-PEA action on the amyloidogenic pathway

The amyloidogenic APP processing is the pathway mainly responsible for Aβ release (mostly $A\beta_{(1-40)}$ and $A\beta_{(1-42)}$) and implies the involvement of β-secretase (BACE1) (O'Brien and Wong, 2011).

In our model, we evaluated the expression of APP, BACE1, and $A\beta_{(1-42)}$ peptide, as well as the effect of um-PEA chronic treatment.

6- and 12-month-old 3xTg-AD mice compared with Non-Tg littermates shown a statistically significant increase of APP and, despite no changes in BACE1 expression, they had a massive $A\beta_{(1-42)}$ amount (Figure 5). At both ages, chronic um-PEA treatment failed in inhibiting APP production (Figure 5a, b). Interestingly, um-PEA was able to strongly reduce $A\beta_{(1-42)}$ levels in both 3xTg-AD and Non-Tg mice at 12 months of age (Figure 5a, d).

Collectively, these results confirm an intense amyloidogenic pathway activity in 3xTg-AD mice, and um-PEA capability to greatly decrease $A\beta_{(1-42)}$ levels.

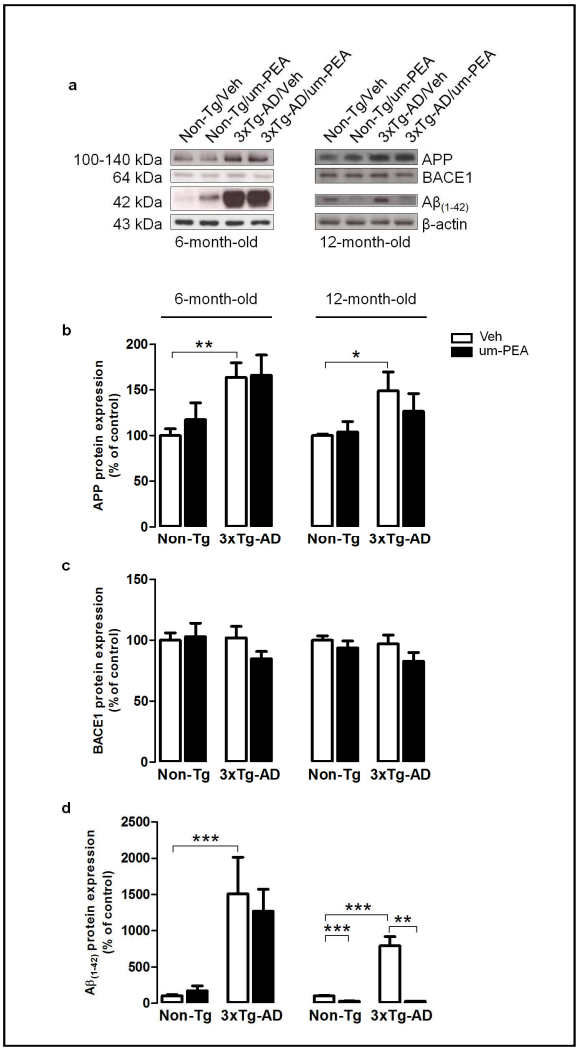

Figure 5 PEA effect on amyloidogenic pathway in hippocampus of 3xTg-AD mice both 6- and 12-month-old

(a) Representative western blots for APP, BACE1 and $A\beta_{(1-42)}$ proteins and **(b-d)** densitometric analyses normalized to β-actin used as loading control. Results are express as percentage of control (Non-Tg/Veh groups). Data are presented as means ± SEM and statistical analysis was performed by two-way ANOVA followed by Bonferroni multiple comparison test (* $p < 0.05$; ** $p < 0.01$; *** $p < 0.001$).

DISCUSSION

Here, we provide the first *in vivo* evidence about the anti-inflammatory and neuroprotective effects of a chronic um-PEA treatment in 3xTg-AD mice. Moreover, original and unique aspect of this study is the treatment schedule, designed to investigate both asymptomatic and frank stages of AD pathology. Current work increases knowledge about the molecular mechanisms involved in AD and suggests a potential new therapeutic approach. We comprehensively examined pathways underlying astrocytic activation, neuroinflammation, and neuronal integrity in 6- and 12-month-old 3xTg-AD mice, relative to Non-Tg, receiving either um-PEA or vehicle for 3 months. Our results clearly indicate that important molecular modifications occur already at early stages, and that um-PEA treatment is able to counteract most of them.

Such results are of great interest since, to date, AD is one of the main public health challenges, and no efficacious treatments are available. The growing demand for new therapeutic tools has prompted researchers to better understand less explored AD hallmarks to manipulate them. In the last two decades, beside old and current pharmacological approaches to hit SPs and NFTs, other strategies aimed at controlling other aspects of this disorder, such as neuroinflammation.

It has been known for a long time that PEA displays marked anti-inflammatory properties in peripheral inflammation models. Recently, its effectiveness has been also demonstrated in models of neurodegenerative disorders presenting inflammatory features, like AD, Parkinson's disease, and multiple sclerosis (D'agostino *et al*., 2012; Esposito *et al*. 2012; Scuderi *et al*., 2014; Rahimi *et al*., 2015). The recent availability of um-PEA, crystalline form of micrometric size that improves the pharmacokinetics and thus the bioavailability (Impellizzeri *et al*., 2014; Petrosino and Di Marzo, 2016), prompted us to test its anti-inflammatory and neuroprotective effects in a transgenic model of AD.

Glia rapidly acts in response to several brain injuries, including Aβ deposits, undergoing important morpho-functional changes that can, in turn, influence disease course. Such modifications are intricate and heterogeneous, and can be crudely identified as hyperreactivity or atrophy (Rodríguez *et al*., 2009; Verkhratsky and Parpura, 2016). Moreover, a direct correlation has been established between glia activation and induction of pro-inflammatory pathways (Orre *et al*., 2014). In our model, we detected alterations of GFAP and S100β, the best-known markers of astrocytic activation, as well as of parameters related to neuroinflammation (i.e., NF-κB, iNOS, IL-1β, TNF-α, and IL-10). Collected results highlighted that the scenario was completely different between the two ages. Indeed, 6-month-old 3xTg-AD mice displayed a mild astrocyte activation and an intense

inflammatory status. Notably, um-PEA revealed its ability to counteract both astrocyte activation and inflammation. Indeed, it significantly reduced GFAP mRNA and blocked NF-κB transactivation, thus reducing the transcription of IL-1β and iNOS. PEA action was also confirmed by the induction of the anti-inflammatory IL-10 cytokine.

Differently, 12-month-old 3xTg-AD mice did not show any sign of neuroinflammation, as expected by the moderate astrocytic atrophy observed at this age. Indeed, transgenic animals exhibited lower GFAP and S100β levels when compared with age-matched Non-Tg. um-PEA treatment caused a marked increase of both S100β and GFAP in 3xTg-AD, but reduced these markers in Non-Tg. The effects of this compound even in old Non-Tg animals are crucial because astrocyte activation in aging is a well-documented phenomenon (Landfield *et al.*, 1977; Yoshida *et al.*, 1996). Our results suggest that, in both genotypes, um-PEA treatment regulates the expression of these proteins, bringing them to the same, likely optimal, levels. Therefore, the pharmacological treatment seems to counteract the negative effect of aging not only in 3xTg-AD, but even in Non-Tg mice, suggesting an important balancing role of this compound.

It is now accepted that both astrocytic activation and atrophy simultaneously occur in AD brains, contributing to neuronal death (Rodríguez *et al.*, 2009). Since our data shown both astrocytic behaviours, we decided to investigate Akt/Gsκ-3β pathway activation. Indeed, it is involved in the phosphorylation of tau proteins which are strictly connected to NFTs development, another key hallmark of AD brain. Here we show, for the first time in an *in vivo* model, um-PEA ability to prevent the alteration in the Akt/Gsκ-3β pathway observed in 6-month-old 3xTg-AD mice, and to reduce tau protein phosphorylation at both ages. The neuroprotective effects of um-PEA were confirmed by fluorescence microscopic detection of MAP2, a structural neuronal marker. Our results highlighted a key role of um-PEA in increasing neuronal survival in 3xTg-AD mice at both ages. Surprisingly, this pro-survival effect was also observed in 6-month-old Non-Tg animals.

By immunofluorescence analysis we observed that 6-month-old 3xTg-AD mice express more MAP2 in comparison with Non-Tg littermates. This curious result could be justified by the mild astrocytic activation observed at this age, whose primary goal is reparative (Myer *et al.*, 2006; Burda and Sofroniew, 2014). It is possible to speculate that this reactive status has not yet reached levels such as to trigger deleterious processes, instead promotes reparative and pro-survival pathways that could support neurons.

Beside NFTs formation, Aβ accumulation in SPs is another AD characteristic hallmark. It has been demonstrated that inflammation accelerates the development of AD phenotype, being responsible for the increment of the amyloidogenic pathway (Wozniak *et al.*, 2007). Based on

current results about reactive gliosis, we explored the main elements involved in the pro-amyloidogenic APP cleavage and the resulting expression of $A\beta_{(1-42)}$, one of the more toxic fragments. Since the presence of the APP_{swe} transgene, we recorded an exacerbation of this protein in 3xTg-AD mice at both ages. Even if any alteration in BACE-1 level was recorded among all experimental groups, a >15-fold increase in $A\beta_{(1-42)}$ expression was observed comparing 3xTg-AD to Non-Tg mice. Our results demonstrated, for the first time, the ability of um-PEA to strongly reduce the expression of $A\beta_{(1-42)}$ in both genotypes at 12 months of age. um-PEA acted, once again, not only in 3xTg-AD, but even in aged Non-Tg animals, suggesting its important role in dampening aging in health and disease.

The current investigation allows a better knowledge of pathology progression in 3xTg-AD mice and demonstrates the therapeutic potential of um-PEA in fighting the aging process, by exerting a combination of anti-inflammatory and neuroprotective effects.

Although our results indicate that, in aged mice, um-PEA treatment caused regulatory effects on pathways mainly involved in AD pathology, more interesting data were obtained in 6-month-old animals. Indeed, AD features of animals treated precociously with um-PEA (starting from 3 months of age, without any clinical sign of disease) seemed to be less pronounced, suggesting the benefit of starting drug treatment very early. It is noteworthy that PEA, by virtue of its high tolerability and safety also demonstrated in humans, could be suitable for long-term treatments that last years, as AD requires.

In conclusion, current results show that the best way to counteract AD is probably starting the pharmacological treatment as soon as possible, pushing researchers to find diagnostic tools for a precocious disease detection.

SECTION IV

High $[K^+]_o$ induced LTP increases hippocampal CA1 dendritic spines area in mouse brain slices

INTRODUCTION

Synaptic plasticity represents the capability of synapses to strengthen or weaken as an adapting mechanism of the brain to react to external and internal stimuli (Malenka and Nicoll, 1999). Long-term depression (LTD) and long-term potentiation (LTP) are two forms of plasticity that can last from minutes to hours. LTP has been first described in the rabbit hippocampus in 1966 by Terje Lømo (Lømo, 1966) and then characterized as a specific synaptic response occurring after strong neuronal stimulations (Bliss and Lømo, 1973). LTP is considered to underlie the processes of learning and memory (Morris *et al*., 1986; Bliss and Collingridge, 1993; Malenka, 1994; Martin *et al*., 2000; Gruart *et al*., 2006), thus explaining why hippocampal region has been the subject of LTP studies from decades.

The LTP phenomenon requires a complex molecular cascade that can be activated in different regions and in different manners. The initial event starts from receptors activation by neurotransmitters and action potential propagation which in turn cause the release of secondary messengers that activate protein kinases (Stepan *et al*., 2015). Dendritic spines are the main structures involved in synaptic potentiation (Harris and Kater, 1994), although presynaptic sites are also implicated. Dendritic spines are rich in actin and thus morphologically highly dynamic. In response to LTP, they undergo shape and cytoskeletal remodeling and eventually increase their volume, features that are thought to be critical for potentiation (Yuste and Bonhoeffer, 2001).

The LTP that takes place in the CA1 region of the hippocampus occurs as a result of postsynaptic N-methyl-D-aspartate receptors (NMDARs) activation (Collingridge *et al*., 1983; Harris *et al*., 1984). The opening of NMDARs channel is voltage-dependent and this is subordinated to the presence of extracellular Mg^{2+} (Mayer *et al*., 1984; Nowak *et al*., 1984). During normal transmission, glutamate released from presynaptic membrane binds both α-amino-3-hydroxy-5-methyl-4-isoxazolepropionic acid receptor (AMPARs) and NMDARs without inducing any potentiation because only AMPARs allow Na^+ postsynaptic influx. Whenever depolarization takes place, Mg^{2+} detaches from the NMDARs channels thereby increasing Ca^{2+} and Na^+ permeability of the postsynaptic membranes through this receptor (Malenka and Nicoll, 1999). Ca^{2+} intake increases AMPARs conductance (via protein kinase) as well as the delivery

and/or clustering of the receptor within the postsynaptic plasma membrane (Malinow and Malenka, 2002) in order to mediate the transmission (Hayashi *et al*., 2000). The increase of Ca^{2+} in the dendritic spines is the actual event that triggers secondary messengers cascade allowing the long-lasting potentiation.

Experimentally, it is possible to induce LTP *in vitro* and *ex vivo* in different manners: for instance, glutamate uncaging onto single spines (Matsuzaki *et al*., 2001) and 10 minutes treatment with 10 mM glycine (Musleh *et al*., 1997) (a NMDARs co-agonist) are two methods able to mimic the natural synaptic strengthen. Moreover, since the 80s it is known that a transient elevation of extracellular K^+ concentration is sufficient to modulate neuronal membrane potential (Balestrino *et al*., 1986) and induce LTP in rat brain slices (Ballyk and Goh, 1992; Fleck *et al*., 1992; Harrison and Alger, 1993; Bernard *et al*., 1994; Roisin *et al*., 1997). This idea comes from the observation that repetitive stimulations at frequency commonly used to induce LTP also causes extracellular K^+ increase (Krnjević *et al*., 1982; Poolos *et al*., 1987) that reaches a concentration of around 8 mM in slices (Nicholson and Hounsgaard, 1983; Svoboda and Syková, 1991). The present study aimed at studying morphological changes in hippocampal CA1 spines after high $[K^+]_o$ (20 mM)-LTP induction by monitoring spines area.

Previous studies performed by this lab confirmed the ability of high $[K^+]_o$ (20mM) to induce LTP, achieving comparable effects obtained by high frequency stimulation (HFS) (data not published). Importantly, the concentration of K^+ in the synaptic cleft after high $[K^+]_o$ treatment was demonstrated to peak at around 8 mM, value consistent with that observed by direct HFS (data not published). The aim of this work is to show that 20 mM K^+ aCSF is able to promote the volume increase of dendritic spines in the same conditions of K^+-induced LTP.

MATERIALS AND METHODS

Stereotaxic injection of rAAV5/CamKIIa-eYFP

9 C57Bl/6 male mice 4 weeks old (Janvier) were housed on a 12-hour light-dark cycle, with *ad libitum* access to food and water. The day of the surgery, animals were deeply anesthetized with 1-1.5% isoflurane and placed in a stereotaxic frame. Short lasting analgesia was provided by injection of 0.05 mg/kg of buprenorphine. Local analgesia was provided by xylocaine (0.2 mg/mL) enough to cover the surface between the skin and the skull before the incision. A volume of 500 nL (5.2×10^{12} virus molecules/ml) at a flow rate of 100 nl/min of rAAV5/CamKIIa-eYFP was injected using the following coordinates: anterior-posterior (AP) -1.85 mm; medio-lateral (ML), ±1.15 mm; and dorso-ventral (DV) -1.00 mm (relative to the bregma) (Figure 1). The needle was kept in the injection site for 8 minutes after the viral infusions and was slowly retracted thereafter. After the surgery, long lasting analgesia was provided by 5mg/kg of carprofen. The viral spreading took place for 3-4 weeks.

Acute slices preparation

Acute brain slices were prepared according to what has been previously described (Rangroo Thrane *et al*., 2013). Briefly, after 3-4 weeks of viral spreading, animals were mildly anesthetized with 1-1.5% isoflurane. After decapitation, the brains were rapidly removed and coronal slices (350 µm) obtained using a vibratome (Leica) in oxygenated (95% O_2/5% CO_2) cold modified Ringer solution composed of (in mM) sucrose 228.0, glucose 11.0, $NaHCO_3$ 26.0, $MgSO_4$ 7.0, KCl 2.5, NaH_2PO_4 1.0, $CaCl_2$ 0.5 (Schwartz *et al*., 2014) (Figure 1).

The brain slices were incubated for 1 hour at +34°C and 30 minutes at room temperature (20-22°C) in continuously oxygenated (95% O_2/5% CO_2) artificial cerebrospinal fluid (aCSF) containing (in mM) NaCl 124.0, $NaHCO_3$ 26.0, glucose 11.0, KCl 2.5, $CaCl_2$ 2.5, $MgCl_2$ 1.3, NaH_2PO_4 1.0.

20mM K^+ LTP induction

After recovery, slices were transferred to a slice chamber and continuously perfused at a rate of 2.5-3.5 ml/min with oxygenated aCSF.

To induce high $[K^+]_o$-LTP, the perfusing aCSF was switched to 20mM K^+ for 50 seconds and then returned to standard aCSF for the next 35 minutes (Figure 1). The 20mM K^+ aCSF

solution had increased KCl and correspondingly reduced NaCl concentration to keep the osmolarity constant.

2-photon imaging

Dendritic spine imaging was carried out right before 20mM K^+ perfusion, and 5, 15, 25 and 35 minutes after high $[K^+]_o$-LTP induction. Image acquisition was performed by a Thorlabs 2-photon microscope using a 20X (20X/1.00W) water immersion objective (Olympus). A laser (InSight DS+, Spectra-Physics) was used to excite YFP at 960nm and the emitted fluorescence was recorded using a 535/50 nm filter. 1024 × 1024 pixels was the image size; 20 frames (each resulting from 32 averages) were acquired for each time points, at depths between 70 and 150 µm from the surface of the slice (Figure 1). At these depths, the concentration of K^+ after superfusion with 20 mM K^+ has been measured to be around 8 mM (unpublished data from KU lab).

Dendritic spine analysis

A total of 267 spines distributed in 27 slices (~10 spines/slice) have been analyzed. ImageJ software was used to process and analyse images.

In order to get a single image for each time point, the 20 frames obtained with each acquisition were co-registered and then averaged. The measurements of the spines area were obtained by manually drawing a line all around the perimeter of single spines for each time point and then measuring the inner area by ImageJ software. YFP signal was used as guide for dendritic spines area.

Statistical analysis

In order to get measurements in the same order of magnitude, all the results are expressed as percentage relative to the baseline (time -2’ 50"). Statistics were performed using the software GraphPad Prism 7 and differences were detected by one-way analysis of variance (ANOVA); multiple comparisons were performed using the Bonferroni’s *post hoc* test.

Data are shown as mean ± SEM. Differences among mean values were considered statistically significant when $p < 0.05$.

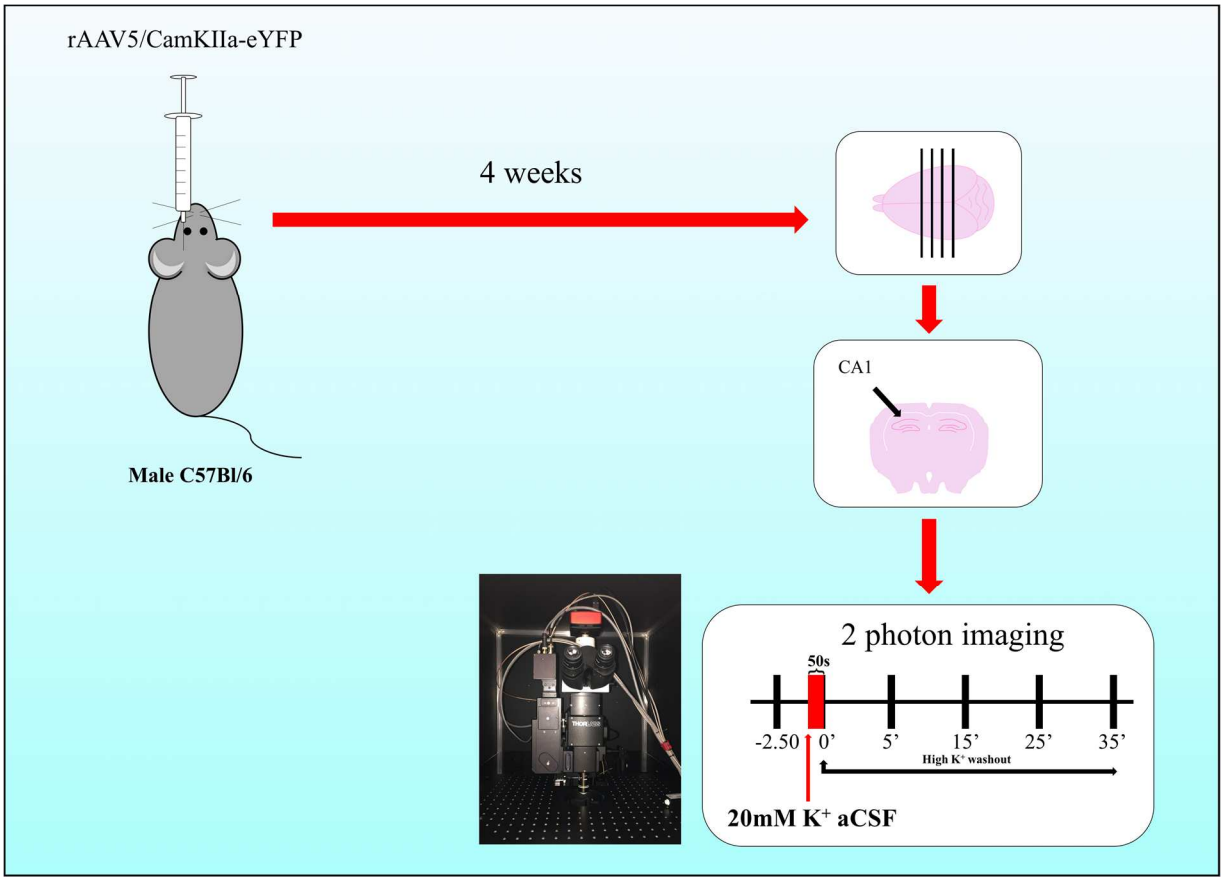

Figure 1 Experimental procedure

RESULTS

Dendritic spines behaviour that involves increasing volume is one of the main features of LTP (Kopec *et al*., 2006). To confirm that 20 mM $[K^+]_o$-LTP is able to induce the same outcome of HFS, we decided to monitor the dendritic spine areas projection since we obtained 2D images by averaging 20 frames for each time point.

The YFP analysis of the total number of spines showed that there is a statistically significant increase of the areas that reaches statistical significance after 15 minutes ($p < 0.01$), and it keeps increasing up to 35 minutes ($p < 0.001$), time point in which maximum pick with an increment of 10.43% ± 1.63 have been registered (Figure 2A). The averaged value of changing during the 35 minutes resulted to be 7.40% ± 0.72.

A closer look to the data revealed that there are different populations of dendrites behaving in different manners (Figure 2): 40.08% of the spines (Figure 2B green; Figure 2C) shows an increased area in each time point; 42.32% of the spine exhibited a “neutral” response (Figure 2G; Figure 2H) including spines (28.8%) with a trend in increasing their area (Figure 2B, yellow) and spines (13.48%) with a trend in decreasing their area (Figure 2B orange); 17.60% of the spines (Figure 2B red, Figure 2E) decreased their area.

By calculating the average of the values for each group of spines, it has been estimated that the increase of the areas of the spines is 25.76% ± 0.99 for the former group (Figure 2D), while the decrease is around 18.8% ± 0.90 for the latter group (Figure 2F).

Taken together these results show that high $[K^+]_o$-LTP induces different morphological changes of dendritic spines, but overall there is an increase of dendritic spines area.

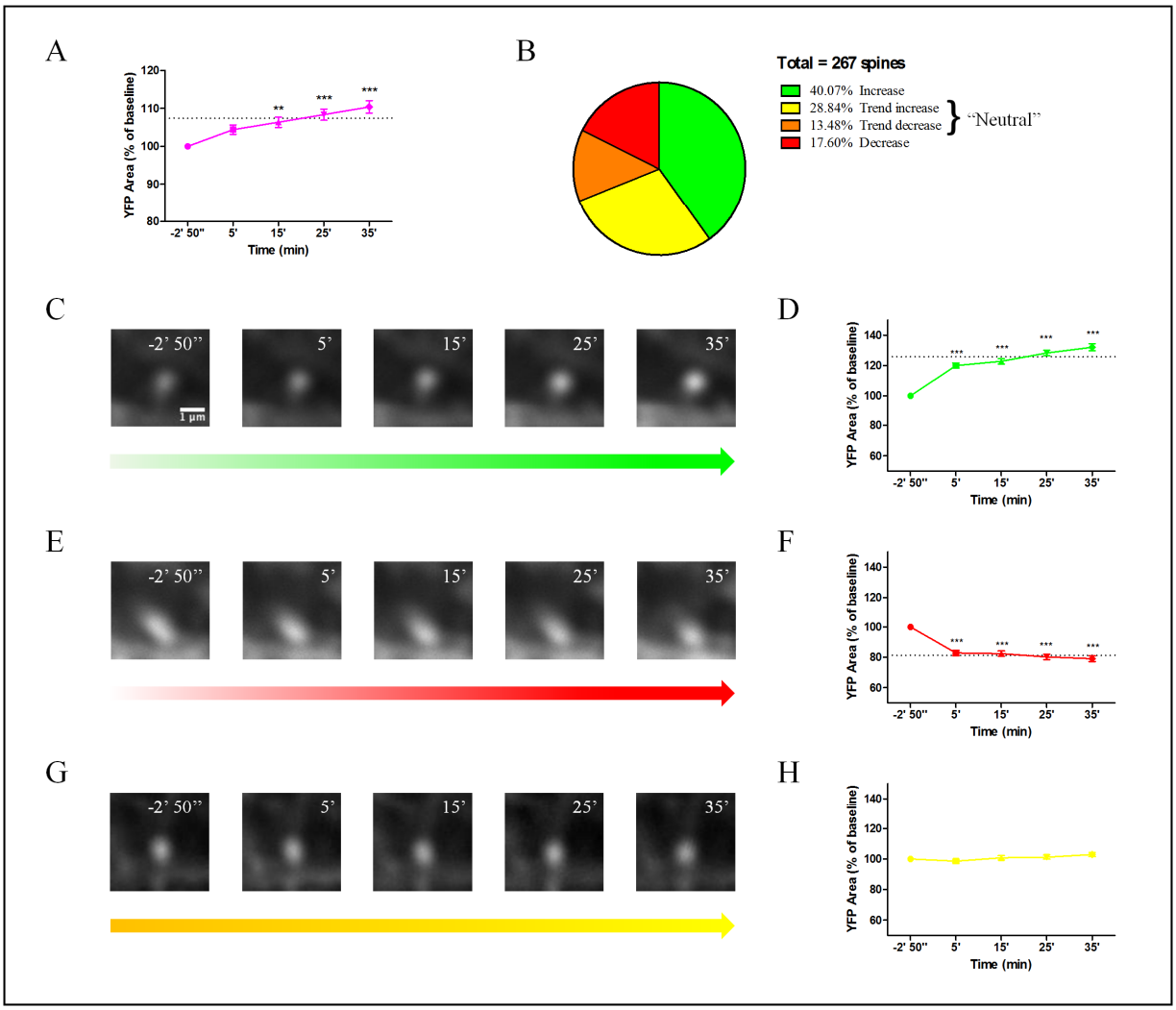

Figure 2 Effect of 20 mM K^+ on dendritic spines area

(A) Measurement of area's changes in the total number of dendritic spines. The dashed line represents the average value of changing during the 35 minutes after high $[K^+]_o$-LTP induction. **(B)** Representation of the different dendritic spines populations divided according to their behaviour in all time points: increase (green) represents all the spines that show an increased area at each time point after high $[K^+]_o$-LTP induction; trend increasing (yellow) represents all the spines that show an increase in at least 2 time points after high $[K^+]_o$-LTP induction; trend decreasing (orange) represents all the spines that show a decrease in 3 time points after high $[K^+]_o$-LTP induction; decrease (red) represents all the spines that show a decreased area at each time point after high $[K^+]_o$-LTP induction. **(C)** Representative images (20X magnification, 17X zoom) of a dendritic spine increasing its area (YFP signal) after high $[K^+]_o$-LTP induction. **(D)** Behaviour of potentiated spines (n = 107) in 35 minutes after high $[K^+]_o$-LTP induction. The dashed line represents the average value of increase during the 35 minute. **(E)** Representative images (20X magnification, 17X zoom) of a dendritic spine decreasing its area (YFP signal) after high $[K^+]_o$-LTP induction. **(F)** Behaviour of shrinking spines (n = 47) in 35 minutes after high $[K^+]_o$-LTP induction. The dashed line represents the averaged value of decrease during the 35 minutes after high $[K^+]_o$-LTP induction. **(G)** Representative images (20X magnification, 17X zoom) of a dendritic spine not changing its area (YFP signal) after high $[K^+]_o$-LTP induction. **(H)** Behaviour of neutral spines (n = 113) in 35 minutes after high $[K^+]_o$-LTP induction.

Data are expressed as percentage of baseline (time -2'55") as means ± SEM of 9 experiments (N = 9; ** $p < 0.01$; *** $p < 0.001$). Statistical analysis was performed by one-way ANOVA followed by Bonferroni's multiple comparison test.

DISCUSSION

The ability of an increased concentration of K^+ to induce neuronal depolarization is a well-established concept (Fleck *et al*., 1992) and recent data collected from this lab have shown that 40-60s of treatment with 20mM K^+ aCSF causes a significant increase in long lasting field excitatory postsynaptic potential (fEPSP) (data not published). This phenomenon seems to share the same mechanisms activated by HFS requiring NMDARs activation and Mg^{2+} detachment from the receptors, and AMPARs involvement in the CA1 hippocampal region (data not published). Moreover, this protocol have shown to trigger a comparable increase of $[K^+]_o$ that is caused by HFS within the dendritic cleft (data not published); this confirmed the physiological importance of reaching a certain concentration of K^+ in the dendritic cleft for the induction of LTP. A crucial feature underlying LTP is the increase of the dendritic spine volume that is observed during both early and late stages of potentiation (Kopec *et al*., 2006).

In this study, we show that exposure of mice acute brain slices to 20 mM K^+ for 50s causes an increase in dendritic spines areas as a consequence of high $[K^+]_o$-LTP induction (Figure 2A). Overall, we found an increase in dendritic spine volume when averaged across the entire population of synapses studied. This finding agrees with the report that fEPSP, a measure of "global" potentiation, also rises in the same conditions.

Surprisingly, we found that there is a population of spines that do not react to the treatment, and another that reacts in the opposite manner, i.e. by decreasing their area. Thus, it is conceivable that the global potentiation registered by fEPSP masks those spines that, supposedly, are not potentiated or even depotentiated or silenced.

The overall increase was statistically significant only starting from 15 minutes after high $[K^+]_o$-LTP induction, and continued up to 35 minutes (Figure 2A). However, it is clear that the increasing event is present already after 5 minutes, as shown in Figure 2D, but the effect is masked by the behaviour of depotentiated spines (Figure 2F).

A possible explanation for our results is offered by the so-called "synaptic tagging hypothesis" first proposed in 1997 by Frey and Morris (Frey and Morris, 1997). Briefly, these authors proposed a model in which LTP induces the sequestration of a pool of proteins synthesis-independent and mRNA (tags) in the surrounding space of the activated dendritic spine; this is one of the way in which early LTP can induce the long-lasting LTP (late-LTP). Recently, the Frey and Morris idea has been further developed by incorporating a mechanism of "competition and cooperation" among spines (Ramiro-Cortés *et al*., 2013). These authors suggest that, since

surrounding spines compete for the same pool of molecules, whenever a stimulus occurs, spines that have been stimulated stronger than others sequestrate the tags, thus winning the competition and being strengthened. The spines that lose the competition can even be removed. Competition can well explain our findings: it is indeed reasonable to suppose that, since the 20 mM perfused solution comes from one side of a chamber, and it has to reach the cells under the surface of the slice, some spines are potentiated sooner and stronger than others, although the final outcome is the induction of a global potentiation of CA1 region synapses.

Altogether, these results provide further support for a role of physiological $[K^+]_o$ increase in inducing LTP in excitatory synapses of the hippocampal CA1 region in mice slices.

Despite the excellence of the results obtained, this study has potential for further improvement aimed at increasing the quality and statistical significance of our data. First of all, it will be necessary to confirm our results by comparing them with a control treatment, which means repeating the experiment in absence of high $[K^+]_o$-LTP. Later, to investigate the mechanism underlying our findings will be necessary. Specifically, to confirm NMDAR dependency the same experiments will be performed in presence of a NMDA antagonist, such as D-(-)-2-Amino-5-phosphonopentanoic acid (AP5).

Furthermore, it will be necessary to overcome some technical limitations to improve signals. We might use transgenic animal model, such as THY1-YFP mice, instead of AAV injection, in order to obtain a better signal-to-noise ratio. In this regard, it has to be pointed out that our choice was guided by the need to be consistent with previous electrophysiological results obtained from KU lab. Improving the image acquisition protocol could be another step. For instance, images could be captured without any averaging, and/or in small z-stacks, which would be helpful to compensate for small movements in z dimension and thus providing a way to follow the spines with more accuracy. The latter strategy could also be useful to estimate volume changes, in addition to area changes.

In sight of the aforementioned arguments, further investigation will be needed.

REFERENCES

Aberle H, Bauer A, Stappert J, Kispert A, Kemler R (1997) beta-catenin is a target for the ubiquitin-proteasome pathway. *EMBO* 16(13):3797-3804.

Allaman I, Gavillet M, Bélanger M, Laroche T, Viertl D, Lashuel HA, *et al.* (2010) Amyloid-beta aggregates cause alterations of astrocytic metabolic phenotype: impact on neuronal viability. *J Neurosci* 30:3326-3338

Alzheimer A (1907) Uber eine eigenartige Erkangkung der Hirnrinde (An unusual illness of the cerebral cortex). *Allgemeine Zeitschr Psychisch-Gerichtliche Medizin* 64:146-148.

Alzheimer's Association Report. (2013) 2013 Alzheimer's disease facts and figures. Alzheimers and Dement. 9:208-245

Anekonda TS (2006) Resveratrol-a boon for treating Alzheimer's disease? *Brain Res Rev* 52:316-326.

Artamonov M, Zhukov O, Shuba I, Storozhuk L, Khmel T, Klimashevsky V, *et al*. (1999) Incorporation of labelled N-acylethanolamine (NAE) into rat brain regions in vivo and adaptive properties of saturated NAE under x-ray irradiation. *Ukr Biokhim Zh* 77(6):51-62.

Balestrino M, Aitken PG, Somjen GG (1986) The effects of moderate changes of extracellular K^+ and Ca^{2+} on synaptic and neural function in the CA1 region of the hippocampal slice. *Brain Res* 377(2):229-239.

Ballyk BA, Goh JW (1992) Elevation of extracellular potassium facilitates the induction of hippocampal long-term potentiation. *J Neurosci Res* 33(4):598-604.

Ben Menachem-Zidon O, Menahem YB, Hur TB, Yirmiya R (2014) Intra-hippocampal transplantation of neural precursor cells with transgenic over-expression of IL-1 receptor antagonist rescues memory and neurogenesis impairments in an Alzheimer's disease model. *Neuropsychopharmacol* 39:401-414.

Bernard J, Lahsaini A, Massicotte G (1994) Potassium-induced long-term potentiation in area CA1 of the hippocampus involves phospholipase activation. *Hippocampus* 4(4):447-453.

Blasko I, Veerhuis R, Stampfer-Kountchev M, Saurwein-Teissl M, Eikelenboom P, Grubeck-Loebenstein B (2000) Costimulatory effects of interferon-gamma and interleukin-1beta or tumor necrosis factor alpha on the synthesis of Abeta1-40 and Abeta1-42 by human astrocytes. *Neurobiol Dis* 7(6 Pt B):682-689.

Blennow K, de Leon MJ, Zetterberg H (2006) Alzheimer's disease. *Lancet* 368:387-403.

Bliss TV, Collingridge GL (1993) A synaptic model of memory: long-term potentiation in the hippocampus. *Nature* 361(6407):31-39.

Bliss TV, Lømo T (1973) Long-lasting potentiation of synaptic transmission in the dentate area of the anaesthetized rabbit following stimulation of the perforant path. *J Physiol* 232(2):331-356.

Block ML, Hong JS (2005) Microglia and inflammation-mediated neurodegeneration: multiple triggers with a common mechanism. *Prog Neurobiol* 76:77-98.

Burda JE, Sofroniew MV (2014) Reactive gliosis and the multicellular response to CNS damage and disease. *Neuron* 81(2): 229-248.

Cadas H, di Tomaso E, Piomelli D (1997) Occurrence and biosynthesis of endogenous cannabinoid precursor, N-arachidonoyl phosphatidylethanolamine, in rat brain. *J Neurosci* 17:1226-1242.

Calignano A, La Rana G, Giuffrida A, Piomelli D (1998) Control of pain initiation by endogenous cannabinoids. *Nature* 394:277-281.

Campolongo P, Ratano P, Ciotti MT, Florenzano F, Nori SL, Marolda R, *et al*. (2013) Systemic administration of substance p recovers Beta amyloid-induced cognitive deficits in rat: involvement of kv potassium channels. *PLoS One* 8:e78036.

Caricasole A, Copani A, Caraci F, Aronica E, Rozemuller AJ, Caruso A, *et al*. (2004) Induction of Dickkopf-1, a negative modulator of the Wnt pathway, is associated with neuronal degeneration in Alzheimer's brain. *J Neurosci* 24:6021-6027.

Caricasole A, Copani A, Caruso A, Caraci F, Iacovelli L, Sortino MA, *et al*. (2003) The Wnt pathway, cell-cycle activation and beta-amyloid: novel therapeutic strategies in Alzheimer's disease. *Trends Pharmacol Sci* 24:233-238.

Cavallini A, Brewerton S, Bell A, Sargent S, Glover S, Hardy C, *et al*. (2013) An unbiased approach to identifying tau kinases that phosphorylate tau at sites associated with Alzheimer disease. *J Biol Chem* 288:23331-23347.

Chen J, Zhou Y, Mueller-Steiner S, Chen LF, Kwon H, Yi S, *et al*. (2005) SIRT1 protects against microglia-dependent amyloid-beta toxicity through inhibiting NF-kappaB signaling. *J Biol Chem* 280(48):40364-40374.

Cleveland DW, Hwo SY, Kirschner MW (1977) Physical and chemical properties of purified tau factor and the role of tau in microtubule assembly. *J Mol Biol* 116(2):227-247.

Cole SL, Vassar R (2008) BACE1 structure and function in health and Alzheimer's disease. *Curr Alzheimer Res* 5:100-120.

Collingridge GL, Kehl SJ, McLennan H (1983) Excitatory amino acids in synaptic transmission in the Schaffer collateral-commissural pathway of the rat hippocampus. *J Physiol* 334:33-46.

Costa B, Conti S, Giagnoni G, Colleoni M (2002) Therapeutic effect of the endogenous fatty acid amide, palmitoylethanolamide, in rat acute inflammation: inhibition of nitric oxide and cyclo-oxygenase systems. *Br J Pharmacol* 137(4):413-420.

Cowley TR, O'Sullivan J, Blau C, Deighan BF, Jones R, Kerskens C, *et al*. (2012) Rosiglitazone attenuates the age-related changes in astrocytosis and the deficit in LTP. *Neurobiol Aging* 33:162-175.

Craft JM, Watterson DM, Van Eldik LJ (2006) Human amyloid beta-induced neuroinflammation is an early event in neurodegeneration. *Glia* 53:484-490.

D'Agostino G, Russo R, Avagliano C, Cristiano C, Meli R, Calignano A (2012) Palmitoylethanolamide protects against the amyloid-β25-35-induced learning and memory impairment in mice, an experimental model of Alzheimer disease. *Neuropsychopharmacol* 37(7):1784-1792.

Dandrea MR, Reiser PA, Gumula NA, Hertzog BM, Andrade-Gordon P (2001) Application of triple immunohistochemistry to characterize amyloid plaque-associated inflammation in brains with Alzheimer's disease. *Biotech Histochem* 76:97-106.

De Felice FG, Wu D, Lambert MP, Fernandez SJ, Velasco PT, Lacor PN, *et al*. (2008) Alzheimer's disease-type neuronal tau hyperphosphorylation induced by A beta oligomers. *Neurobiol Aging* 29:1334-1347.

De Ferrari GV, Inestrosa NC (2000) Wnt signaling function in Alzheimer's disease. *Brain Res Rev* 33(1) :1-12.

de Oliveira RM, Pais TF, Outeiro TF (2010) Sirtuins: common targets in aging and in neurodegeneration. *Curr Drug Targets* 11:1270-1280.

Dehghani L, Hashemi-Beni B, Poorazizi E, Khorvash F, Shaygannejad V, Sedghi M, *et al*. (2013) Evaluation of neural gene expression in serum treated embryonic stem cells in Alzheimer's patients. *J Res Med Sci* 18(Suppl 1):S20-S23.

Di Filippo M, Sarchielli P, Picconi B, Calabresi P (2008) Neuroinflammation and synaptic plasticity: theoretical basis for a novel, immune-centred, therapeutic approach to neurological disorders. *Trends Pharmacol Sci* 29:402-412.

Donato R, Cannon BR, Sorci G, Riuzzi F, Hsu K, Weber DJ, *et al*. (2013) Functions of S100 proteins. *Curr Mol Med* 13:24-57.

Donato R, Heizmann CW (2010) S100B protein in the nervous system and cardiovascular apparatus in normal and pathological conditions. *Cardiovasc Psychiatry Neuro*l 2010:929712.

Dubois B, Feldman HH, Jacova C, Cummings JL, Dekosky ST, Barberger-Gateau P, *et al*. (2010) Revising the definition of Alzheimer's disease: a new lexicon. *Lancet Neurol* 9:1118-1127.

Engel T, Hernandez F, Avila J, Lucas JJ (2006) Full reversal of Alzheimer’s disease-like phenotype in a mouse model with conditional overexpression of glycogen synthase kinase-3. *J Neurosci* 26(19):5083-5090.

Espinosa A, Alegret M, Valero S, Vinyes-Junque G, Hernandez I, Mauleon A, *et al*. (2015) A longitudinal follow-up of 550 mild cognitive impairment patients: evidence for large conversion to dementia rates and detection of major risk factors involved. *J Alzheimers Dis* 34:769-780.

Esposito E, Impellizzeri D, Mazzon E, Paterniti I, Cuzzocrea S (2012) Neuroprotective activities of palmitoylethanolamide in an animal model of Parkinson's disease. *PLoS One* 7(8):e41880.

Esposito G, Scuderi C, Lu J, Savani C, De Filippis D, Iuvone T, *et al*. (2008) S100B induces tau protein hyperphosphorylation via Dickopff-1 up-regulation and disrupts the Wnt pathway in human neural stem cells. *J Cell Mol Med* 12:914-927.

Esposito G, Scuderi C, Valenza M, Togna GI, Latina V, De Filippis D, *et al*. (2011) Cannabidiol reduces Abeta-induced neuroinflammation and promotes hippocampal neurogenesis through PPARgamma involvement. *PLoS One* 6:e28668.

Ferreira ST, Clarke JR, Bomfim TR, De Felice FG (2014) Inflammation, defective insulin signaling, and neuronal dysfunction in Alzheimer's disease. *Alzheimers Dement* 10:S76-S83.

Fleck MW, Palmer AM, Barrionuevo G (1992) Potassium-induced long-term potentiation in rat hippocampal slices. *Brain Res* 580(1-2):100-105.

Frank-Cannon TC, Alto LT, McAlpine FE, Tansey MG (2009) Does neuroinflammation fan the flame in neurodegenerative diseases. *Mol Neurodegener* 4:47.

Franklin A, Parmentier-Batteur S, Walter L, Greenberg DA, Stella N (2003) Palmitoylethanolamide increases after focal cerebral ischemia and potentiates microglial cell motility. *J Neurosci* 23:7767-7775.

Frankola KA, Greig NH, Luo W, Tweedie D (2011) Targeting TNF-alpha to elucidate and ameliorate neuroinflammation in neurodegenerative diseases. *CNS Neurol Disord Drug Targets* 10:391-403.

Frey U, Morris RG (1997) Synaptic tagging and long-term potentiation. *Nature* 385(6616):533-536.

Fuller S, Steele M, Munch G (2010) Activated astroglia during chronic inflammation in Alzheimer's disease–do they neglect their neurosupportive roles. *Mutat Res* 690:40-49.

Gabuzda D, Yankner BA (2013) Physiology: Inflammation links ageing to the brain. *Nature* 497(7448): 197-198.

Gan L, Mucke L (2008) Paths of convergence: sirtuins in aging and neurodegeneration. *Neuron* 58:10-14.

Gatti A, Lazzari M, Gianfelice V, Di Paolo A, Sabato E, Sabato AF (2012) Palmitoylethanolamide in the treatment of chronic pain caused by different etiopathogenesis. *Pain Med* 13:1121-1130.

Gentleman SM, Nash MJ, Sweeting CJ, Graham DI, Roberts GW (1993) Beta-amyloid precursor protein (beta APP) as a marker for axonal injury after head injury. *Neurosci Lett* 160:139-144.

Griffin WS (2006) Inflammation and neurodegenerative diseases. *Am J Clin Nutr* 83:470S-474S.

Griffin WS (2011) Alzheimer's-Looking beyond plaques. *F1000 Med Rep* 3:24.

Griffith CM, Xie MX, Qiu WY, Sharp AA, Ma C, Pan A, *et al*. (2016) Aberrant expression of the pore-forming KATP channel subunit Kir6.2 in hippocampal reactive astrocytes in the 3xTg-AD mouse model and human Alzheimer's disease. *Neuroscience* 336:81-101.

Grillo SL, Keereetaweep J, Grillo MA, Chapman KD, Koulen P (2013) N-Palmitoylethanolamine depot injection increased its tissue levels and those of other acylethanolamide lipids. *Drug Des Devel Ther* 7:747-752.

Grimes CA1, Jope RS (2001) The multifaceted roles of glycogen synthase kinase 3beta in cellular signaling. *Prog Neurobiol* 65(4):391-426.

Gruart A, Muñoz MD, Delgado-García JM (2006) Involvement of the CA3-CA1 synapse in the acquisition of associative learning in behaving mice. *J Neurosci* 26(4):1077-1087.

Haigis MC, Sinclair DA (2010) Mammalian sirtuins: biological insights and disease relevance. *Annu Rev Pathol* 5:253-295

Hallenbeck J (2010) How inflammation modulates central nervous system vessel activation and provides targets for intervention-a personal perspective. *Ann N Y Acad Sci* 1207:1-7.

Hanger DP, Hughes K, Woodgett JR, Brion JP, Anderton BH (1992) Glycogen synthase kinase-3 induces Alzheimer's disease-like phosphorylation of tau: generation of paired helical filament epitopes and neuronal localisation of the kinase. *Neurosci Lett* 147(1):58-62.

Harris EW, Ganong AH, Cotman CW (1984) Long-term potentiation in the hippocampus involves activation of Nmethyl-D-aspartate receptors. *Brain Res* 323(1):132-137.

Harris KM, Kater SB (1994) Dendritic spines: cellular specializations imparting both stability and flexibility to synaptic function. *Annu Rev Neurosci* 17:341-371.

Harrison CM, Alger BE (1993) Perfusion with high potassium plus glutamate can cause LTP erasure or persistent loss of neuronal responsiveness in the CA1 region of the hippocampal slice. *Brain Res* 602(1):175-179.

Harting K, Knöll B (2010) SIRT2-mediated protein deacetylation: an emerging key regulator in brain physiology and pathology. *Eur J Cell Biol* 89:262-269.

Hayashi Y, Shi SH, Esteban JA, Piccini A, Poncer JC, Malinow R (2000) Driving AMPA receptors into synapses by LTP and CaMKII: requirement for GluR1 and PDZ domain interaction. *Science* 287(5461):2262-2267.

Heneka MT, O'Banion MK, Terwel D, Kummer MP (2010) Neuroinflammatory processes in Alzheimer's disease. *J Neural Transm* 117:919-947.

Hirokawa N (1994) Microtubule organization and dynamics dependent on microtubule-associated proteins. *Curr Opin Cell Biol* 6:74-81.

Hoppe JB, Rattray M, Tu H, Salbego CG, Cimarosti H (2013) SUMO-1 conjugation blocks beta-amyloid-induced astrocyte reactivity. *Neurosci Lett* 546:51-56.

Howitz KT., Bitterman KJ, Cohen HY, Lamming DW, Lavu S, Wood JG, *et al.* (2003) Small molecule activators of sirtuins extend Saccharomyces cerevisiae lifespan. *Nature* 425:191-196

Impellizzeri D, Bruschetta G, Cordaro M, Crupi R, Siracusa R, Esposito E, *et al*. (2014) Micronized/ultramicronized palmitoylethanolamide displays superior oral efficacy compared to nonmicronized palmitoylethanolamide in a rat model of inflammatory pain. *J Neuroinflammation* 11:136.

Inestrosa NC, Montecinos-Oliva C, Fuenzalida M (2012) Wnt signaling: role in Alzheimer disease and schizophrenia. *J Neuroimmune Pharmacol* 7:788-807.

Jefremov V, Zilmer M, Zilmer K, Bogdanovic N, Karelson E (2007) Antioxidative effects of plant polyphenols: from protection of G protein signaling to prevention of age-related pathologies. *Ann N Y Acad* Sci 1095:449-457.

Jiang X, Takahashi N, Ando K, Otsuka T, Tetsuka T, Okamoto T (2003) NF-kappa B p65 transactivation domain is involved in the NF-kappa B-inducing kinase pathway. *Biochem Biophys Res Commun* 301(2):583-590.

Jope RS, Yuskaitis CJ, Beurel E (2007) Glycogen synthase kinase-3 (GSK3): inflammation, diseases, and therapeutics. *Neurochem Res* 32 (4-5):577-595.

Julien C, Tremblay C, Emond V, Lebbadi M, Salem N Jr, Bennett DA, *et al*. (2009) Sirtuin 1 reduction parallels the accumulation of tau in Alzheimer disease. *J Neuropathol Exp Neurol* 68:48-58.

Kapoor A, Collino M, Castiglia S, Fantozzi R, Thiemermann C (2010) Activation of peroxisome proliferator-activated receptor-beta/delta attenuates myocardial ischemia/reperfusion injury in the rat. *Shock* 34:117-124.

Keppel Hesselink JM, de Boer T, Witkamp RF (2013) Palmitoylethanolamide: a natural body-own anti-inflammatory agent, effective and safe against influenza and common cold. *Int J Inflam* 2013:151028.

Kim D, Nguyen MD, Dobbin MM, Fischer A, Sananbenesi F, Rodgers JT, *et al*. (2007) SIRT1 deacetylase protects against neurodegeneration in models for Alzheimer's disease and amyotrophic lateral sclerosis. *EMBO J* 26:3169-3179.

Kim W, Kim M, Jho EH (2013) Wnt/beta-catenin signalling: from plasma membrane to nucleus. *Biochem J* 450:9-21.

Koistinaho J, Malm T, Goldsteins G (2011) Glycogen synthase kinase-3beta: a mediator of inflammation in Alzheimer's disease. *Int J Alzheimers Dis* 2011:129753.

Koistinaho M, Ort M, Cimadevilla JM, Vondrous R, Cordell B, Koistinaho J, *et al*. (2001) Specific spatial learning deficits become severe with age in beta -amyloid precursor protein transgenic mice that harbour diffuse beta -amyloid deposits but do not form plaques. *Proc Natl Acad Sci USA* 98:14675-14680.

Kopec CD, Li B, Wei W, Boehm J, Malinow R (2006) Glutamate receptor exocytosis and spine enlargement during chemically induced long-term potentiation. *J Neurosci* 26(7):2000-2009.

Kosaraju J, Holsinger RM, Guo L, Tam KY (2016) Linagliptin, a dipeptidyl deptidase-4 inhibitor, mitigates mognitive deficits and p athology in the 3xTg-AD Mouse Model of Alzheimer's Disease. *Mol Neurobiol* [Epub ahead of print].

Krnjević K, Morris ME, Reiffenstein RJ (1982) Stimulation-evoked changes in extracellular K^+ and Ca^{2+} in pyramidal layers of the rat's hippocampus. *Can J Physiol Pharmacol* 60(12):1643-1657.

Landfield PW, Rose G, Sandles L, Wohlstadter TC, Lynch G (1977) Patterns of astroglial hypertrophy and neuronal degeneration in the hippocampus of ages, memory-deficient rats. *J Gerontol* 32(1):3-12.

Lawrence T (2009) The Nuclear Factor NF-κB Pathway in Inflammation. *Cold Spring Harb Perspect Biol* 1(6):a001651.

Li HL, Wang HH, Liu SJ, Deng YQ, Zhang YJ, Tian Q, *et al*. (2007a) Phosphorylation of tau antagonizes apoptosis by stabilizing beta-catenin, a mechanism involved in Alzheimer's neurodegeneration. *Proc Natl Acad Sci USA* 104(9) :3591-3596.

Li Y, Yokota T, Gama V, Yoshida T, Gomez JA, Ishikawa K, *et al*. (2007b) Bax-inhibiting peptide protects cells from polyglutamine toxicity caused by Ku70 acetylation. *Cell Death Differ* 14:2058-2067.

Li Y, Zhou W, Tong Y, He G, Song W (2006) Control of APP processing and Abeta generation level by BACE1 enzymatic activity and transcription. *FASEB J* 20:285-292.

Lo Verme J, Fu J, Astarita G, La Rana G, Russo R, Calignano A, *et al*. (2005) The nuclear receptor peroxisome proliferator-activated receptor-alpha mediates the anti-inflammatory actions of palmitoylethanolamide. *Mol Pharmacol* 67:15-19.

Lo Verme J, Russo R, La Rana G, Fu J, Farthing J, Mattace-Raso G, *et al*. (2006) Rapid broad-spectrum analgesia through activation of peroxisome proliferator-activated receptor-alpha. *J Pharmacol Exp Ther* 319(3):1051-1061.

Lømo T (1966) Frequency potentiation of excitatory synaptic activity in the dentate area of the hippocampal formation *Acta Physiol Scand* 68(Suppl. 277):128.

Lu T, Pan Y, Kao SY, Li C, Kohane I, Chan J, *et al*. (2004) Gene regulation and DNA damage in the ageing human brain. *Nature* 429:883-891.

Luo Y, Bolon B, Kahn S, Bennett BD, Babu-Khan S, Denis P, *et al*. (2001) Mice deficient in BACE1, the Alzheimer's beta-secretase, have normal phenotype and abolished beta-amyloid generation. *Nat Neurosci* 4:231-232.

Luterman JD, Haroutunian V, Yemul S, Ho L, Purohit D, Aisen PS, *et al*. (2000) Cytokine gene expression as a function of the clinical progression of Alzheimer disease dementia. *Arch Neurol* 57:1153-1160.

Luthi-Carter R, Taylor DM, Pallos J, Lambert E, Amore A, Parker A, *et al*. (2010) SIRT2 inhibition achieves neuroprotection by decreasing sterol biosynthesis. *Proc Natl Acad Sci USA* 107:7927-7932.

Mackie K, Stella N (2006) Cannabinoid receptors and endocannabinoids: evidence for new players. *AAPS J* 8:E298-E306.

Malenka RC (1994) Synaptic plasticity in the hippocampus: LTP and LTD. *Cell* 78(4):535-538.

Malenka RC, Nicoll RA (1999) Long-term potentiation-a decade of progress? *Science* 285(5435):1870-1874.

Malinow R, Malenka RC (2002) AMPA receptor trafficking and synaptic plasticity. *Annu Rev Neurosci* 25:103-126.

Martin SJ, Grimwood PD, Morris RG (2000) Synaptic plasticity and memory: an evaluation of the hypothesis. *Annu Rev Neurosci* 23:649-711.

Matsuzaki M, Ellis-Davies GCR, Nemoto T, Miyashita Y, Iino M, Kasai H (2001) Dendritic spine geometry is critical for AMPA receptor expression in hippocampal CA1 pyramidal neurons. *Nature Neurosci* 4:1086-1092.

Mayer ML, Westbrook GL, Guthrie PB (1984) Voltage-dependent block by Mg^{2+} of NMDA responses in spinal cord neurons. *Nature* 309(5965):261-263.

McGeer EG, McGeer PL (1999) Brain inflammation in Alzheimer disease and the therapeutic implications. *Curr Pharm Des* 5:821-836.

McGeer PL, McGeer EG (2013) The amyloid cascade-inflammatory hypothesis of Alzheimer disease: implications for therapy. *Acta Neuropathol* 126:479-497.

Meda L, Baron P, Scarlato G (2001) Glial activation in Alzheimer's disease: the role of Abeta and its associated proteins. *Neurobiol Aging* 22:885-893.

Medeiros R, LaFerla FM (2013) Astrocytes: conductors of the Alzheimer disease neuroinflammatory symphony. *Exp Neurol* 239:133-138.

Menard C, Bastianetto S, Quirion R (2013) Neuroprotective effects of resveratrol and epigallocatechin gallate polyphenols are mediated by the activation of protein kinase C gamma. *Front Cell Neurosci* 7:281.

Michan S, Sinclair D (2007) Sirtuins in mammals: insights into their biological function. *Biochem J* 404:1-13.

Minghetti L (2004) Cyclooxygenase-2 (COX-2) in inflammatory and degenerative brain diseases. *J Neuropathol Exp Neurol* 63:901-910.

Morris RG (2001) Episodic-like memory in animals: psychological criteria, neural mechanisms and the value of episodic-like tasks to investigate animal models of neurodegenerative disease. *Philos Trans R Soc Lond B Biol Sci* 356:1453-1465.

Morris RG, Anderson E, Lynch GS, Baudry M (1986) Selective impairment of learning and blockade of long-term potentiation by an N-methyl-D-aspartate receptor antagonist, AP5. *Nature* 319(6056):774-776.

Mrak RE (2009) Neuropathology and the neuroinflammation idea. *J Alzheimers Dis* 18:473-481.

Mrak RE, Griffin WS (2001a) Interleukin-1, neuroinflammation, and Alzheimer's disease. *Neurobiol Aging* 22:903-908.

Mrak RE, Griffin WS (2001b) The role of activated astrocytes and of the neurotrophic cytokine S100B in the pathogenesis of Alzheimer's disease. *Neurobiol Aging* 22:915-922.

Murillo-Rodriguez E, Desarnaud F, Prospero-Garcia O (2006) Diurnal variation of arachidonoylethanolamine, palmitoylethanolamide and oleoylethanolamide in the brain of the rat. *Life Sci* 79:30-37.

Musleh W, Bi X, Tocco G, Yaghoubi S, Baudry M (1997) Glycine-induced long-term potentiation is associated with structural and functional modifications of alpha-amino-3-hydroxyl-5-methyl-4-isoxazolepropionic acid receptors. *Proc Natl Acad Sci USA* 94(17):9451-9456.

Myer DJ, Gurkoff GG, Lee SM, Hovda DA, Sofroniew MV (2006) Essential protective roles of reactive astrocytes in traumatic brain injury. *Brain* 129:2761-2772.

Nicholson C, Hounsgaard J (1983) Diffusion in the slice microenvironment and implications for physiological studies. *Fed Proc* 42(12):2865-2868.

Nowak L, Bregestovski P, Ascher P, Herbet A, Prochiantz A (1984) Magnesium gates glutamate-activated channels in mouse central neurons. *Nature* 307(5950):462-465.

O'Brien RJ, Wong PC (2011) Amyloid precursor protein processing and Alzheimer's disease. *Annu Rev Neurosci* 34:185-204.

O'Callaghan JP, Sriram K (2005) Glial fibrillary acidic protein and related glial proteins as biomarkers of neurotoxicity. *Expert Opin Drug Saf* 4:433-442.

Oddo S, Caccamo A, Kitazawa M, Tseng BP, LaFerla FM (2003a) Amyloid deposition precedes tangle formation in a triple transgenic model of Alzheimer's disease. *Neurobiol Aging* 24:10631070.

Oddo S, Caccamo A, Shepherd JD, Murphy MP, Golde TE, Kayed R, *et al*. (2003b) Triple-transgenic model of Alzheimer's disease with plaques and tangles: intracellular Abeta and synaptic dysfunction. *Neuron* 39(3):409-421.

Olabarria M, Noristani HN, Verkhratsky A, Rodríguez JJ (2010) Concomitant astroglial atrophy and astrogliosis in a triple transgenic animal model of Alzheimer's disease. *Glia* 58:831-838.

Orre M, Kamphuis W, Osborn LM, Jansen AH, Kooijman L, Bossers K, *et al*. (2014) Isolation of glia from Alzheimer's mice reveals inflammation and dysfunction. *Neurobiol Aging* 35(12):2746-1760.

Osborn LM, Kamphuis W, Wadman WJ, Hol EM (2016) Astrogliosis: An integral player in the pathogenesis of Alzheimer's disease. *Prog Neurobiol* 144:121-141.

Outeiro TF, Kontopoulos E, Altmann SM, Kufarev I, Strathearn KE, Amore AM, *et al*. (2007) Sirtuin 2 inhibitors rescue alpha-synuclein-mediated toxicity in models of Parkinson's disease. *Science* 317:516-519.

Outeiro TF, Marques O, Kazantsev A (2008) Therapeutic role of sirtuins in neurodegenerative disease. *Biochim Biophys Acta* 1782:363-369.

Paxinos G, Watson C (2007) The rat brain in stereotaxic coordinates.

Petrosino S, Di Marzo V (2016) The pharmacology of palmitoylethanolamide and first data on the therapeutic efficacy of some of its new formulations. *Br J Pharmacol*. [Epub ahead of print]

Petrosino S, Iuvone T, Di Marzo V (2010) N-palmitoyl-ethanolamine: Biochemistry and new therapeutic opportunities. *Biochimie* 92:724-727.

Petrosino S, Schiano Moriello A, Cerrato S, Fusco M, Puigdemont A, De Petrocellis L, *et al*. (2016) The anti-inflammatory mediator palmitoylethanolamide enhances the levels of 2-arachidonoylglycerol and potentiates its actions at transient receptor potential vanilloid type-1 channels. *Br J Pharmacol* 173:1154-1162.

Poolos NP, Mauk MD, Kocsis JD (1987) Activity-evoked increases in extracellular potassium modulate presynaptic excitability in the CA1 region of the hippocampus. *J Neurophysiol* 58(2):404-416.

Prince M, Wimo A, Guerchet M, Ali GC, Wu YT, Prina M (2015) *Alzheimer's Disease International. World Alzheimer Report 2015. The Global Impact of Dementia An analysis of prevalence, incidence, cost and trends.*

Qin W, Chachich M, Lane M, Roth G, Bryant M, de Cabo R, *et al*. (2006a) Calorie restriction attenuates Alzheimer's disease type brain amyloidosis in Squirrel monkeys (Saimiri sciureus). *J Alzheimers Dis* 10:417-422.

Qin W, Yang T, Ho L, Zhao Z, Wang J, Chen L, *et al*. (2006b) Neuronal SIRT1 activation as a novel mechanism underlying the prevention of Alzheimer disease amyloid neuropathology by calorie restriction. *J Biol Chem* 281:21745-21754.

Querfurth HW, LaFerla FM (2010) Alzheimer's disease. *N Engl J Med* 362:329-344.

Rahimi A, Faizi M, Talebi F, Noorbakhsh F, Kahrizi F, Naderi N (2015) Interaction between the protective effects of cannabidiol and palmitoylethanolamide in experimental model of multiple sclerosis in C57BL/6 mice. *Neuroscience* 290:279-287.

Ramiro-Cortés Y, Hobbiss AF, Israely I (2013) Synaptic competition in structural plasticity and cognitive function. *Philos Trans R Soc Lond B Biol Sci* 369(1633):20130157.

Rangroo Thrane V, Thrane AS, Wang F, Cotrina ML, Smith NA, Chen M, *et al*. (2013) Ammonia triggers neuronal disinhibition and seizures by impairing astrocyte potassium buffering. *Nat Med* 19(12):1643-1648.

Repetto G, del Peso A, Zurita JL (2008) Neutral red uptake assay for the estimation of cell viability/cytotoxicity. *Nat Protoc* 3:1125-1131.

Rodrigues EM, Weissmiller AM, Goldstein LS (2012) Enhanced beta-secretase processing alters APP axonal transport and leads to axonal defects. *Hum Mol Genet* 21:4587-4601.

Rodríguez JJ, Olabarria M, Chvatal A, Verkhratsky A (2009) Astroglia in dementia and Alzheimer's disease. *Cell Death Differ* 16(3):378-385.

Roisin MP, Leinekugel X, Tremblay E (1997) Implication of protein kinase C in mechanisms of potassium-induced long-term potentiation in rat hippocampal slices. *Brain Res* 745(1-2):222-230.

Rojo LE, Fernandez JA, Maccioni AA, Jimenez JM, Maccioni RB (2008) Neuroinflammation: implications for the pathogenesis and molecular diagnosis of Alzheimer's disease. *Arch Med Res* 39:1-16.

Romano A, Pace L, Tempesta B, Lavecchia AM, Macheda T, Bedse G, *et al*. (2014) Depressive-like behaviour is paired to monoaminergic alteration in a murine model of Alzheimer's disease. *Int J Neuropsychopharmacol* 18(4).

Sastre M, Klockgether T, Heneka MT (2006) Contribution of inflammatory processes to Alzheimer's disease: molecular mechanisms. *Int J Dev Neurosci* 24:167-176.

Savonenko A, Xu GM, Melnikova T, Morton JL, Gonzales V, Wong MP, *et al*. (2005) Episodic-like memory deficits in the APPswe/PS1dE9 mouse model of Alzheimer's disease: relationships to beta-amyloid deposition and neurotransmitter abnormalities. *Neurobiol Dis* 18:602-617.

Sawmiller D, Habib A, Li S, Darlington D, Hou H, Tian J, *et al*. (2016) Diosmin reduces cerebral Aβ levels, tau hyperphosphorylation, neuroinflammation, and cognitive impairment in the 3xTg-AD mice. *J Neuroimmunol* 299:98-106.

Schwartz N, Temkin P, Jurado S, Lim BK, Heifets BD, Polepalli JS, *et al*. (2014) Decreased motivation during chronic pain requires long-term depression in the nucleus accumbens. *Science* 345(6196):535-542.

Schwartz N, Temkin P, Jurado S, Lim BK, Heifets BD, Polepalli JS, *et al*. (2014) Decreased motivation during chronic pain requires long-term depression in the nucleus accumbens. *Science* 345(6196):535-542.

Scuderi C, Esposito G, Blasio A, Valenza M, Arietti P, Steardo L Jr, *et al*. (2011) Palmitoylethanolamide counteracts reactive astrogliosis induced by beta-amyloid peptide. *J Cell Mol Med* 15:2664-2674.

Scuderi C, Steardo L (2013) Neuroglial roots of neurodegenerative diseases: therapeutic potential of palmitoylethanolamide in models of Alzheimer's disease. *CNS Neurol Disord Drug Targets* 12:62-69.

Scuderi C, Stecca C, Iacomino A, Steardo L (2013) Role of astrocytes in major neurological disorders: the evidence and implications. *IUBMB Life* 65:957-961.

Scuderi C, Stecca C, Valenza M, Ratano P, Bronzuoli MR, Bartoli S *et al*. (2014). Palmitoylethanolamide controls reactive gliosis and exerts neuroprotective functions in a rat model of Alzheimer's disease. *Cell Death Dis* 5:e1419.

Scuderi C, Valenza M, Stecca C, Esposito G, Carratu MR, Steardo L (2012) Palmitoylethanolamide exerts neuroprotective effects in mixed neuroglial cultures and organotypic hippocampal slices via peroxisome proliferator-activated receptor-alpha. *J Neuroinflammation* 9:49.

Selkoe DJ (2001) Alzheimer's disease: genes, proteins, and therapy. *Physiol Rev* 81(2):741-766.

Sexton CE, Mackay CE, Lonie JA, Bastin ME, Terriere E, O'Carroll RE, *et al*. (2010) MRI correlates of episodic memory in Alzheimer's disease, mild cognitive impairment, and healthy aging. *Psychiatry Res* 184:57-62.

Sheerin AH, Zhang X, Saucier DM, Corcoran ME (2004) Selective antiepileptic effects of N-palmitoylethanolamide, a putative endocannabinoid. *Epilepsia* 45:1184-1188.

Shih RH, Wang CY, Yang CM (2015) NF-kappaB Signaling Pathways in Neurological Inflammation: A Mini Review. *Front Mol Neurosci* 8:77.

Skaper SD, Facci L, Romanello S, Leon A (1996) Mast cell activation causes delayed neurodegeneration in mixed hippocampal cultures via the nitric oxide pathway. *J Neurochem* 66:1157-1166.

Spires-Jones TL, Fox LM, Rozkalne A, Pitstick R, Carlson GA, Kazantsev AG (2012) Inhibition of sirtuin 2 with sulfobenzoic acid derivative AK1 is non-toxic and potentially neuroprotective in a mouse model of frontotemporal dementia. *Front Pharmacol* 3:42.

Steardo L Jr, Bronzuoli MR, Iacomino A, Esposito G, Steardo L, Scuderi C (2015) Does neuroinflammation turn on the flame in Alzheimer's disease? Focus on astrocytes. *Front Neurosci*. 9:259.

Steiner J, Bogerts B, Schroeter ML, Bernstein HG (2011) S100B protein in neurodegenerative disorders. *Clin Chem Lab Med* 49:409-424.

Stepan J, DineJ, Eder M (2015) Functional optical probing of the hippocampal trisynaptic circuit in vitro: network dynamics, filter properties, and polysynaptic induction of CA1 LTP. *Front Neurosci* 9:160.

Sun AY, Wang Q, Simonyi A, Sun GY (2010) Resveratrol as a therapeutic agent for neurodegenerative diseases. *Mol Neurobiol* 41:375-383.

Svoboda J, Syková E (1991) Extracellular space volume changes in the rat spinal cord produced by nerve stimulation and peripheral injury. *Brain Res* 560(1-2):216-224.

Tang BL, Chua CE (2008**)** SIRT1 and neuronal diseases. *Mol Aspects Med* 29(3):187-200.

Theuns J, Van Broeckhoven C (2000) Transcriptional regulation of Alzheimer's disease genes: implications for susceptibility. *Hum Mol Genet* 9:2383-2394.

Tuppo EE, Arias HR (2005) The role of inflammation in Alzheimer’s disease. *Int J Biochem Cell Biol* 37:289-305.

Vairano M, Dello Russo C, Pozzoli G, Battaglia A, Scambia G, Tringali G, *et al*. (2002) Erythropoietin exerts anti-apoptotic effects on rat microglial cells in vitro. *Eur J Neurosci* 16:584-592.

Verkhratsky A, Butt AM (2007) Glial Neurobiology. United Kingdom: John Wiley and Sons Ltd.

Verkhratsky A, Olabarria M, Noristani HN, Yeh CY, Rodriguez JJ (2010) Astrocytes in Alzheimer's disease. *Neurotherapeutics* 7(4):399-3412.

Verkhratsky A, Parpura V (2010) Recent advances in (patho)physiology of astroglia. *Acta Pharmacol Sin* 31:1044-1054.

Verkhratsky A, Parpura V (2016) Astrogliopathology in neurological, neurodevelopmental and psychiatric disorders. *Neurobiol Dis* 85:254-261.

Verkhratsky A, Rodríguez JJ, Parpura V (2013) Astroglia in neurological diseases. *Future Neurol*. 8(2):149-158.

Verkhratsky A, Sofroniew MV, Messing A, deLanerolle NC, Rempe D, Rodriguez JJ, *et al*. (2012) Neurological diseases as primary gliopathies: a reassessment of neurocentrism. *ASN Neuro* 4(3):e00082.

Wozniak MA, Itzhaki RF, Shipley SJ, Dobson CB (2007) Herpes simplex virus infection causes cellular beta-amyloid accumulation and secretase upregulation. *Neurosci Lett* 429(2-3):95-100.

Wyss-Coray T (2006) Inflammation in Alzheimer disease: driving force, bystander or beneficial response. *Nat Med* 12:1005-1015.

Wyss-Coray T, Rogers J (2012) Inflammation in Alzheimer disease-a brief review of the basic science and clinical literature. *Cold Spring Harb Perspect Med* 2(1):a006346.

Yoshida T, Goldsmith SK, Morgan TE, Stone DJ, Finch CE (1996) Transcription supports age-related increases of GFAP gene expression in the male rat brain. *Neurosci Lett* 215(2): 107-110.

Yuan J, Zhang J, Wong BW, Si X, Wong J, Yang D, *et al*. (2005) Inhibition of glycogen synthase kinase 3beta suppresses coxsackievirus-induced cytopathic effect and apoptosis via stabilization of beta-catenin. *Cell Death Differ* 12(8):1097-1106.

Yuste R, Bonhoeffer T (2001) Morphological changes in dendritic spines associated with long-term synaptic plasticity. *Annu Rev Neurosci* 24:1071-1089.

Zamanian JL, Xu L, Foo LC, Nouri N, Zhou L, Giffard RG, *et al*. (2012) Genomic analysis of reactive astrogliosis. *J Neurosci* 32: 6391-6410.

Zenzmaier C, Marksteiner J, Kiefer A, Berger P, Humpel C (2009) Dkk-3 is elevated in CSF and plasma of Alzheimer's disease patients. *J Neurochem* 110:653-661.

Zhang Z, Hartmann H, Do VM, Abramowski D, Sturchler-Pierrat C, Staufenbiel M, *et al*. (1998) Destabilization of beta-catenin by mutations in presenilin-1 potentiates neuronal apoptosis. *Nature* 395(6703):698-702.

Zhu LQ, Wang SH, Liu D, *et al*. (2007) Activation of glycogen synthase kinase-3 inhibits long-term potentiation with synapse-associated impairments. *J Neurosci* 27(45):12211-12220.